

THE TROPICAL CIRCULATION IN A CHANGING CLIMATE

Dissertation

zur Erlangung des Doktorgrades
an der Fakultät für Mathematik, Informatik und Naturwissenschaften
im Fachbereich Geowissenschaften der Universität Hamburg

vorgelegt von

Elina Plesca

Hamburg

2018

Als Dissertation angenommen vom Fachbereich
der Geowissenschaften der Universität Hamburg.

Folgende Gutachter empfehlen die Annahme der Dissertation:

Prof. Dr. Stefan A. Buehler
und Dr. Verena Grützun

Tag der Disputation: Hamburg, den 29. Juni 2018

Abstract

The tropical atmospheric overturning circulations are likely weakening under increased CO₂ forcing. However, insufficient understanding of the circulations' dynamics diminishes the full confidence in such a response. Here I address two distinct aspects of the circulation change as it is represented in a series of CMIP5 (Coupled Model Intercomparison Project Phase 5) idealized experiments: the robustness of the Walker circulation in a warming climate and the fast response of the tropical overturning circulation to CO₂ forcing.

The first study investigates the changes in the Pacific Walker circulation under anthropogenic forcing and the sensitivity of its weakening response to internal variability, General Circulation Model (GCM) configuration, and indexing method. The sensitivity to internal variability is analyzed by using a 68-member ensemble of the MPI-ESM-LR model; the influence of model physics is analyzed by using the 28-member CMIP5 multi-model ensemble. Three simple circulation indices, based on mean sea-level pressure, 500 hPa vertical velocity and 200 hPa velocity potential, are computed for each member of the two ensembles. The analysis uses the outputs of the CMIP5 idealized transient climate simulations with 1% per year CO₂ increase from pre-industrial level, and investigates the detected circulation response until the moment of CO₂ doubling (70 years). Depending on the indexing method, it is found that 50-93% of the MPI-ESM-LR and 54-75% of the CMIP5 ensemble members project significant negative trends in the circulation's intensity. This large spread in the ensembles reduces the confidence that a weakening circulation is a robust feature of climate change. Furthermore, the similar magnitude of the spread in both ensembles shows that the Walker circulation response is strongly influenced by natural variability, even on a 70-year period.

In the second part of this thesis I analyze CMIP5 idealized climate experiments with abrupt quadrupling of atmospheric CO₂ to understand the fast response of the tropical overturning circulation to this forcing and the main contributors to this response. I define a measure for the circulation intensity based on pressure velocity in the tropical subsidence regions. In doing so, I play on the advantage of the subsidence regions in being dynamically stable and on the fact that, from a measurement point of view, the observation of these regions is prone to less uncertainty than the convective regions. Also, the subsidence regions are less sensitive to the GCM's cloud and precipitation parametrization schemes. My method allows to decompose the circulation intensity relative change (with respect to a control state) into a sum of the relative

changes in subsidence area, static stability and atmospheric cooling rate. Also, I use aqua planet and realistic planet experiments to look into the effect of the land-sea differentiated heating on the total change in circulation strength. I find that on average the tropical circulation slows down and this change is dominated by the cooling rate reduction, as the other factors show a positive change. The cooling rate reduction results from the direct radiative effect of increased CO₂ concentration in the atmosphere. I find that even in a realistic planet setup the circulation change is dominated by the changes in the subsidence regions over the oceans, but the land-sea differentiated heating also contributes to the slow-down of the circulation by driving the vertical expansion of the tropics. A brief analysis of the circulation changes in a coupled climate experiment suggests that the fast response of the circulation is detectable at time scales smaller than 1 year: another mechanism leading to the circulation weakening takes over around this time range, i.e. the increased static stability in response to the surface temperature rise occurring as a result of the CO₂ greenhouse effect.

Zusammenfassung

Die tropischen Umwälzzirkulationen schwächen sich wahrscheinlich bei erhöhtem CO₂-Antrieb ab. Ein unzureichendes Verständnis der Dynamik der Zirkulationen verringert jedoch die Verlässlichkeit einer solchen Reaktion. Hier gehe ich auf zwei verschiedene Aspekte der Zirkulationsveränderung ein, die in einer Reihe von idealisierten Experimenten im Rahmen des CMIP5 Modellvergleichs untersucht werden: die Robustheit der Walker-Zirkulation in einem sich erwärmenden Klima und die schnelle Reaktion der tropischen Umwälzzirkulation auf den CO₂-Antrieb.

Die erste Studie untersucht die Veränderungen der pazifischen Walker-Zirkulation unter anthropogenem Einfluss und die Sensitivität ihrer Abschwächung im sich erwärmenden Klima bezüglich interner Variabilität, der Konfiguration des allgemeinen Zirkulationsmodells (General Circulation Model oder GCM) und der Indexierungsmethode. Die Sensitivität bezüglich interner Variabilität wird mit Hilfe eines Ensembles aus 68 verschiedenen Realisierungen des MPI-ESM-LR Modells analysiert. Der Einfluss der Modellphysik wird mit Hilfe des CMIP5 Ensembles aus 28 Modellen analysiert. Drei einfache Zirkulationsindizes, basierend auf dem durchschnittlichen Meeresspiegeldruck, auf der 500 hPa Vertikalgeschwindigkeit und auf dem 200 hPa Geschwindigkeitspotenzial werden für jedes Mitglied der zwei Ensembles berechnet. Die Analyse verwendet die Ergebnisse der idealisierten CMIP5 transienten Klimasimulationen mit einem CO₂-Anstieg von 1% pro Jahr seit dem vorindustriellen Niveau und untersucht die nachgewiesene Zirkulationsreaktion bis zum Zeitpunkt der CO₂-Verdopplung (70 Jahre). Abhängig von der Indexierungsmethode wird festgestellt, dass 50-93% der MPI-ESM-LR und 54-75% der CMIP5-Ensemblemitglieder signifikante negative Trends in der Zirkulationsintensität projizieren. Diese große Streuung in den Ensembles verringert das Vertrauen, dass eine sich abschwächende Zirkulation ein robustes Merkmal des Klimawandels ist. Die ähnliche Größe der Streuung in beiden Ensembles zeigt darüber hinaus, dass die Änderung der Walker-Zirkulation stark von der natürlichen Variabilität beeinflusst wird, selbst bei einem Betrachtungszeitraum von 70 Jahren.

Im zweiten Teil dieser Dissertation analysiere ich idealisierte CMIP5 Klimaexperimente mit abrupter Vervierfachung des atmosphärischen CO₂, um die schnelle Reaktion der tropischen Umwälzzirkulation auf diesen Antrieb zu verstehen und die wichtigsten Faktoren für diese Reaktion zu finden. Ich definiere ein Maß für die Zirkulationsintensität basierend auf der Druck-

geschwindigkeit in den tropischen Subsidenzgebieten. Dabei nutze ich den Vorteil, dass die Subsidenzgebiete dynamisch stabil sind, und den Vorteil, dass die Beobachtung dieser Regionen aus messtechnischer Sicht weniger unsicher als die der konvektiven Regionen ist. Außerdem reagieren die Subsidenzgebiete weniger empfindlich auf die Parametrisierungsschemata für Wolken- und Niederschlag des GCM. Meine Methode erlaubt es, die relative Änderung der Zirkulationsintensität (in Bezug auf einen Kontrollzustand) in eine Summe der relativen Änderungen im Subsidenzgebiet, der statischen Stabilität und der atmosphärischen Abkühlrate zu zerlegen. Außerdem benutze ich Vergleiche zwischen Experimenten, die einen reinen Aqua-Planeten simulieren und realistischen Experimenten, die auch die Landverteilung berücksichtigen, um die Wirkung der differenzierten Land-See-Erwärmung auf die Gesamtveränderung der Zirkulationsstärke zu untersuchen. Mein Ergebnis ist, dass sich die tropische Zirkulation durchschnittlich verlangsamt und diese Veränderung durch die Reduktion der Abkühlrate dominiert wird, da die anderen Faktoren eine positive Veränderung zeigen. Die Reduktion der Abkühlungsraten resultiert aus dem direkten Strahlungseffekt der erhöhten CO_2 -Konzentration in der Atmosphäre. Zudem zeige ich, dass selbst in den realistischen Simulationen die Zirkulationsänderung von den Veränderungen in den Subsidenzregionen über den Ozeanen dominiert wird. Dabei trägt allerdings auch die unterschiedlich starke Erwärmung von Land und Ozean zur Verlangsamung der Zirkulation bei, indem sie die vertikale Ausdehnung der Tropen vorantreibt. Eine kurze Analyse der Zirkulationsänderungen in einem gekoppelten Klimaexperiment legt nahe, dass die schnelle Reaktion der Zirkulation innerhalb von Zeitskalen unter einem Jahr nachweisbar ist. Ein weiterer Mechanismus, der zur Schwächung der Zirkulation führt, wird in diesem Zeitbereich dominant: die erhöhte statische Stabilität in Reaktion auf den Anstieg der Oberflächentemperatur infolge des CO_2 -Treibhauseffekts.

Contents

Abstract	iii
Zusammenfassung	v
1 Introduction	1
1.1 The atmospheric circulation in the tropics	1
1.2 Anthropogenic CO ₂ emissions' impact on the tropical circulation	3
1.3 Motivation and research questions	5
1.4 Research approach	8
1.5 Outline	11
2 Data	12
2.1 The CMIP5 experiments	12
2.2 The ERA-Interim reanalysis	14
2.3 The ENSO index dataset	15
3 The change of Walker circulation under CO₂ forcing	16
3.1 Walker circulation indices	16
3.2 The simulation of the Walker circulation in ERA-Interim	18
3.3 The natural variability signal in the Walker circulation change	21
3.4 The CMIP5 detected Walker circulation change	24
3.5 Ensemble members' differences and the detected ensemble spread	28
4 The fast response of the tropical circulation to CO₂ forcing	37
4.1 The subsidence mass flow metric	37
4.2 The circulation response in the aqua-planet experiments	41
4.3 The circulation response in the AMIP experiments	45
4.4 Does CO ₂ impact the variability of the circulation?	48
4.5 The slow response of the tropical circulation to CO ₂ forcing	52
5 Conclusions and outlook	57
5.1 Conclusions	57
5.2 Outlook	62

Contents	viii
Bibliography	66
List of Tables	74
List of Figures	75
Acknowledgements	80

1 Introduction

Thermodynamical changes induced by the anthropogenic greenhouse gas emission are already observable at global scale. At regional scale, however, the atmospheric circulation plays an important role in modifying weather and climate. An understanding of the expected circulation changes and the associated risks will provide crucial information for the global, regional and local decision-making process in the effort to mitigate and to adapt to climate change. Here I investigate two different aspects of the tropical circulation change, with the over-arching goal of advancing our understanding of the mechanisms driving the change and the sensitivity of the circulation to the anthropogenic CO₂ forcing. The first aspect is the robustness of the Walker circulation slowdown and its sensitivity to natural variability and climate model configuration. The second aspect of circulation change is the fast response of the tropical overturning circulation to a CO₂ increase, i.e. the direct effect of CO₂ increase on the circulation.

1.1 The atmospheric circulation in the tropics

Compared to the mid- and high-latitudes, the meridional temperature gradients in the tropics are much less pronounced. As a consequence, the weather and climate in the tropics are shaped predominantly by the contrast between the heat capacities of land and ocean. Over land, due to the low heat capacity of soil and vegetation, air temperature and moisture exhibit a large diurnal amplitude compared to the less ample variation over the ocean. Additionally, over land we find a clear seasonal migration of the wet weather systems. This migration is much less pronounced over the ocean. This uneven distribution of heat/moisture sources and sinks throughout the tropics, at different space and time scales, maintains strong convective systems and extensive subsidence areas, which characterize the tropical atmospheric circulation. Within the tropics, the atmospheric motion manifests itself on climate time scale through several large scale features: the trade winds, the ITCZ (Intertropical Convergence Zone), and the Hadley, Walker, and monsoon circulations.

The trade winds are the predominant easterlies shaping the surface zonal air flow between around 20°S and 20°N. This region is populated by trade wind shallow cumulus clouds controlled by the convection induced by the warm surface. The trade winds supply the air mass and moisture

needed to fuel the ITCZ, which represents a discontinuous region of strong convection clusters driven by the convergence of surface equatorward-moving air masses. Due to axial tilting and differential distribution of land masses in the Southern and Northern Hemispheres, the ITCZ exhibits a clear seasonal cycle and its position shifts between 5°S and 7°N throughout the year [Donohoe et al., 2013]. By maintaining a strong vertical flux of sensible and latent heat from the surface to the upper troposphere, as well as a weaker net upward mass flux, the ITCZ drives the Hadley circulation, which is the largest atmospheric meridional flow feature in the Earth's climate system [McIlveen, 2010]. In the upper troposphere, this circulation feeds air mass and heat pole- and eastward to the subtropical high pressure zones (Fig. 1.1), such as the Azores, the Bolivian or the North Pacific Highs. In these regions, in the lower troposphere, the air motion turns equator- and westward and feeds the trade wind region, thus closing the Hadley Cell. As mentioned above, the differential heating of land and ocean induces seasonal disturbances in this large circulation system, especially in the Northern Hemisphere. This monsoon circulation manifests itself through a change in wind speed and direction (and subsequent change in precipitation) in boreal summer, most prominently over South Asia and West Africa.

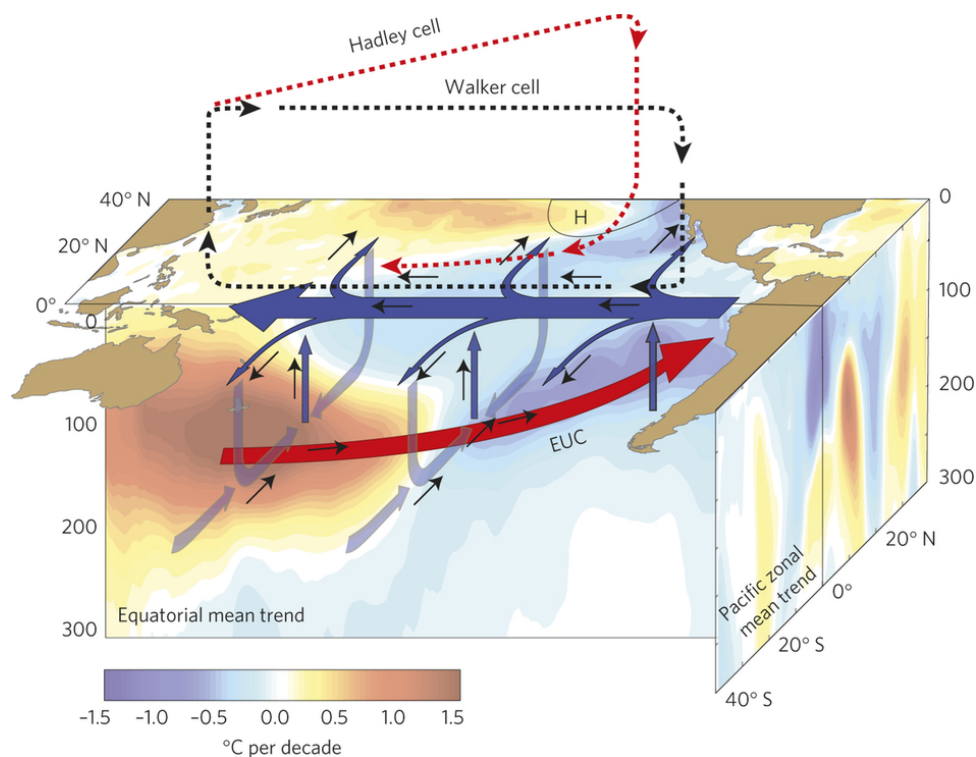


Figure 1.1: Schematic of the atmospheric circulation over the tropical Pacific Ocean and its relationship to the ocean circulation. The *color shading* describes the anomalous ocean circulation with the help of the equatorial and meridional mean trend in water temperature down to the 300 m depths as detected in the 1992–2011 period reanalysis (reprinted by permission from Springer Customer Service Centre GmbH: Nature Climate Change, England et al. [2014], © 2014).

Aside from the Hadley Cells, the tropical atmospheric circulation features the Walker Cells, the largest being the Pacific Walker Cell. This component of the atmospheric circulation is influenced by the Pacific Ocean circulation along the equator. On average, the Humboldt current transports cold water northward towards the equatorial East Pacific, maintaining a shallow mixed layer and thermocline in this region, while the West Pacific in the region of the Maritime Continent retains a warm and deep mixed layer and thermocline. The trade winds sustain this east-to-west slope of the thermocline, thus creating the conditions for the strong updraft region over the Maritime Continent and the subsidence region in the Eastern Pacific, featuring the two vertical branches of the Pacific Walker Cell (Fig. 1.1). Though the motion within the Cell is fuelled by the trade winds, the temperature gradient over the equatorial Pacific has a large impact on the size and intensity of the Cell. This impact is emphasized by ENSO (El Niño Southern Oscillation). This quasi-periodic oscillation has two phases determined by the sea-surface temperature (SST) anomaly over the equatorial Eastern to Central Pacific: El Niño (positive) phase, characterized by significant positive SST anomaly, and La Niña (negative) phase, which represents an extreme case of the mean conditions, with significant negative SST anomaly. Consequently, during an El Niño event, the Pacific Walker Cell is slowed down or even reversed, while it is strengthened during La Niña. By having a significant impact on the vertical circulation along the full length of the equator, ENSO's influence extends on the variability of the climate in the subtropics and the temperate zone as well as on that of the tropics [Gershunov and Barnett, 1998; Diaz et al., 2001; Alexander et al., 2002].

1.2 Anthropogenic CO₂ emissions' impact on the tropical circulation

In the last two centuries, the anthropogenic emissions of CO₂ and other greenhouse gases have been impacting the Earth system in various inter-related ways. By reshaping the radiative signature of the atmosphere and driving the rise of surface temperature, these emissions affect the dynamics of the climate system.

The latest investigations based on the CMIP5 (Coupled Model Intercomparison Project Phase 5, see Taylor et al. [2012]) General Circulation Models (GCMs) show a consensus on the weakening of the tropical atmospheric circulation in response to global climate change [Held and Soden, 2006; Vecchi and Soden, 2007; Gastineau et al., 2009; Bony et al., 2013; Shepherd, 2014; Kociuba and Power, 2015]. The components of the tropical circulation, however, respond differently to the anthropogenic climate change. Though the tropics already exhibit expansion trends by up to 2° of latitude per decade [Davis and Birner, 2013], the ITCZ becomes narrower and more vigorous in a warmer climate, with Byrne and Schneider [2016] pointing out the strengthening of the meridional moist static energy gradient as the dominant mechanism for this

change. For the Hadley circulation, the CO₂ forcing may cause a weakening of the northern cell, but a strengthening of the southern cell [Ma and Xie, 2013]. At the same time, there is substantial evidence that both cells widen [Lu et al., 2008; Davis and Birner, 2013; Albern et al., 2018].

The Walker circulation will likely respond to the increased CO₂ concentration by weakening at a higher rate than the Hadley circulation [Vecchi and Soden, 2007]. Conversely, the observations of the past two decades have shown a strengthening of the Pacific Walker Cell, which is related, according to England et al. [2014] and McGregor et al. [2014], to the post-2000 global surface temperature hiatus and the increased subsurface ocean heat uptake (Fig. 1.1). Kociuba and Power [2015] found this variation (i.e. the recent strengthening of the Walker circulation) to be difficult to simulate by the state-of-the-art CMIP5 GCMs in coupled climate experiments with prescribed natural and anthropogenic forcings from observations in the last 150 years (the CMIP5 historical experiment; Taylor et al. [2012]). However, Ma and Zhou [2016] suggest in their study, based on non-coupled climate experiments with prescribed sea surface temperatures from observations (the AMIP experiment; Taylor et al. [2012]), that there is reasonably good performance in the simulation of the strengthened circulation by the CMIP5 models. This may relate to the insufficient understanding of the drivers of the Walker circulation and its internal variability. Therefore, there is a high degree of uncertainty in simulating the behaviour of the Walker circulation arising from this lack of understanding its dynamical mechanisms and from the model performance in representing the impact of external forcing of the factors determining the changes in the circulation.

The thermodynamical mechanism for the circulation weakening, according to Held and Soden [2006], consists of the imbalance between the increase in atmospheric moisture driven by the temperature rise and the slower precipitation rate change. Lu et al. [2008] show that the stronger increase in static stability compared to the increase in diabatic heating as a response to warming weakens the overturning circulation. Another discussed mechanism is the advection of dry air from the subsidence regions towards the strong convection regions, thus decreasing the horizontal extent of the convection, but increasing its vertical extent, as well as the vertical extent of the tropical troposphere [Chou et al., 2009; Chou and Chen, 2010]. Additionally, Ma et al. [2012] suggest that the cooling/warming of the convective/subsiding regions as a result of enhanced advection of vertical stratification causes the tropical circulation slowdown.

One would expect that both the increase in CO₂ itself and the subsequent climate system feedbacks, such as surface heating, play a role for the circulation slowdown, but their relative contributions are still unclear. Most recent studies show that the increase in surface temperature dominates and causes a decrease in the circulation intensity, by enhancing the atmospheric stability of the lower troposphere [Vecchi and Soden, 2007; He and Soden, 2015]. At the same

time, [Zelinka and Hartmann \[2010\]](#) and [Bony et al. \[2013\]](#) argue that even in the absence of surface temperature increase the tropical circulation will weaken if CO₂ concentration rises. This relates to the radiative effect of CO₂ on the atmospheric cooling rate, as the latter weakens and therefore reduces the vertical atmospheric motion. In addition, there is insufficient certainty on the circulation's natural variability [[Power and Kociuba, 2011b](#); [Kociuba and Power, 2015](#)], which may mask the CO₂ induced weakening. The regional aspects of climate change introduce further uncertainty: [Ma and Xie \[2013\]](#) argue that a large part of the intermodel spread in the tropical overturning circulation is driven by the patterns in sea surface temperature change; [Gaetani et al. \[2017\]](#) and [Li and Ting \[2017\]](#) suggest, on the example of the Asian and West African monsoons, that at regional scales the circulation actually strengthens under CO₂ forcing.

1.3 Motivation and research questions

The effects of the increasing CO₂ concentrations in the last two centuries have been investigated mostly from the point of view of thermodynamical response of the climate system [[Shepherd, 2014](#)]. This allows us to build an understanding of the expected changes in the global patterns of climate variables, but still leaves a wide margin for uncertainty in regional climate changes. The regional response to anthropogenic forcing is highly dependent on atmospheric circulation (global and regional), but GCMs have yet to provide a high confidence level in simulating and projecting these circulation changes [[Shepherd, 2014](#)].

Referring to the above mentioned mechanisms responsible for the response of the tropical circulation to anthropogenic CO₂ forcing, there are various sources of uncertainty, as well as sources for the intermodel spread of the response, that one needs to consider for an investigation, such as the ones depicted in [Fig. 1.2](#):

current understanding: the climate system is a coupled atmosphere-ocean system. The changes in the atmospheric dynamics need to also account for the ocean dynamics. At the moment, the processes in the ocean are still less understood than the atmospheric processes and this impacts the performance of the GCMs and the confidence in the detected changes;

drivers of the circulation: the proper representation of these drivers in the GCMs (e.g. temperature gradients, land-ocean contrast, seasonal, interannual, decadal variability modes) raises the confidence level in the detected variation;

drivers of change: the various mechanisms leading to the likely weakening of the tropical atmospheric circulation were mentioned above. However, these mechanisms do not act

individually and their impact differs in time and space. Therefore, a good understanding of their interaction is needed to assess the potential changes;

natural variability: the effect of the increased CO₂ is superimposed on the natural variability. The latter depends on external factors (e.g. solar cycle, obliquity, precession) and internal factors (seasonal cycles, variability modes at various time scales, volcanic activity). A good representation of this variability is thus needed to insure realistic simulations;

spatial scale: though thermodynamics dominate at the global scale, regional changes are highly sensitive to circulation changes [Shepherd, 2014];

the interaction between large- and small-scale processes: the small-scale processes, such as cloud or convective systems, go along with the large-scale circulations, but are much more variable in time and space, as well as a big source of uncertainty for the climate representation;

circulation intensity quantification: there are a multitude of metrics for the intensity of the tropical circulation, in general, and for its components, in particular. Besides presenting various facets of the circulation, each of the metrics is subject to the CO₂ impact on its base-parameter;

GCM configuration and parametrization schemes: though the intermodel spread within the General Circulation Models suite has a decreasing trend, we still find a large uncertainty in the detected changes. IPCC [2013] states that the largest uncertainty is likely to arise from the precipitation and cloud parametrizations.

In this work, I investigate two distinct aspects of the change in tropical atmospheric circulation, touching upon most of the uncertainty sources listed above.

In the first part of this thesis, I look into the robustness of the projected change of the Pacific Walker circulation in an idealized coupled climate experiment and the sensitivity of the findings to natural variability, GCM physics and quantification method. The research questions addressed here are:

- What is the most probable response of the Walker circulation to a gradual CO₂ increase?
- How robust is this response?
- Does the choice of metric for the Walker circulation intensity matter?
- What are the reasons for the intermodel spread?
- How does the detected change compare to the natural variability of the circulation?

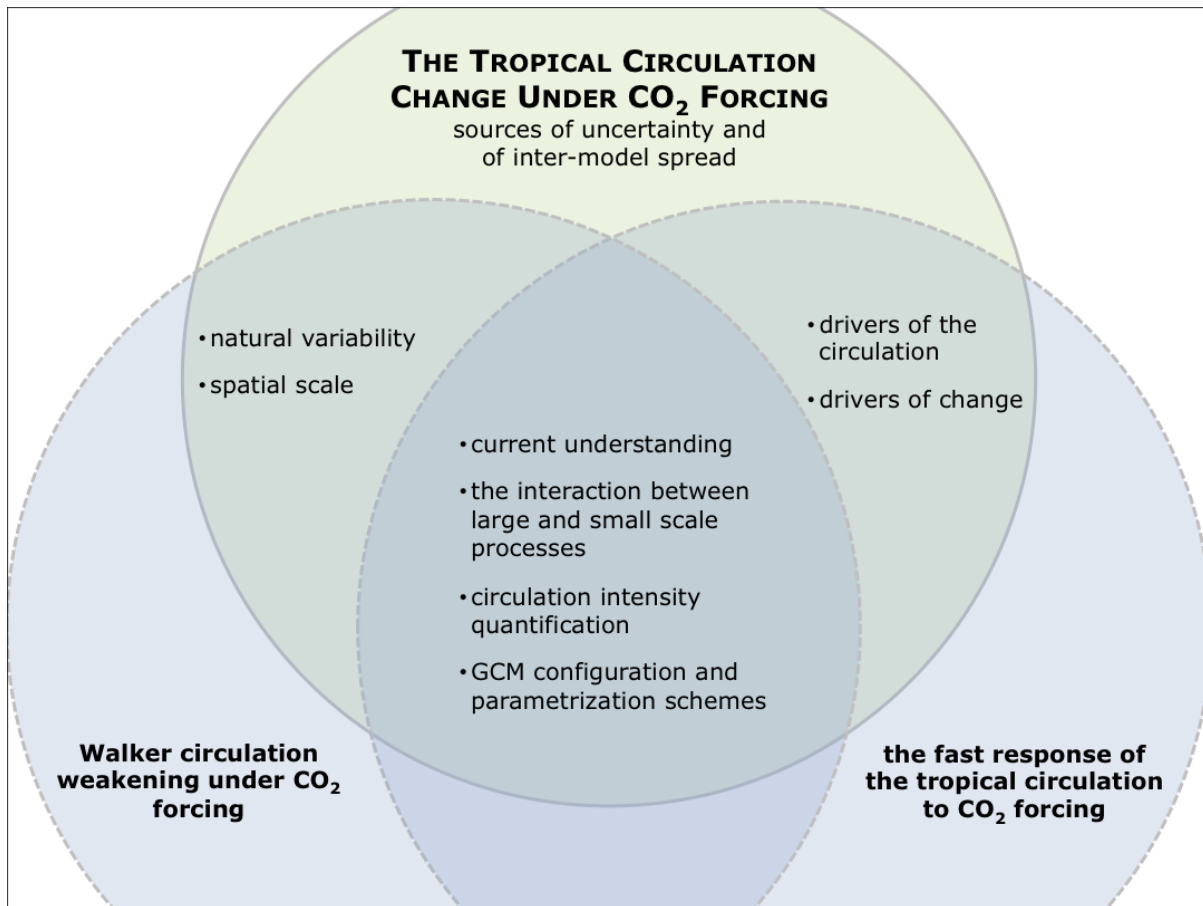


Figure 1.2: Sources of uncertainty and of intermodel spread in the assessment of the change in tropical circulation under anthropogenic CO₂ forcing investigated in this work.

In the second part, the direct role of CO₂ forcing on the tropical circulation is assessed using a series of simple idealized climate experiments. This relates to the fast response of the circulation to the forcing, as opposed to the slow response that is shaped not only by the change in CO₂ concentrations, but also by the subsequent climate feedbacks, such as the surface temperature increase or the atmospheric moisture content increase. The following research questions guide this part of the work:

- How does the tropical circulation change as response to the CO₂ forcing, but with no surface temperature adjustment?
- What are the relative contributions of the change in radiative heating rate and in static stability to the total change in circulation intensity?
- How does the effect of land-sea contrast on the circulation change compare to the CO₂ impact?
- Is the fast response detectable in the coupled experiments?

1.4 Research approach

Taking into account the sources of uncertainty and intermodel spread noted in the previous Section, the analysis setup for both parts of this work aims to address several sources each (Fig. 1.2).

First, I look into the variation of the Walker circulation in a CMIP5 idealized transient climate simulation (Chapter 3), which describes a climate state close to present conditions. In particular, I investigate the robustness of the weakening of the circulation in a CMIP5 transient climate experiment, namely the benchmark 1% per year increase in CO₂ concentration (from pre-industrial levels to quadrupling of concentration), referred to henceforth by its CMIP5 label 1pctCO2. The novelty of my approach is that I consider not only the GCM configuration and the initial conditions for the experiment as uncertainty sources, but also the method used to quantify the intensity of the Walker circulation. In other words, I inspect the detected circulation response from three distinct perspectives: the internal variability, the GCM configuration and the indexing method.

The influence of internal variability on the detection of a weakening Walker circulation will be deduced from the outputs of a 68-member ensemble of the MPI-ESM-LR model [Stevens et al., 2013]. The members of this ensemble differ only in initial conditions: the initial climate state for each member is derived from distinct time windows of the control run of this model.

The second ensemble used in this work comprises 28 CMIP5 GCMs (one realization each). The initial conditions for the 1pctCO2 outputs differ as in the case of the MPI ensemble, because each experiment is run from a mean control state subject to the model physics. But this ensemble also includes a signal of the differences between the model configurations and parametrization schemes. As mentioned in Bony et al. [2013] and Shepherd [2014], the simulation of the dynamical aspect of climate change is quite dependent on the interaction between the simulations of large-scale systems and small-scale processes. Under this consideration, I analyze the outputs of this ensemble from the aspect of the non-linear effects caused by the model configuration in addition to the effect of natural variability.

The third investigated factor is the indexing method applied for quantifying the intensity of the Pacific Walker Cell. The need to include this factor arises from the fact that most studies rely on a single indexing method to describe the intensity of the circulation (e.g. Wang [2002], Tanaka et al. [2004], Vecchi et al. [2006], Bayr et al. [2014]). Consequently, additional spread in the projected responses of the Pacific Walker Cell may be caused by the internal variability and the response of the index's base parameter to increased CO₂ forcing (see Chapter 12 in IPCC

[2013]). My analysis provides a comparative view on three simple, widely-used indices and the circulation response differences that arise from their application:

- The first index relates to the main driver of the Pacific Walker Cell, which is the temperature gradient between the East and West Pacific. This gradient is accompanied by a pressure gradient across the Pacific. Under these considerations, this perhaps most intuitive index for the Pacific Walker Circulation is based on the mean sea-level pressure (MSLP) difference between the East and West equatorial Pacific [Vecchi et al., 2006]. This index will be referred to as MSLP-index.
- The second index reflects the dynamics of the cell: the ω_{500} -index is derived from the 500 hPa vertical velocity anomaly difference between the East and West equatorial Pacific [Wang, 2002].
- The third index was introduced by Tanaka et al. [2004] as a characteristic of the circulation in the upper troposphere. It is based on the annual deviation from the zonal mean of the 200 hPa velocity potential, and will be referred to as the χ_{200} -index.

As mentioned above, the response of the index's base parameter to increasing forcing may induce additional uncertainty in the Walker circulation projection. The three indices investigated in this paper are based on parameters highly sensitive to regional cloud and precipitation pattern changes (e.g. surface pressure) and thus are subject to the uncertainty of cloud and precipitation representation in GCMs [Held and Soden, 2006; Power and Kociuba, 2011a,b; Bony et al., 2013]. I acknowledge that there are other indices quantifying the circulation intensity from anomalies extending over several atmospheric layers (e.g. based on the zonal mass stream function, see Yu and Zwiers [2010]). Nonetheless, I chose these three simple, all quasi-surface indices, as their derivations are comparable and each of them reflects the circulation at different levels in the atmosphere. This will further allow me to look into the sensitivity of the Walker circulation response to the representation of various processes within the Walker Cell.

The time series of the three indices are derived for the two ensembles mentioned above. Following this derivation, index-based differences between trends in the Pacific Walker Cell intensity are analyzed, as well as the correlation of the indices. Models will be grouped depending on their Walker circulation response, attempting to reveal possible sources of uncertainty and inconsistency between GCMs. I start from the premise that differences among models may also be detected in the patterns of parameters whose response to climate change is robust among the CMIP5 models, such as global mean surface temperature increase and mean outgoing longwave radiation decrease over the tropical Pacific (see Chapter 12 in IPCC [2013]).

In the second part of this work (Chapter 4), I develop a metric for the circulation intensity that allows the quantification of this CO₂ radiative effect on the total change in tropical circulation, while investigating the fast response of the tropical overturning circulation to climate change, i.e. the direct effect of CO₂ increase on the circulation. It is common to investigate the tropical overturning circulation through the prism of both the convective and the subsiding regions in the atmosphere. Most metrics for the intensity of the circulation are based on the dynamics in the convective regions, on the difference between the convecting and subsiding regions for a certain parameter (e.g. vertical velocity), and/or on the tropical precipitation patterns (e.g. [Bony et al. \[2013\]](#); [Ma and Xie \[2013\]](#); [He and Soden \[2015\]](#)). However, [Rybka and Tost \[2014\]](#), [Shepherd \[2014\]](#), [Su et al. \[2014\]](#), and [Merlis \[2015\]](#) suggest that the cloud, precipitation and convection parametrizations cause most of the uncertainty in the GCM simulation of atmospheric circulation. The metric introduced here considers the vertical pressure velocity ω in the tropical subsidence regions, and, therefore, reduces the impact of this uncertainty (i.e. induced by the cloud and precipitation parametrizations) on my results. My metric gives the opportunity to decompose the relative change in circulation into a sum of relative changes in atmospheric cooling rate, stratification and subsidence area. This decomposition allows me to quantify the fast response of the circulation to CO₂ increase, as well as to determine the main drivers of this response. This allows for a better understanding of the mechanisms affecting this change.

Another process to be considered when analyzing atmospheric circulation is the differential heating of land and ocean surfaces, which acts as additional forcing both at regional and global scales. To account for this, I study first the simple idealized case of the aqua planets, without axial tilting, therefore no seasons and zonal asymmetries [[Medeiros et al., 2015](#)]. Then I compare these results to the results obtained from AMIP (Atmospheric Model Intercomparison Project, see [Taylor et al. \[2012\]](#)) experiments. These experiments are set up on an Earth-like planet, but the climate system is limited to the atmosphere only, with sea surface temperature and sea ice being prescribed to modern patterns. To put my findings in the context of a coupled climate system, I carry out a brief similar investigation on the CMIP5 idealized coupled climate experiment with an abrupt CO₂ quadrupling from pre-industrial levels.

This study setup helps to quantify and decompose the fast response of the tropical atmospheric circulation into the contributions of radiative cooling rate change and atmospheric stratification change. By comparing the aqua planet and Earth-like planet results, I address the question whether the fast response of the circulation is dominated by the land-sea differential heating. The results presented here are based on an ensemble of eight CMIP5 GCMs participating in both the aqua-planet and AMIP experiments.

1.5 Outline

The results of this thesis are presented as follows:

Chapter 2 contains the description of the datasets used in this thesis, as well as that of the CMIP5 idealized climate experiments and of the ERA-Interim reanalysis;

Chapter 3 firstly presents the Walker circulation indices (Section 3.1). Then I discuss the Walker circulation variation in ERA-Interim (Section 3.2), in the MPI-ESM-LR ensemble (Section 3.3), and in the CMIP5 ensemble (Section 3.4). Section 3.5 analyses the intermodel differences and the potential reasons for the intermodel spread;

Chapter 4 describes the new method for the quantification of the tropical circulation intensity in Section 4.1; the circulation change and its drivers are discussed for the aqua-planet experiments in Section 4.2, for the AMIP experiment in Section 4.3. Section 4.4 presents a brief analysis of the change in circulation variability. Section 4.5 puts the previous results in the perspective of the coupled climate experiments.

Chapter 5 summarizes the main conclusions of the thesis and presents a brief outlook for the findings.

Note: This thesis contains excerpts from the following two publications:

1. Plesca, E., Grützun, V., and Buehler, S. A. (2018). How robust is the weakening of the Pacific Walker circulation in CMIP5 idealized transient climate simulations? *Journal of Climate*, **31**(1): 81–97
2. Plesca, E., Buehler, S. A., Grützun, V. (2018, in review). The fast response of the tropical circulation to CO₂ forcing. Submitted to *Journal of Climate*

2 Data

2.1 The CMIP5 experiments

This work is based on the intercomparison of results from 28 General Circulation Models (GCMs) participating in the Coupled Model Intercomparison Project Phase 5 (CMIP5). The CMIP5 experiments provide a wide range of climate system setups that allow the assessment of various drivers of change, anthropogenic, as well as natural [Taylor et al., 2012]. In accordance with the research approach described in Section 1.4, a distinct set of experiments will be used for each of the two main parts of this thesis. The list of experiments from the CMIP5 framework relevant to this work is presented below (the first two will be investigated in Chapter 3, the rest in Chapter 4):

piControl multicentury pre-industrial control experiment, the climate system is considered to be in quasi-equilibrium, with unforced variability;

1pctCO2 idealized experiment with 1% per year increase in CO₂ concentration relative to mean pre-industrial levels, run until quadrupling of concentration (140 years);

historical coupled climate experiment forced by observed atmospheric concentrations (of natural and anthropogenic origin), with time-evolving land cover. This experiment is used here mostly as a source of mean surface temperature patterns, as well as mean concentration of atmospheric absorption species;

aquaControl aqua-planet idealized control experiment [Taylor et al., 2012; Medeiros et al., 2015]. The aqua planet is an idealized Earth-size planet covered by water, with no axial tilting, and an uncoupled climate system. The radiation scheme uses the mean concentrations of the absorption species from the historical experiment for the 1979–2008 period;

aqua4xCO2 aqua-planet idealized experiment set up based on aquaControl, but with sudden CO₂ concentration quadrupling from aquaControl. The surface temperature is prescribed to the aquaControl mean. Therefore, the climate system response in aqua4xCO2 represents the effect of the increase in CO₂, and is not subject to the change in surface processes resulting from increased surface temperature;

amip uncoupled amip control experiment (from AMIP – Atmospheric Model Intercomparison Project). This experiment is set up similarly to aquaControl, but this time an Earth-like planet is considered. In the amip experiment the atmospheric composition follows the 1979–2008 mean historical values, and sea surface temperature and sea ice are prescribed to the 1979–2008 historical values;

amip4xCO2 amip idealized experiment, with the CO₂ concentration abruptly quadrupled compared to the amip values. The sea surface temperature is held fixed to the amip values, but the land is allowed to heat;

aqua4K aqua-planet experiment with atmospheric composition kept to aquaControl values, but the surface temperature is abruptly increased by 4 K;

amip4K amip experiment with atmospheric composition kept to amip values, but the surface temperature is abruptly increased by 4 K;

abrupt4xCO2 idealized coupled experiment with an abrupt quadrupling in CO₂ concentration from piControl mean values. Though an equilibrium climate state is not yet reached, most outputs for this experiment are limited to 140 years.

For the investigation of the change in Walker circulation intensity I use monthly mean outputs of two GCM ensembles for the piControl and 1pctCO2 experiments. The first ensemble consists of 68 members resulting from running the MPI-ESM-LR model [Giorgetta et al., 2013; Stevens et al., 2013] for 1pctCO2 with slightly perturbed initial climate state at each run, derived from different time windows in piControl (referred to onward as the MPI ensemble). The second ensemble comprises monthly outputs for the CMIP5 1pctCO2 experiment from 28 GCMs listed in Tab. 2.1 (referred to as CMIP5 ensemble). The version of the MPI-ESM-LR model applied for obtaining the MPI ensemble is different from the model version in the CMIP5 ensemble, therefore differences in values and responses are to be expected.

For consistency reasons, the GCM ensemble analyzed for the assessment of the fast response of the tropical circulation to CO₂ is limited to 8 models that had been run for the aqua-planet experiments, marked in Tab. 2.1. The length of the time series for both aqua-planet experiments is 5 years, for the amip experiments it is 30 years. Throughout the study I will compare the mean control climate state (referred onward as aquaControl/amip or control climate) to the quasi-equilibrium reached by the climate system after the sudden change in CO₂ forcing occurs (referred onward as aqua4xCO2/amip4xCO2 or forced climate).

In both parts of the research for every CMIP5 GCM one realization of the model was considered, namely the r1i1p1 realization [Taylor et al., 2012].

The CMIP5 data were accessed through the German Climate Computing Centre (DKRZ) ESGF-CoG node.

Table 2.1: Details of the CMIP5 General Circulation Models

Model	Horizontal grid (lat×lon)	TCR _{TP} [K]	Aqua-planet	Institute	Reference
ACCESS1-3	145×192	1.669		Commonwealth Scientific and Industrial Research Organisation and Bureau of Meteorology, Australia	Bi et al. [2013]
BCC-CSM1-1	64×128	1.284		Beijing Climate Center, China	Wu et al. [2014]
BCC-CSM1-1-M	160×320	1.551		Meteorological Administration	Wu et al. [2014]
CanESM2	64×128	1.835		Canadian Centre for Climate Modelling and Analysis	Arora et al. [2011]
CCSM4	192×288	1.350	+	National Center for Atmospheric Research, USA	Meehl et al. [2012]
CESM1-BGC	192×288	1.367		Community Earth System Model Contributors, USA	Long et al. [2013]
CMCC-CM	240×480	2.106		Centro Euro-Mediterraneo per i Cambiamenti Climatici, Italy	Scoccimarro et al. [2011]
CNRM-CM5	128×256	1.644	+	Centre National de Recherches Meteorologiques, Meteo-France	Voldoire et al. [2013]
CNRM-CM5-2	128×256	1.532			Voldoire et al. [2013]
CSIRO-Mk3-6-0	96×192	1.602		Commonwealth Scientific and Industrial Research Organisation and Queensland Climate Change Centre of Excellence, Australia	Rotstayn et al. [2012]
FGOALS-g2	60×128	1.408		Institute of Atmospheric Physics, Chinese Academy of Sciences, and Tsinghua University, China	Li et al. [2013]
FGOALS-s2	108×128	1.682			Bao et al. [2013]
GFDL-CM3	90×144	1.892		NOAA Geophysical Fluid Dynamics Laboratory, USA	Donner et al. [2011]
GFDL-ESM2G	90×144	1.303			Dunne et al. [2012]
GFDL-ESM2M	90×144	1.336			Dunne et al. [2012]
GISS-E2-H	90×144	1.569		NASA Goddard Institute for Space Studies, USA	Schmidt et al. [2014]
HadGEM2-ES	145×192	2.127	+	Met Office Hadley Centre, UK	Collins et al. [2011]
INMCM4	120×180	1.095		Institute for Numerical Mathematics, Russia	Volodin et al. [2010]
IPSL-CM5A-LR	96×96	2.032	+	Institute Pierre Simon Laplace, France	Dufresne et al. [2013]
IPSL-CM5A-MR	143×144	2.056			Dufresne et al. [2013]
IPSL-CM5B-LR	96×96	1.413			Hourdin et al. [2013]
MIROC-ESM	64×128	1.844	+	Japan Agency for Marine-Earth Science and Technology, Atmosphere and Ocean Research Institute (University of Tokyo), and National Institute for Environmental Studies	Watanabe et al. [2011]
MIROC5	128×256	1.388			Watanabe et al. [2010]
MPI-ESM-LR	96×192	1.843 (1.547 ± 0.080)	+	Max Planck Institute for Meteorology, Germany	Stevens et al. [2013]
MPI-ESM-MR	96×192	1.971	+		Giorgetta et al. [2013]
MRI-CGCM3	160×360	1.392	+	Meteorological Research Institute, Japan	Yukimoto et al. [2012]
NorESM1-M	96×144	1.108		Norwegian Climate Centre	Bentsen et al. [2013]
NorESM1-ME	96×144	1.186			Bentsen et al. [2013]

2.2 The ERA-Interim reanalysis

ERA-Interim is a global atmospheric reanalysis dataset produced by the European Centre for Medium-Range Weather Forecasts (ECMWF) [Dee et al., 2011]. The dataset covers the period from 1979 until present and is updated every month. In the framework of my research questions and considering that the climate experiments I analyse are idealized, I use the ERA-Interim 1979–2014 monthly means as a 'reality check' of my results. I acknowledge that this dataset is subject to the biases of the ECMWF Integrated Forecasting System (IFS), version IFS (Cy31r2)

from 2006 and cannot be treated as the true state of the climate, but nonetheless represents a reliable reference dataset. The spatial resolution of the dataset used here is $0.75^\circ \times 0.75^\circ$ on 60 vertical levels from the surface up to 0.1 hPa.

2.3 The ENSO index dataset

The tropical circulation, in general, and the Pacific Walker circulation, in particular, are strongly modulated by the El Niño Southern Circulation (ENSO). For comparison between the ENSO phase and the variation of the circulation, I use the Ocean Niño Index (ONI). This index represents a 3-month running mean SST anomaly in the Niño 3.4 region (5°S - 5°N , 120° - 170°W), according to the ERSST.v5 SST dataset. ONI takes into account the rapid surface temperature increase since 1950 and calculates the sea surface anomalies with reference to their contemporary climatology [\[NOAA CPC, 2018\]](#).

3 The change of Walker circulation under CO₂ forcing

In this Chapter I present the analysis of the time series for the Pacific Walker circulation indices. The indices are described in Section 3.1. Further, I discuss separately the results for ERA-Interim (Section 3.2), the MPI ensemble (Section 3.3), those for the CMIP5 ensemble (Section 3.4) and look into ensemble members' differences that relate to the detected ensemble spread (Section 3.5).

3.1 Walker circulation indices

Three indices for the intensity of the Pacific Walker Cell are compared in this work. The first index relates to the main driver of the Walker circulation - the temperature gradient across the tropical Pacific, which may also be derived from the pressure gradient. The MSLP-index is computed following Vecchi et al. [2006], and is equal to the difference between the MSLP anomaly (deviation from the mean MSLP for the experiment time range – 140 years that corresponds to the moment of CO₂ quadrupling) averaged over two spatial boxes as shown in Fig. 3.1a: the East equatorial Pacific box (160°W-80°W, 5°S-5°N) and the West equatorial Pacific box (80°E-160°E, 5°S-5°N).

The second index, named ω_{500} -index, looks into the vertical motion in the ascending and subsiding branches of the Pacific Walker Cell. It is derived from the mean 500 hPa vertical velocity anomaly (deviation from the mean 500 hPa vertical velocity for the experiment time range – 140 years that corresponds to the moment of CO₂ quadrupling) difference between the East equatorial Pacific (160°W-120°W, 5°S-5°N) and the West equatorial Pacific (120°E-160°E, 5°S-5°N), as described in Wang [2002] (Fig. 3.1b).

The third method of indexing the Walker circulation is based on the decomposition of the 200 hPa velocity potential field in three orthogonal spatial patterns - zonal, time mean eddy, and transient eddy components, each describing the Hadley, Walker, and monsoon circulations, respectively [Tanaka et al., 2004]. Following this method, the 200 hPa vertical velocity zonal mean, describing the intensity of the meridional flow and the Hadley circulation, is removed from the time series. Afterwards, the χ_{200} -index of the Walker circulation is defined as the maximum value over the West Pacific in the 12-month running mean field of this deviation

from the zonal mean (Fig. 3.1c). The definition of the index provides an indication of the approximate geographical position for the ascending branch of the cell in addition to the intensity quantification.

Note that the reference boxes for the MSLP-index and ω_{500} -index differ (Fig. 3.1a and 3.1b), and the reference grid point for the χ_{200} -index varies between time steps. Also, because for the χ_{200} -index the seasonality of the index is removed by applying a 12-month running mean, I apply the same averaging method to the time series of the MSLP-index and the ω_{500} -index to ensure equivalent comparison.

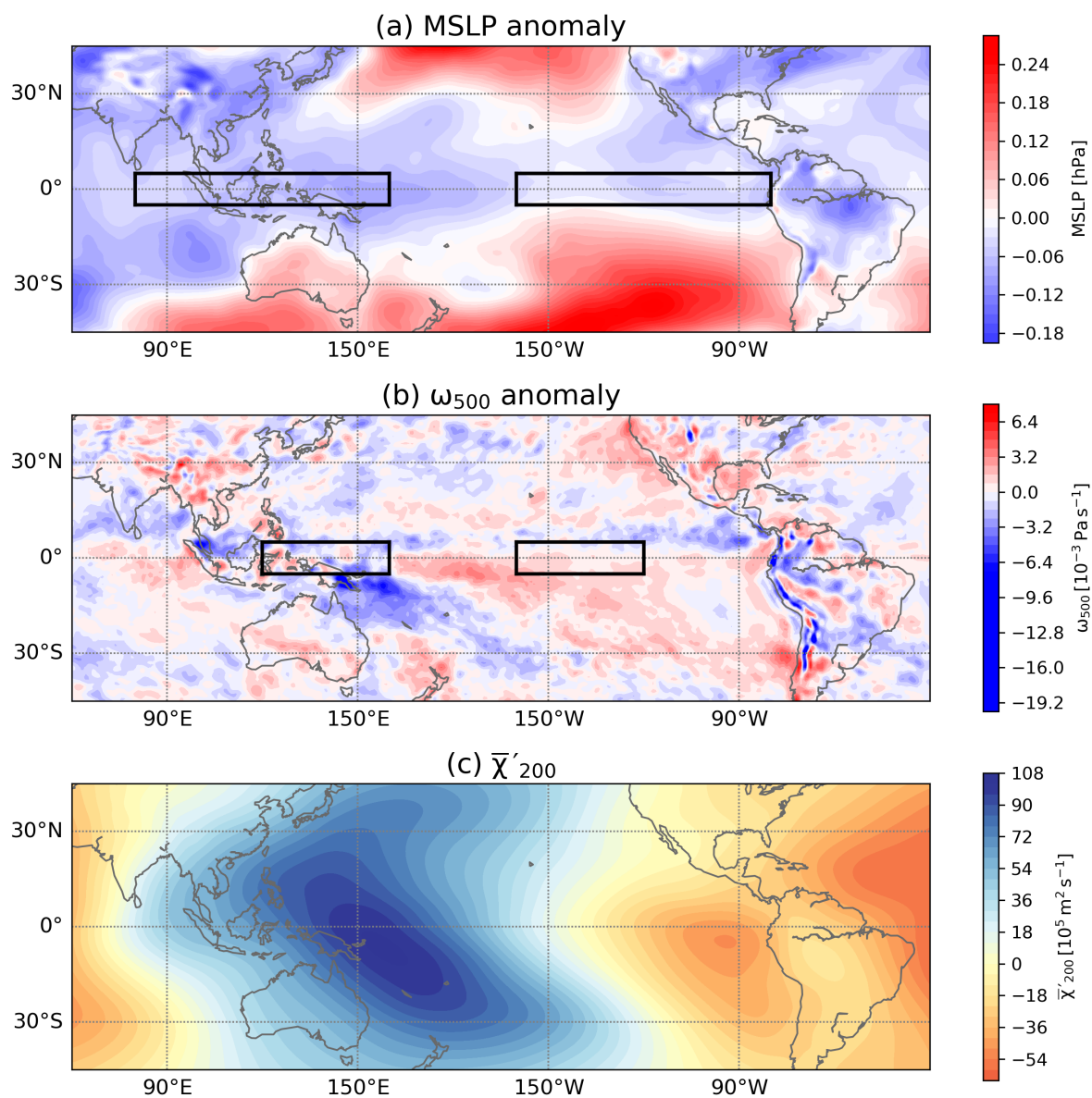


Figure 3.1: ERA-Interim reanalysis 1979–2008 mean fields for the parameters used to derive (a) the MSLP-index, (b) the ω_{500} -index, and (c) the χ_{200} -index. The Western and Eastern Pacific boxes used for the first two indices are marked in (a) and (b).

To investigate the relationship between the change in the Walker circulation and the mean surface temperature change, I look into transient climate response (TCR), which was first introduced by Cubasch et al. [2001] as the mean global surface temperature change ΔT by the time of CO₂ doubling under a scenario equivalent to the 1pctCO₂ experiment. TCR is usually applied to characterize the mean climate state in a transient climate, being different from equilibrium climate sensitivity (ECS), which reflects the changes of the system after equilibrium is reached [Gregory and Forster, 2008]. TCR is most commonly calculated as the mean global ΔT for years 61-80 of the 1pctCO₂ output, after the control run mean global temperature is removed. Gregory and Forster [2008] introduce a new method for TCR calculation, from the radiative forcing at the time of CO₂ doubling and the climate resistance parameter, thus removing the need to use the control runs of the models. By deriving TCR with both methods, as well as with linear regression of the time series, I find that the difference between TCR derived with the Gregory and Forster [2008] method and with linear regression is of the order of 10^{-3} K for the MPI ensemble and of the order of 10^{-2} K for the CMIP5 ensemble. The difference between these methods and the first method is of the order of 10^{-1} K for both ensembles. Considering that the method introduced by Gregory and Forster [2008] accounts for the gradual increase in forcing and for the climate system resistance to the changes induced by this forcing, I will consider this as reference method for the calculation of TCR.

However, the comparison of global TCR to Walker circulation changes introduces additional uncertainty to answering the research questions, as global TCR is also subject to variations in the subtropical and polar regions' circulation. Consequently, in the framework of this thesis, I define the tropical Pacific transient climate response (TCR_{TP}) equal to ΔT in the region within the (80°E-80°W, 30°S-30°N) box by the time of CO₂ doubling. This box covers all regions used in the derivation of the Walker circulation indices. At the same time, TCR_{TP} cannot be derived directly by using the Gregory and Forster [2008] method, since that method relies on global averages. To simplify the calculation of TCR_{TP}, I use the linear regression method (Tab. 2.1). This is justified by the small difference between this and the Gregory and Forster [2008] methods.

3.2 The simulation of the Walker circulation in ERA-Interim

The ERA-Interim mean value of the MSLP-, ω_{500} - and χ_{200} -index is 4.099 ± 83.576 Pa, $(0.299 \pm 18.853) \times 10^{-3}$ Pa s⁻¹ and $(108.764 \pm 10.012) \times 10^5$ m²s⁻¹, respectively (Tab. 3.1). Fig. 3.2 shows the time series of these indices, which visually explain the high variance detected above. It is also evident that the Walker circulation is directly linked to ENSO, as the periods of extremely weak Walker Cell coincide with the extreme El Niño events (e.g. 1983–1984,

1997–1998). It is remarkable that the MSLP and the ω_{500} indices' minima precede the El Niño minima by 4–5 months, while the χ_{200} -index minima practically coincide with the El Niño events. Therefore, the changes in the circulation in the lower and mid troposphere change the east to west wind stress regime over the equatorial Pacific and amplify the sea surface anomaly, while the upper troposphere is directly sensitive to the changes in the boundary layer.

I also acknowledge that the definitions of the MSLP- and ω_{500} -indices suggest the time mean of these indices should tend to zero. However, the choice of the spatial boxes used to derive the mean anomalies in the convection and subsidence branches of the Walker Cell can explain the non-null values. The western boxes used in the derivation of the indices include considerable land mass, especially the MSLP-index (Fig. 3.1). Therefore, in comparison with the eastern box, the western anomalies will also arise from the effect of land-sea contrast. Another reason for a non-null mean value could be related to the difference between the convection and subsidence areas – the former is more aggregated than the latter and the eastern box may not contain the entire subsidence area related to the Pacific Walker Cell. Despite this feature of the index definition, I consider the ERA-Interim indices' time series a reliable reference dataset, comparable with values obtained in previous studies for time series of observation and/or reanalysis datasets [Wang, 2002; Tanaka et al., 2004; Vecchi et al., 2006].

Table 3.1: Statistical results for the ERA-Interim reanalysis dataset

	ERA-Interim
MSLP-index ^a [Pa]	4.099 ± 83.576
ω_{500} -index ^a [10 ⁻³ Pa s ⁻¹]	0.299 ± 18.853
χ_{200} -index ^a [10 ⁵ m ² s ⁻¹]	108.764 ± 10.012
<i>all months in the Walker circulation index time series</i>	
corr(MSLP-index, ω_{500} -index) ^b	0.753
corr(MSLP-index, χ_{200} -index) ^b	0.427
corr(ω_{500} -index, χ_{200} -index) ^b	0.613
<i>months in the Walker circulation index time series with extreme circulation intensity</i>	
corr(MSLP-index, ω_{500} -index) _{extr} ^b	0.884
corr(MSLP-index, χ_{200} -index) _{extr} ^b	-0.400
corr(ω_{500} -index, χ_{200} -index) _{extr} ^b	-0.110

^a For each index, I calculate the mean of its time series and the standard deviation of its detrended time series. The table presents the averages of these values and their variance within the dataset.

^b $corr(x,y)$ - Pearson correlation coefficient between x and y .

As mentioned above, the three indices describe a distinct feature of the Pacific Walker Cell each, are subject to thermodynamical and circulation processes at different levels in the atmosphere, and are built on different basis variables and geographical regions. Tab. 3.1 gives

time series statistics, including trend and correlation coefficient statistics, for the reanalysis and the investigated indices. The reanalysis dataset reveals a fairly good correlation between the MSLP- and the ω_{500} -index (0.753), as well as between the ω_{500} - and the χ_{200} -index (0.613), but quite low between the MSLP- and the χ_{200} -index (0.427). Here I consider again the relation between ENSO and the Walker circulation – El Niño events relate to weakened circulation. The La Niña events are consistent with a strengthened Pacific Walker Cell (Fig. 3.2), but the index deviation from the mean in these periods is significantly smaller than in the El Niño periods [Tanaka et al., 2004]. I therefore correlate the months with circulation intensity outside 1σ from the mean of the time series for all three indices (hereafter named extreme cases). It is found that all the identified extreme cases relate to a strongly weakened circulation. While the correlation coefficient between the MSLP- and ω_{500} - indices becomes larger, it becomes negative and considerably smaller for the correlations between the χ_{200} -index and these two indices, respectively. This results from the latter reaching a minimum of intensity 4-5 months later than the first two indices (Fig. 3.2), suggesting a slower response of the upper troposphere to a weaker circulation. Considering the differences between indices' definitions and the medium to high correlation between the time series, the correlation results for the ERA-Interim time series are deemed realistic.

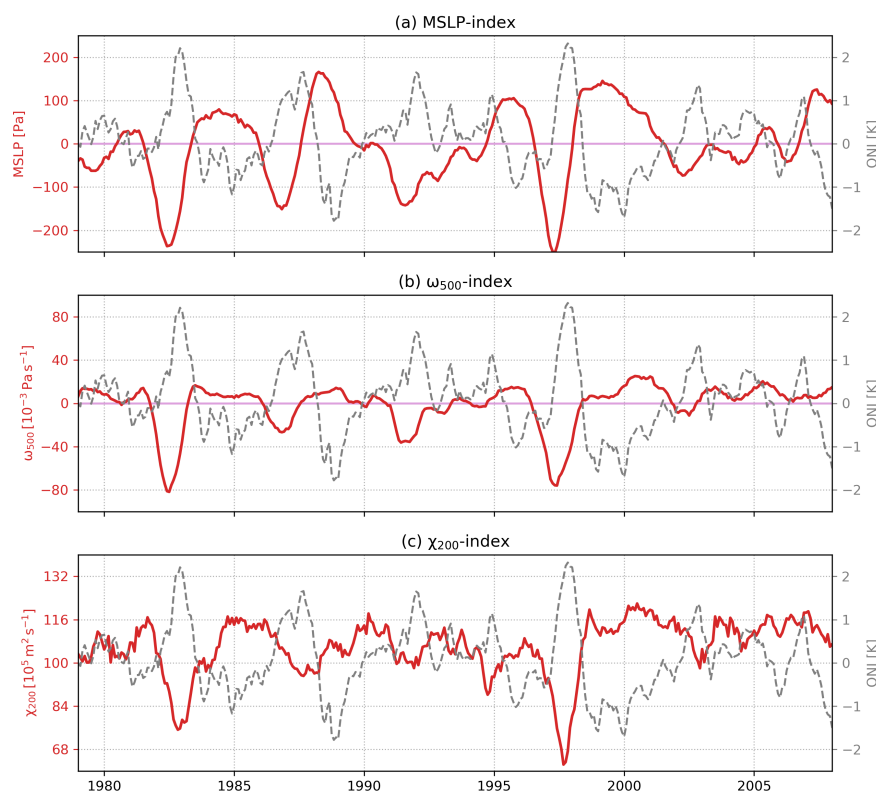


Figure 3.2: ERA-Interim reanalysis 1979–2008 time series for (a) the MSLP-index, (b) the ω_{500} -index, and (c) the χ_{200} -index. In every plot the ONI-index is presented in *dashed line*, with values on the second y-axis.

3.3 The natural variability signal in the Walker circulation change

As stated above, the purpose of using the MPI ensemble is to study the impact of natural variability on the Walker circulation trend. Averaging over the 68-members of the MPI ensemble, the mean value over the time series of the MSLP-, ω_{500} - and χ_{200} -index is -0.038 ± 0.398 Pa, $(0.019 \pm 0.049) \times 10^{-3}$ Pa s $^{-1}$ and $(134.213 \pm 0.869) \times 10^5$ m 2 s $^{-1}$, respectively (Tab. 3.2). These mean values differ from the ERA-Interim mean values, but the high variance within the reanalysis still places them within 1σ (standard deviation) from the mean for the first two indices and around 2σ from the mean for the χ_{200} -index. The ERA-Interim mean value shows a stronger Walker circulation in comparison to the MPI ensemble mean if the MSLP- and ω_{500} - indices are applied, but slower if the χ_{200} -index is applied. Here I acknowledge that these differences arise from (1) the setup of the CMIP5 1pctCO2 experiment as an idealized climate experiment, (2) the distinct configuration of the ECMWF IFS model on which the ERA-Interim reanalysis is based (compared to the configuration of the MPI-ESM-LR model), (3) the different time extent for the averaging, which takes into account more internal variability modes for the CMIP5 experiment than for ERA-Interim, and (4) the fact that ERA-Interim relies on a period which was shown to have a strengthened Walker circulation [England et al., 2014].

Table 3.2: Statistical results for the MPI ensemble

	MPI ensemble	
	mean	σ
MSLP-index ^a [Pa]	-0.038 ± 0.398	75.542 ± 6.787
ω_{500} -index ^a [10^{-3} Pa s $^{-1}$]	0.019 ± 0.049	9.574 ± 0.945
χ_{200} -index ^a [10^5 m 2 s $^{-1}$]	134.213 ± 0.869	10.019 ± 0.739
<i>all months in the Walker circulation index time series</i>		
corr(MSLP-index, ω_{500} -index) ^b	-0.435 ± 0.136	
corr(MSLP-index, χ_{200} -index) ^b	0.398 ± 0.062	
corr(ω_{500} -index, χ_{200} -index) ^b	0.256 ± 0.084	
<i>months in the Walker circulation index time series with extreme circulation intensity</i>		
corr(MSLP-index, ω_{500} -index) _{extr} ^b	-0.214 ± 0.359	
corr(MSLP-index, χ_{200} -index) _{extr} ^b	0.574 ± 0.213	
corr(ω_{500} -index, χ_{200} -index) _{extr} ^b	0.299 ± 0.221	
<i>variations of parameters until CO$_2$ doubling</i>		
MSLP-index trend [Pa dec $^{-1}$]	-1.553 ± 0.398	
ω_{500} -index trend [10^{-3} Pa s $^{-1}$ dec $^{-1}$]	-0.725 ± 0.753	
χ_{200} -index trend [10^5 m 2 s $^{-1}$ dec $^{-1}$]	-1.113 ± 0.592	

^a For each index and each ensemble member, I calculate the mean of its time series (140-years period, which corresponds to CO $_2$ quadrupling), and the standard deviation of its detrended time series. The table presents the averages of these values and their variance within the ensemble.

^b $corr(x,y)$ - Pearson correlation coefficient between x and y .

The correlation within the MPI-ensemble, interestingly, is inconsistent with the reanalysis, showing not only smaller correlation coefficients, but also negative correlation between the MSLP- and the ω_{500} -index (Tab. 3.2). The latter may be caused by various factors, such as the definition of the indices, discrepancies between the surface pressure and vertical velocity response to circulation intensity change, the physical approximations and parametrization scheme of the MPI-ESM-LR. A thorough analysis of this feature is beyond the scope of this work, but may serve as a good test case for the performance of a GCM. Having the above-mentioned negative correlation in mind, I find that, while looking into the extreme cases for this ensemble, the MSLP- and the ω_{500} - indices are practically uncorrelated. While the mean ensemble correlation between the χ_{200} -index and the other two increases for the extreme cases, its variance also becomes larger. The reasons for such values stated for the ERA-Interim data set apply here as well, along with the fact that, for the MPI ensemble, the time lag between the minima in the χ_{200} -index and the other two indices' time series is around 7-8 months. The interesting fact that the correlation between different indexing methods is stronger in reanalysis than in GCM simulations was also noticed by Davis and Birner [2016], albeit for the Hadley circulation and the width of the tropical belt instead of the Walker circulation. The reason for this apparently general behaviour is unclear: it may be caused by insufficient precision in the GCM simulation of the circulation, but also might simply be due to the much higher resolution of the reanalysis.

The trends in the intensity of the Pacific Walker Cell were derived by applying time linear regression to the three indices' time series. The mean trends over the MPI ensemble, index-wise, until the moment of CO₂ doubling (70 years) and quadrupling (140 years), are shown in Tab. 3.2. On average, independent of the chosen index, the Walker circulation slows down by the time CO₂ doubles. Compared to the ensemble mean standard deviation of the indices, the trend suggests a decrease in the intensity of the cell by 2.1% σ , 7.6% σ and 11.1% σ per decade for the MSLP-, ω_{500} - and χ_{200} -index, respectively (Tab. 3.2). But the percentage of members simulating a weakening circulation varies among indices. Here I consider as significant the trends with $\geq 80\%$ confidence level and I observe the following for each of the indices' time series:

1. MSLP-index: 49 out of 68 ensemble members show significant trends, whereof 34 are negative (suggesting a weakening Walker circulation by the moment of CO₂ doubling);
2. ω_{500} -index: 59 out of 68 ensemble members show significant trends, whereof 54 are negative;
3. χ_{200} -index: 63 out of 68 ensemble members show significant trends, all negative.

These results suggest a degree of sensitivity of the circulation projection to surface processes, which induces additional variability for the indices. The lower troposphere branch of the Pacific Walker Cell is highly dependent on the thermodynamics and atmospheric circulation within the boundary layer, and is also influenced by the atmosphere-ocean coupling. The MSLP-index, which is characterising the intensity of this section of the cell, shows the lowest percentage of significant trends (72%) and the lowest percentage of ensemble members projecting a weakening circulation by the doubling of CO₂ (50% of all ensemble members and 69% of the ensemble members with significant trends). Conversely, in the case of the ω_{500} -index, which describes the change in the ascending branch of the cell and is less sensitive to surface processes, there are more ensemble members which have a significant trend (87%). Also, the probability of a weakening circulation is higher if this index is considered, as 79% of ensemble members project the weakening (92% of the ensemble members with significant trends). The upper troposphere is significantly more stable than its lower and middle parts and exhibits less variability on monthly scales. As a result, for the χ_{200} -index time series I find significant trends in 93% of the ensemble members and all these members suggest a weakening circulation. To conclude, the detection of trends in the intensity of the Walker circulation is affected by the sensitivity of the base parameter to surface processes, including the atmosphere-ocean coupling in the lower troposphere. Also, some of the variability may be a result of the index definition: while [Tanaka et al. \[2004\]](#) separate the Walker circulation from the Hadley and monsoon circulations, the other two indices might still contain significant variability modes originating from these circulations.

The most robust feature in the response of the climate system to increased CO₂ forcing is mean surface temperature rise. Previous studies show that the tropical overturning circulation is slower in a warmer climate [[Held and Soden, 2006](#); [Vecchi and Soden, 2007](#); [Bony et al., 2013](#); [Chadwick et al., 2013](#)]. In this regard, I examined the relationship between the change in the intensity of the Walker circulation and the change in mean surface temperature in the tropical Pacific region. Considering the above, negative correlation between the Walker circulation trend and surface temperature variation should be expected. The MPI ensemble tropical mean ΔT by CO₂ doubling, TCR_{TP}, is 1.547 K and has a low variance, as shown in [Tab. 3.2](#). The trends detected in the Walker circulation indices have considerably higher variance ([Tab. 3.2](#)), therefore high correlation between TCR_{TP} and the circulation changes across the ensemble is less probable, as seen in [Tab. 3.3](#). TCR_{TP} has the highest absolute correlation coefficient value with the MSLP-index trend, which is expected considering the dependence of the MSLP-index on surface temperature changes. The ω_{500} -index trend shows the highest variance within the MPI ensemble ([Tab. 3.2](#)), which may in turn explain the detected insignificant correlation coefficients. If only ensemble members with significant detected trends are considered, the correlation between the changes in the circulation and in the surface temperature slightly improves for the MSLP- and χ_{200} - indices, but this does not hold for the ω_{500} -index.

Table 3.3: MPI ensemble correlation between the change in Walker circulation on one side and TCR_{TP} and the OLR trend (until CO_2 doubling) on the other side (selected runs/GCMs refer to the runs/GCMs that show a significant trend in the Walker circulation intensity until CO_2 doubling)

	Correlation with TCR_{TP}		Correlation with OLR trend	
	all runs	selected runs	all runs	selected runs
MSLP-index	-0.774	-0.826	0.131	0.144
ω_{500} -index	0.152	0.150	-0.156	-0.179
χ_{200} -index	-0.534	-0.546	0.489	0.498

As mentioned in the definition of the χ_{200} -index, this method also provides an indication of the location of the ascending branch of the Cell. By analyzing the time series of the coordinates for the maximum value of χ_{200} , I find that 90% of the MPI ensemble members suggest an eastward shift of the ascending branch, consistent with previous findings [Bayr et al., 2014].

In conclusion of this Section, based on the MPI ensemble, I note that internal variability alone causes a significant spread in the response of the Pacific Walker circulation to increasing CO_2 forcing. The robustness of a weakening circulation is diminished by the differences between the trends detected in the time series of the three indices and by the relatively low correlation between these indices. In general, the χ_{200} -index provides the highest confidence in the detected trend, and in the sign of the circulation's intensity change, leading me to rely on it for further studies. At the same time, this index is a proxy for the upper tropospheric divergence of flow resulting from the circulation, being less representative for the ascending branch or the lower tropospheric flow within the Pacific Walker Cell. Consequently, in future studies, the choice of index should depend on the scope and region of study.

3.4 The CMIP5 detected Walker circulation change

In this Section I look into another kind of ensemble, the CMIP5 model ensemble. Here, each ensemble member has different model physics. Initial conditions also differ, but the main source of differences is generally seen in the GCM configuration. The 28 members of the CMIP5 ensemble render time averaged MSLP- and ω_{500} - indices slightly different in value and variance from the case of the MPI ensemble. As in the case of the MPI ensemble, these values differ from the ERA-Interim resulting averages (Tab. 3.4). The χ_{200} -index shows a CMIP5 ensemble mean value smaller than the MPI ensemble value, but which is closer to ERA-Interim to a degree of one standard deviation. The considerations stated in the previous Section on the differences between datasets are also valid for this ensemble. Moreover, these differences and the higher

variance come from the non-linear effects of the numerical approximations and parametrization schemes characteristic to each GCM. Under these considerations, I assume that the simulations capture the Walker circulation reasonably well.

The correlation between indices is low and significantly more varying within this ensemble compared to both the MPI ensemble and the reanalysis values. The differences between the physics of the CMIP5 GCMs make it impossible to conclude on the correlations between the indices on ensemble level (both for the entire time series and for the extreme cases), even though for specific models some coefficients are large. For example, the correlation between the MSLP- and χ_{200} -index for MIROC-ESM equals to 0.855, but is quite low between ω_{500} - and χ_{200} -index (0.322) and MSLP- and χ_{200} -index (0.179). The large variance of the correlation coefficients suggests a different response of the circulation at different vertical levels, pointing to a probable degree of discontinuity in the vertical in some GCMs, and/or to a need to adjust the indices to the particular GCM.

Table 3.4: Statistical results for the CMIP5 ensemble

	CMIP5 ensemble	
	mean	σ
MSLP-index ^a [Pa]	0.129 ± 0.446	71.545 ± 21.732
ω_{500} -index ^a [10 ⁻³ Pa s ⁻¹]	-0.015 ± 0.087	13.027 ± 4.922
χ_{200} -index ^a [10 ⁵ m ² s ⁻¹]	119.241 ± 25.425	11.041 ± 3.506
<i>all months in the Walker circulation index time series</i>		
corr(MSLP-index, ω_{500} -index) ^b	0.203 ± 0.548	
corr(MSLP-index, χ_{200} -index) ^b	0.337 ± 0.262	
corr(ω_{500} -index, χ_{200} -index) ^b	0.307 ± 0.243	
<i>months in the Walker circulation index time series with extreme circulation intensity</i>		
corr(MSLP-index, ω_{500} -index) _{extr} ^b	0.380 ± 0.664	
corr(MSLP-index, χ_{200} -index) _{extr} ^b	0.535 ± 0.385	
corr(ω_{500} -index, χ_{200} -index) _{extr} ^b	0.367 ± 0.422	
<i>variations of parameters until CO₂ doubling</i>		
MSLP-index trend [Pa dec ⁻¹]	-4.477 ± 4.328	
ω_{500} -index trend [10 ⁻³ Pa s ⁻¹ dec ⁻¹]	-0.516 ± 1.101	
χ_{200} -index trend [10 ⁵ m ² s ⁻¹ dec ⁻¹]	-0.395 ± 0.955	

^a For each index and each ensemble member, I calculate the mean of its time series (140-years period, which corresponds to CO₂ quadrupling), and the standard deviation of its detrended time series. The table presents the averages of these values and their variance within the ensemble.

^b $corr(x,y)$ - Pearson correlation coefficient between x and y .

Table 3.5: CMIP5 ensemble correlation between the change in Walker circulation on one side and TCR_{TP} and the OLR trend (until CO_2 doubling) on the other side (selected runs/GCMs refer to the runs/GCMs that show a significant trend in the Walker circulation intensity until CO_2 doubling)

	Correlation with TCR_{TP}		Correlation with OLR trend	
	all runs	selected runs	all runs	selected runs
MSLP-index	-0.338	-0.323	-0.273	-0.150
ω_{500} -index	0.047	-0.094	0.174	0.104
χ_{200} -index	-0.370	-0.454	-0.213	-0.213

As seen in Tab. 3.4, the mean CMIP5 ensemble trend in the Pacific Walker Cell is negative, regardless of the chosen index. On average, in the period until CO_2 doubling the circulation is slowing down by 6.3% σ , 4.0% σ and 3.6% σ per decade for the MSLP-, ω_{500} - and χ_{200} -index, respectively (Tab. 3.4). The values of the mean trend differ significantly from the MPI ensemble and their variance is considerably larger. Fig. 3.3 depicts the Walker circulation 70-years trends (until CO_2 doubling) and 140-years trends (until CO_2 quadrupling) over the CMIP5 ensemble. Independent of the index, at least 70% of the ensemble members show significant trends, as defined in the previous Section (24 out of 28 for the MSLP-index, 20 out of 28 for the ω_{500} -index, 23 out of 28 for the χ_{200} -index). A weakening Pacific Walker Cell is simulated by:

1. 21 out of 24 members with significant trend in the MSLP-index time series;
2. 15 out of 20 members with significant trend in the ω_{500} -index time series;
3. 17 out of 23 members with significant trend in the χ_{200} -index time series.

Compared to the MPI ensemble, looking at the ability to detect significant trends, the CMIP5 ensemble shows less sensitivity to surface processes. However, the number of members and the distinct configuration of the GCMs caution against drawing conclusions from this difference in sensitivity.

Nonetheless, as it was also true in the case of the MPI ensemble, the same ensemble member may suggest a different sign for the change in the circulation intensity depending on the chosen index (Fig. 3.3). As the 1pct CO_2 experiment set up in CMIP5 allows investigation of changes until quadrupling of CO_2 , I note in Fig. 3.3 that some models reveal significantly different trends in the circulation from the start of the experiment until doubling of CO_2 (70 years period) than until quadrupling (140 years period) - e.g. BCC-CSM1-1, FGOALS-s2, MIROC-ESM. I find that these differences of trends hold even if the period from the moment of CO_2 doubling until that of quadrupling is considered. This finding leads to the conclusion that the intensity change

is non-linear and changes not only as a result of increasing forcing, but also partly due to the internal variability of the Pacific Walker circulation and its driving factors.

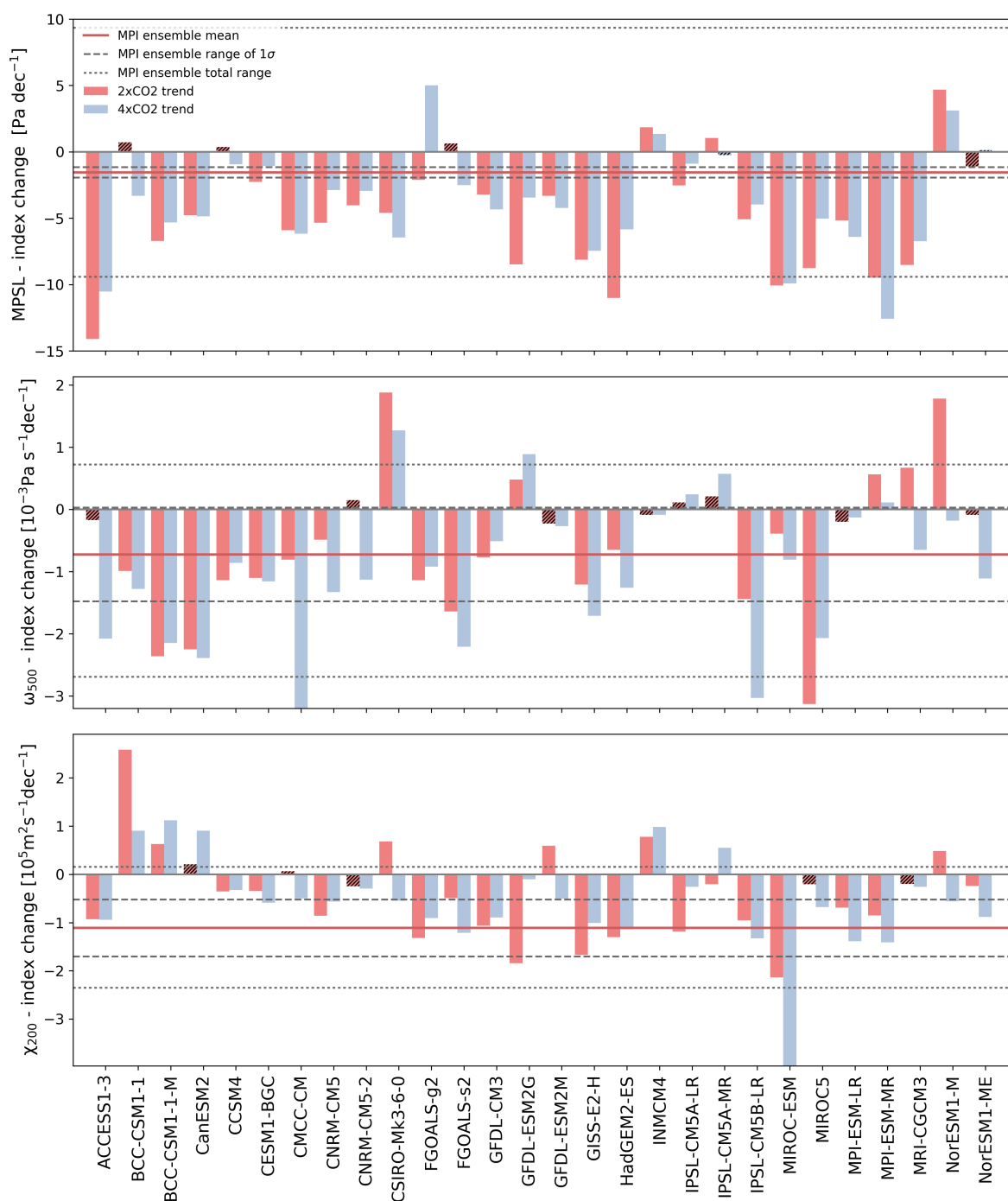


Figure 3.3: Pacific Walker Cell intensity trends detected for the CMIP5 ensemble 1pctCO₂ experiment output. Trends detected until CO₂ doubling are shaded *red*, until CO₂ quadrupling - *blue* (hatched bars denote trends with confidence level below 80%). The *red solid line* represents the MPI ensemble mean trend, the *dashed lines* - the range of 1σ variance, the *dotted lines* - the total spread of the MPI ensemble.

To assess the importance of increased forcing for the circulation change, I look again into the TCR_{TP} as a robust indicator of the response of the climate system to higher CO_2 concentration. Fig. 3.4 depicts the change in circulation as a function of TCR_{TP} , for each member of both investigated ensembles. There is one subfigure for each circulation index. As clearly visible, the CMIP5 ensemble mean TCR_{TP} , 1.592 K (Tab. 3.4), does not differ significantly from the MPI ensemble mean TCR_{TP} , but the GCMs' distinct configurations lead to a much higher variance ($\sigma = 0.302$ K). These large variances of TCR_{TP} and of the Walker circulation indices affect the detection of correlation between these parameters, giving significantly different values compared to the MPI ensemble (Tab. 3.5). Limiting the correlation only to the GCMs showing significant trends does not improve the correlation either.

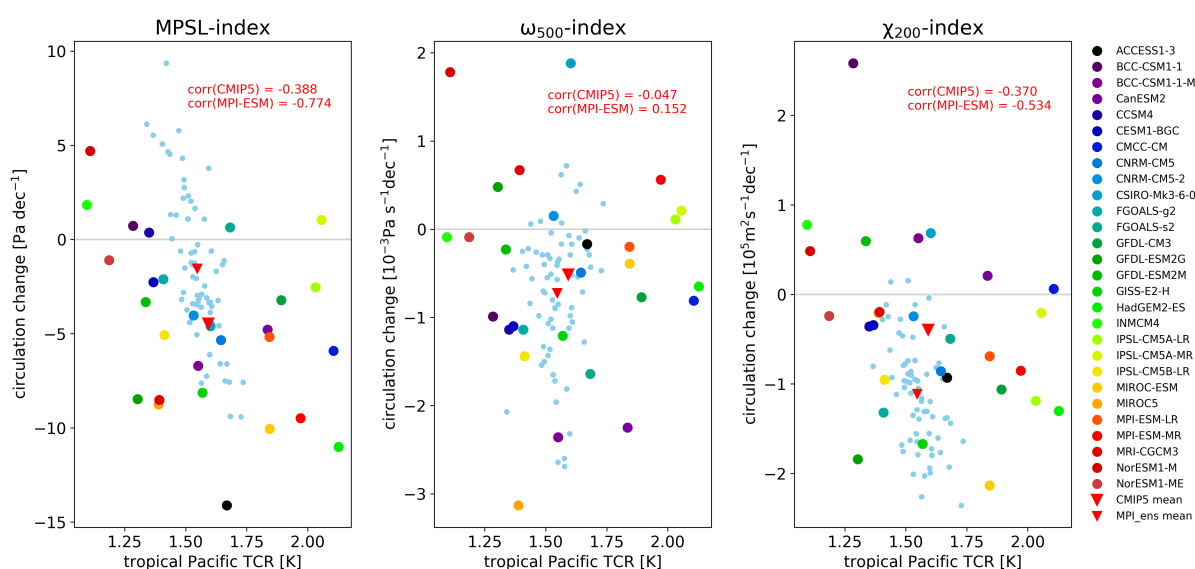


Figure 3.4: Pacific Walker Cell intensity trend until CO_2 doubling compared to the TCR_{TP} in the CMIP5 and MPI ensembles' output of the 1pct CO_2 experiment (the values corresponding to the MPI ensemble are denoted by circles with smaller diameter). The correlation coefficient between the two sets is given for each ensemble separately.

In summary, it is interesting to note that, although somewhat larger, the spread in the detected Walker circulation intensity change found in the CMIP5 ensemble is of comparable magnitude to the spread found in the MPI ensemble.

3.5 Ensemble members' differences and the detected ensemble spread

Judging from Fig. 3.4, it is apparently sufficient to use one GCM ensemble (in this case the MPI ensemble) to obtain the variance of the Walker circulation trends under increased CO_2

forcing. In other words, it appears on first sight as if natural variability alone could account for the observed intermodel spread in Walker circulation response. I investigated this point further, looking for differences between GCM representation of the Walker circulation in a control unforced climate experiment and for qualitative differences between Walker circulation response spread in the two different ensembles.

Before looking into these differences, I rank the MPI and CMIP5 ensemble members in ascending order by each Walker circulation index time series trend. Fig. 3.5 shows the order of the ensemble members arranged according to their mean rank across the three indices. The figure draws again attention to the difference between the trends detected in the time series of the three indices - unless by mean rank, the low correlation between index rankings makes it difficult to indicate which model shows the largest weakening or strengthening of the Walker circulation. Further, I use the 5th and 95th percentile of the mean rank (rank_m) across each ensemble to distinguish 2 groups of MPI-ESM-LR runs and of CMIP5 GCMs (Fig. 3.5):

1. low-ranking ensemble members (LRMs) or members that project the strongest weakening of the Walker circulation: MPI-ESM-LR runs with $\text{rank}_m \leq 17$ (MPI ensemble 5th percentile) and GCMs with $\text{rank}_m \leq 10$ (CMIP5 ensemble 5th percentile);
2. high-ranking ensemble members (HRMs) or members that project the smallest weakening of the Walker circulation or even its strengthening: model runs with $\text{rank}_m \geq 58$ (MPI ensemble 95th percentile) and GCMs with $\text{rank}_m \geq 23$ (CMIP5 ensemble 95th percentile).

In order to investigate the simulation of the Walker circulation by the CMIP5 ensemble members, I look into the background naturally-forced CMIP5 experiment, namely piControl. A time mean for this control run of the meridional cross-section over the equatorial Pacific (between 10°N and 10°S) of the vertical velocity field, hereinafter ω_X , can be used to give an indication of the characteristics of the Pacific Walker Cell simulation in the respective GCM and the locations of the corresponding ascending and subsiding branches. Fig. 3.6a presents such a cross-section obtained from the output of the MPI-ESM-LR model, showing a clear differentiation between the convective region in blue shading over the Maritime Continent and the subsidence region in red shading over the Central and East Pacific. The wave-like features visible in the cross-section for this model, as well as MPI-ESM-MR (Fig. 3.6b), are numerical artifacts resulting from spectral ringing (personal comment of Thorsten Mauritsen). To facilitate the comparison of the Pacific Walker Cell representation between the 28 members of the CMIP5 ensemble, I calculate the layer-thickness-weighted vertical mean of ω_X , referred onward as $\bar{\omega}_X$. The minimum value of $\bar{\omega}_X$ corresponds to the region of strongest convection, and the maximum value to the region with strongest subsidence. As seen in Fig. 3.6b, the general expected $\bar{\omega}_X$ pattern of the Pacific Walker Cell is identifiable in all the models: I find a convective region

over the Maritime Continent and a subsidence region over the East Pacific. There is also a region of ascending motion starting around 280°E eastward, but this is induced by orography. Nonetheless, there is a large variance of the Walker circulation simulation among the CMIP5 GCMs, especially in the zonal extent and in the average intensity of vertical velocity in these regions. Considering this background experiment variance, I infer that the GCM numerical configuration and its parametrization schemes influence the representation of the Pacific Walker Cell and its variation under various forcings. I further investigate the change in $\bar{\omega}_X$ at the moment of CO₂ doubling (averaging over year 60-80 of the 1pctCO₂ output) with respect to the piControl mean, in particular for the CMIP5 ensemble LRMs and HRMs. Fig. 3.6c shows this change on the primary y-axis (solid lines) and the background pattern on the secondary y-axis (dotted lines).

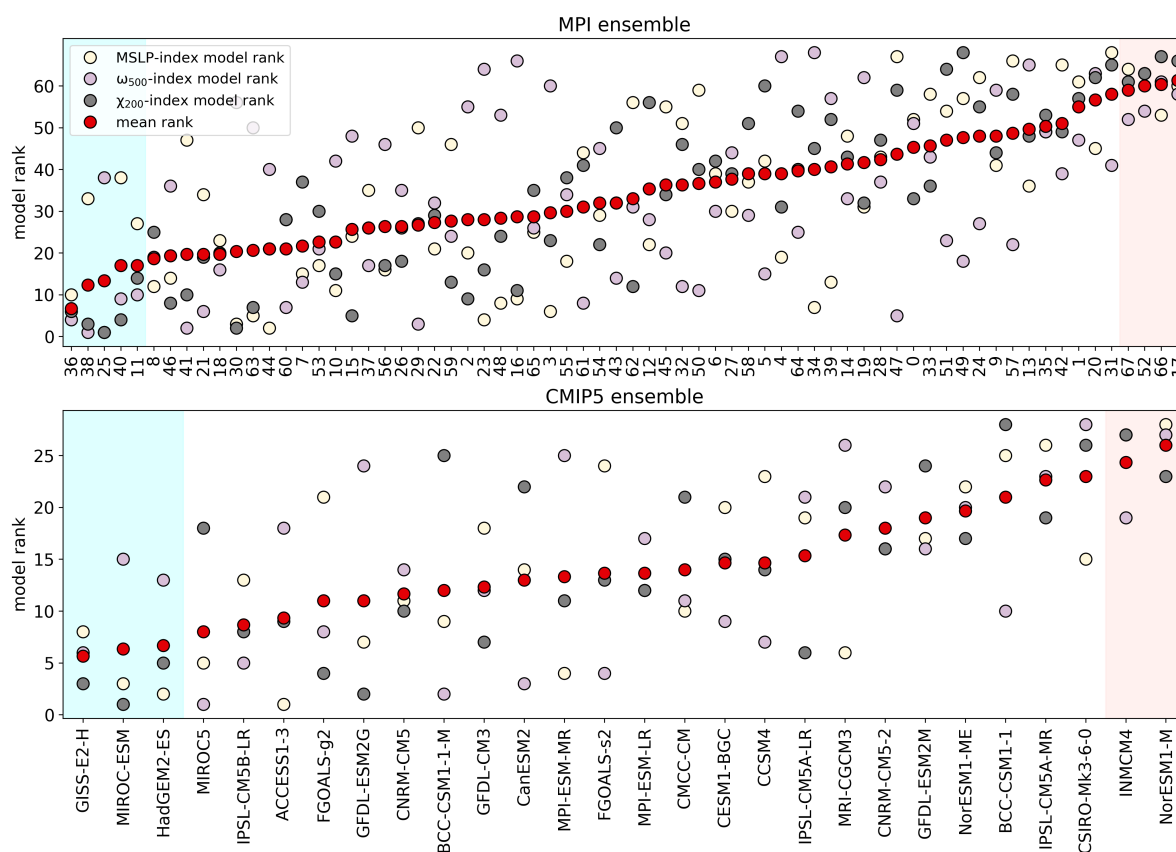


Figure 3.5: MPI and CMIP5 ensemble members' index-based ranking (in ascending order) according to the projected trend in the intensity of the Pacific Walker Cell until CO₂ doubling within the 1pctCO₂ experiment (MPI-ESM-LR runs and GCMs are ordered according to their mean rank). The *blue shading* denotes the low-ranking ensemble members (LRM, projecting on average the strongest weakening of the Walker circulation), the *red shading* - high-ranking members (HRM, projecting on average the smallest weakening of the Walker circulation or its strengthening).

There is no clear distinction between the LRMs and HRMs in the piControl experiment. So, apparently, the difference in the response between the LRMs and HRMs is not caused by them having different representation of the Walker circulation to start with, but by other intermodel differences that only become apparent upon forcing. The HRMs show significantly less variance in the change across the equatorial Pacific than the LRMs. Also, the HRM ensemble members suggest a slightly intensified convection in the ascending branch and small change in the subsidence area, which is consistent with a circulation that either shows insignificant change or one that strengthens. Conversely, the LRMs clearly show a shift of the convecting branch eastward from the Maritime Continent and a general increase in ascending motion across the Pacific, which is related to a slower circulation. Again, the fact that in the background experiments the low-ranking and the high-ranking ensemble members do not show clear differences suggests that the distinct response found for the Pacific Walker Cell is mostly induced by the CO₂ forcing and the response of the climate system elements to this forcing (e.g. clouds, precipitation, surface temperature, atmospheric stratification, atmosphere-ocean heat exchange).

As mentioned in Section 3.3, increased surface temperature is one of the robust responses of the climate to CO₂ concentration increase and may serve as an intermediate parameter to identify drivers of the circulation response variation. The circulation may be investigated inclusively from the point of view of the related cloudiness and/or outgoing longwave radiation (OLR). The latter is modulated, among others, by clouds, precipitation, and aerosols. Currently, because of the low confidence in aerosol-cloud interaction radiative feedback [see Chapter 8 in IPCC [2013]], the parametrization of clouds and convection is responsible for most uncertainty in climate models, including in the projection of OLR variation at intra- and interannual time scale. Here I look into the spatial structure of OLR change and surface temperature increase by the doubling of CO₂, as simulated by the ensembles, and investigate the differences among ensemble members in the region of the tropical Pacific. Although the correlation of surface temperature increase, OLR trend, and Walker indices trends is low (Tab. 3.3 and 3.5), the differences in the regional response of temperature and OLR may be indicative of the origin in Walker circulation change differences among models.

Fig. 3.7 describes for each of the two ensembles the mean ensemble change in OLR with respect to the piControl mean, as well as the change detected in the LRM and HRM groups. Fig. 3.7a and 3.7b show that the patterns in the mean control OLR (obtained from averaging over the monthly outputs of the piControl CMIP5 experiment) are quite similar between the MPI and CMIP5 ensembles, despite the small differences over the central Pacific and Eastern Indian Ocean - Australia regions, where the MPI ensemble suggests less cloudiness. Consequently,

I deem it reasonable to look into the CO₂-forced OLR changes in both ensembles, aiming to identify the effect of internal variability and of GCM configuration on the mean change.

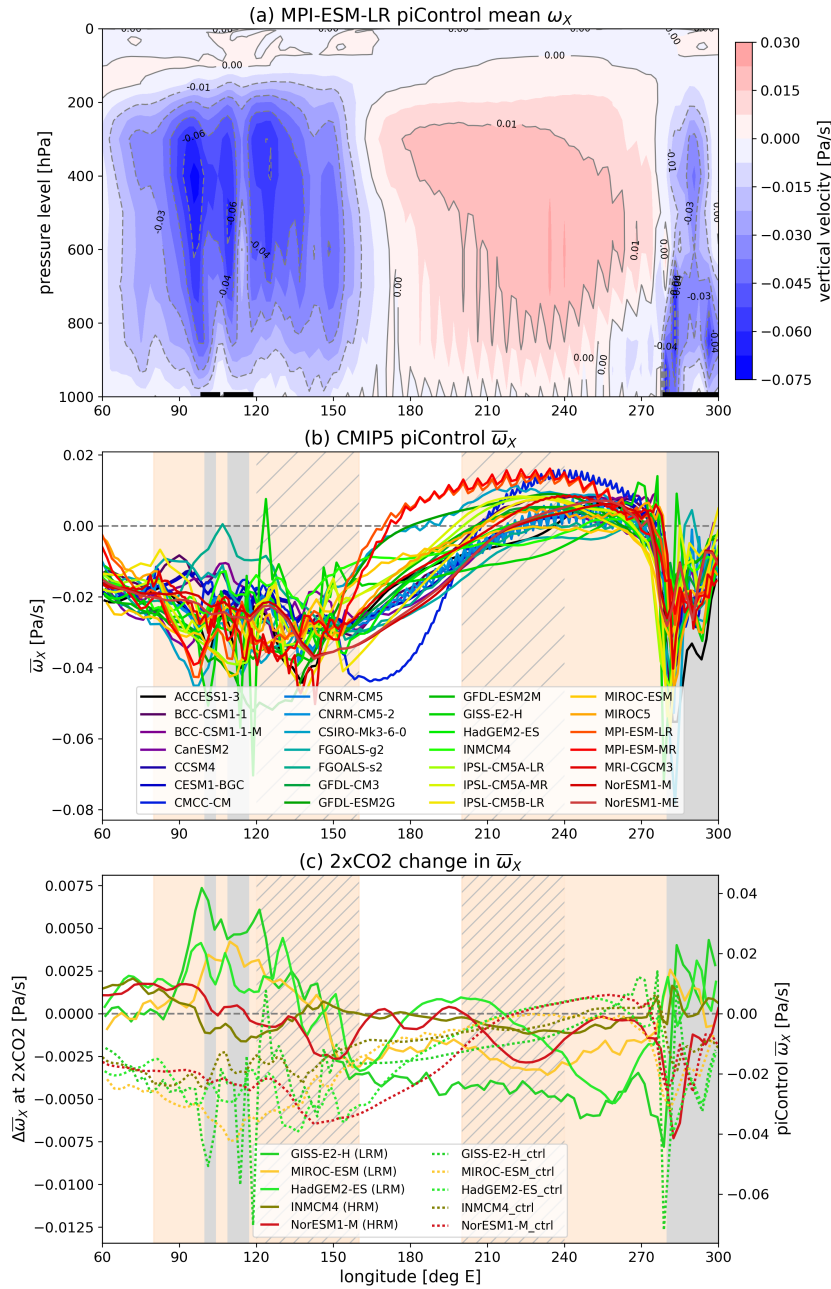


Figure 3.6: (a) Meridional cross-section of vertical velocity ω_x between 10°N and 10°S, calculated for the mean piControl output of MPI-ESM-LR. (b) CMIP5 ensemble vertically-weighted mean $\bar{\omega}_x$ of the meridional cross-section presented above. (c) Changes in $\bar{\omega}_x$ at the moment of CO₂ doubling with respect to the control run for the CMIP5 ensemble LRM (GISS-E2-H, MIROC-ESM, HadGEM2-ES) and HRMs (INMCM4, NorESM1-M).

Notes: The *thick black lines* at the bottom of plot (a), as well as the *grey stripes* in (b) and (c), represent land surface on the equator, corresponding to Sumatra, Borneo and South America. The *beige stripes* in (b) and (c) refer to the zonal extent of the boxes used to compute the MSLP-index; the *hatched stripes* refer to the zonal extent of the boxes used to compute the ω_{500} -index.

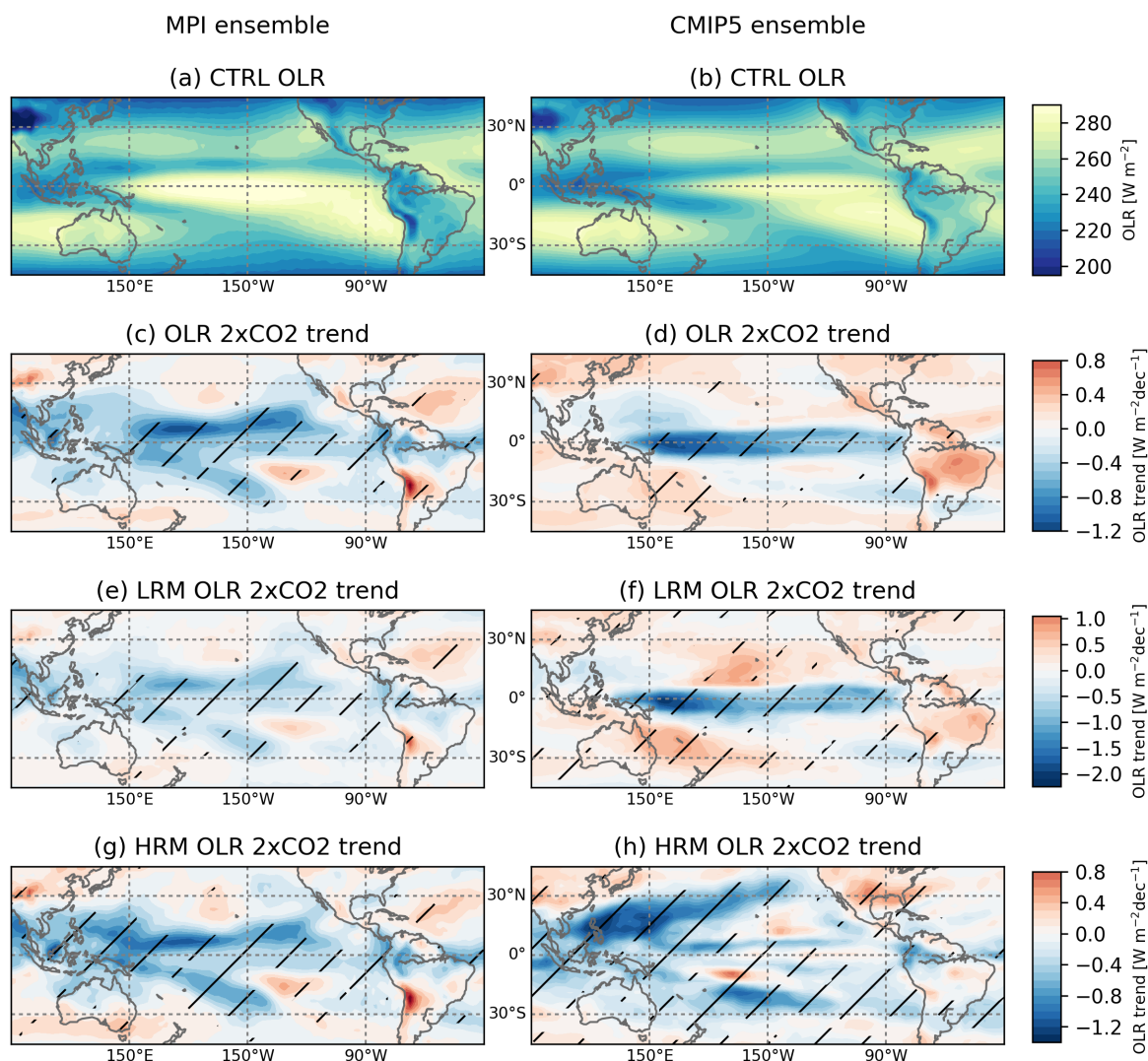


Figure 3.7: (a), (b) - Ensemble mean OLR in the pre-industrial control experiment (piControl) for the MPI and CMIP5 ensembles, respectively. (c), (d) - Ensemble mean trend in OLR variation until CO₂ doubling in the 1pctCO2 output. (e), (f) - Mean trend in OLR variation until CO₂ doubling in the 1pctCO2 output, averaged for the low-ranking ensemble members (LRM). (g), (h) - Mean OLR trend until CO₂ doubling, averaged for the high-ranking ensemble members (HRM). *Note:* Regions with trends having $\geq 80\%$ confidence level are hatched.

This comparison reveals significant differences between the mean ensemble OLR change: the MPI ensemble shows an increasing cloudiness not only across the central Pacific, but also over the Maritime Continent, whereas the CMIP5 ensemble does not (Fig. 3.7c and 3.7d). Also, the presence and intensification of the southern branch of the Intertropical Convergence Zone (ITCZ) is much more pronounced in the MPI ensemble. The CMIP5 mean OLR change reveals a strong increase of cloudiness immediately to the east of the Maritime Continent. Therefore, not only the previous studies [Bayr et al., 2014] and the χ_{200} -index analysis project this shift of

the ascending branch of the cell (75% of the CMIP5 GCMs simulate it; not shown), it is also confirmed by the OLR change pattern.

I note that the MPI ensemble mean OLR change pattern is preserved in both the LRM and HRM means (Fig. 3.7e and 3.7g): increasing cloudiness along the equator and the Maritime Continent, visible southern branch of the ITCZ. The difference between these groups of the MPI ensemble members is mostly in magnitude, not the sign of the trend. This can be seen in Fig. 3.8, which shows mean OLR trend differences between HRM and LRM models. Hatching there indicates where the trend changes sign between LRM and HRM models, and subplot (a) shows that this does not occur over the tropical Pacific for the MPI ensemble. However, it is also visible that, compared to the HRM group, the LRM group projects almost no increase in cloudiness over the Maritime Continent, but eastward from this region. This is once more consistent with an eastward shift of the Walker Cell ascending branch in a climate with slower circulation.

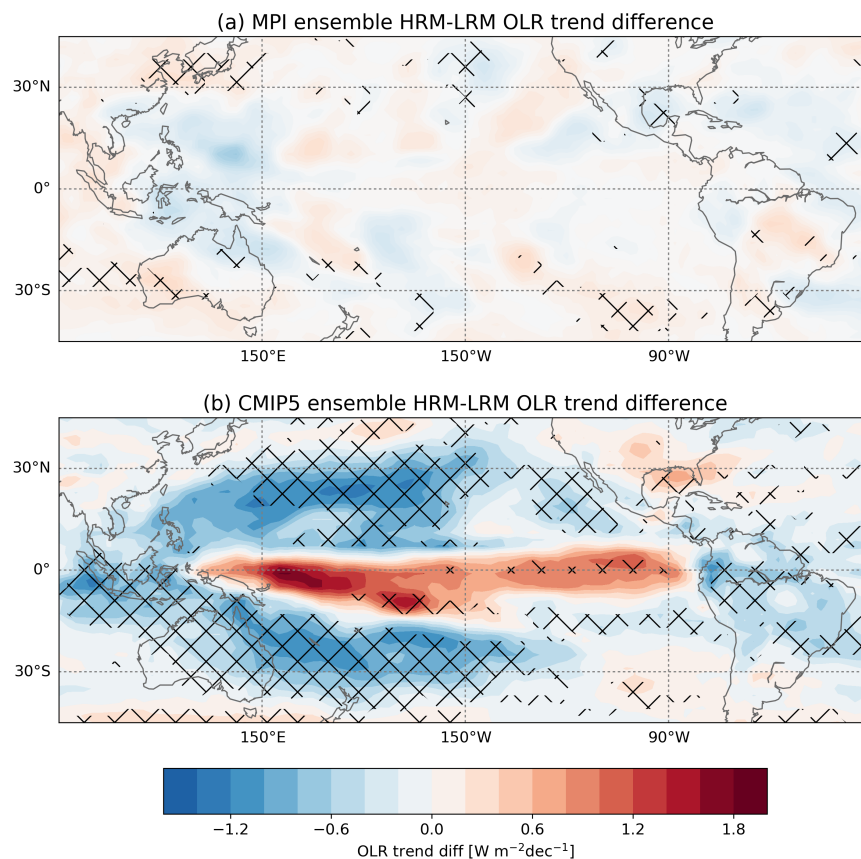


Figure 3.8: Mean OLR trend difference between HRMs and LRMs for the MPI ensemble (a) and the CMIP5 ensemble (b). The *crossed hatching* shows the regions where the sign of the trend differs between LRMs and HRMs. *Blue areas without hatching* are where the models with less circulation slowdown (HRM) have a stronger increase in cloudiness (lower OLR) than the areas with a stronger circulation slowdown (LRM).

Fig. 3.7f and 3.7h show the mean OLR trend for the CMIP5 LRM models (GISS-E2-H, MIROC-ESM, HadGEM2-ES) and HRM models (INMCM4, NorESM1-M), respectively. Compared to the results from the MPI ensemble, the patterns in the OLR trend differ significantly between the two groups of GCMs. Also, the area showing different sign in the trends is much larger (Fig. 3.8b), including parts of the Maritime continent and of the tropical Pacific. The LRM group (Fig. 3.7f) is characterized by a strong significant negative OLR trend to the east of the Maritime Continent. This is indicative of increasing cloudiness related to the intensification of convection in this region and the eastward shift of the ascending branch of the Pacific Walker Cell. The HRM subplot (Fig. 3.7f) suggests, on the other hand, only small increase in cloudiness over the equatorial region of the Maritime Continent, but a strongly intensified cloudiness over its northern region, consistent with more active convection in the Pacific Walker Cell. Also, in the OLR trends in the HRM model I identify a pronounced southern branch of the ITCZ in the South-Western Pacific, which cannot be found in the LRM models.

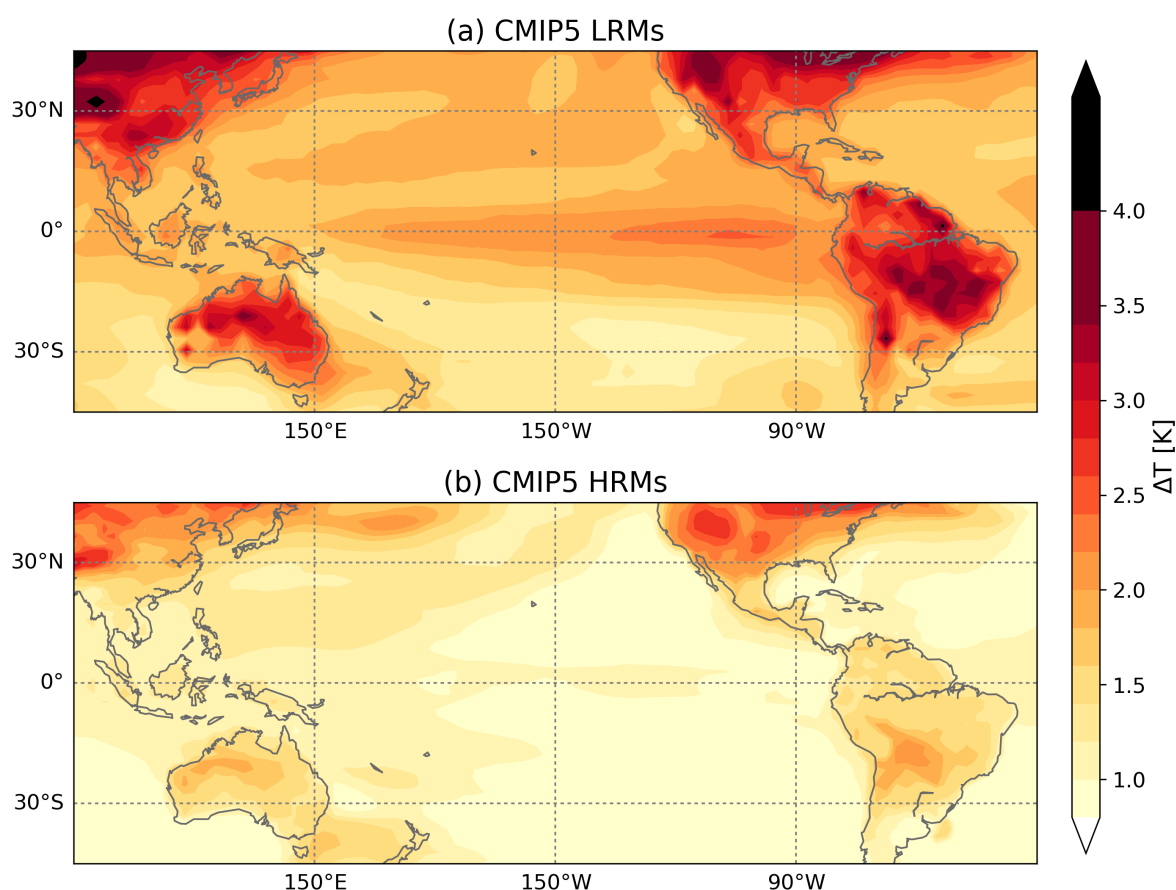


Figure 3.9: Surface temperature change at the moment of CO₂ doubling in the 1pctCO₂ experiment output, averaged for the LRM (a) and HRM (b) CMIP5 models.

A similar picture to the differences in OLR trend between the LRM and HRM ensemble members emerges in the surface temperature change over the tropical Pacific (Fig. 3.9). The

LRM ensemble members show overall a larger increase of surface temperature across the equatorial Pacific and especially over the Eastern Pacific, a pattern compatible with an El Niño state of the climate system and a slower Walker circulation. The temperature variation over the Maritime Continent is also smaller but more uniform in the HRMs than in the LRMs, consistent with a non-changing or strengthening circulation (Fig. 3.7f and 3.7h).

This analysis of the relation between the changes in OLR over the tropical Pacific and the variation of the Walker Pacific Cell dynamics shows that even if the detected variances of the circulation trends in the two ensembles are similar, this variability is caused by different factors. For the Walker circulation trends in the MPI ensemble, which are driven by internal variability, the patterns in OLR change are comparable (differing mostly in magnitude) between the runs projecting the most weakened circulation and the runs projecting the less changing or strengthening circulation. On the other hand, the CMIP5 ensemble shows that a GCM with a strong decrease in the intensity of the Walker Cell will likely have a drier Maritime Continent, a significant eastward shift of the ascending branch of the cell, and a warmer East and Central Pacific by CO₂ doubling than a GCM with a stronger circulation. It has been suggested by [Bony et al. \[2013\]](#) and [Su et al. \[2014\]](#) that these intermodel differences arise most probably from the differences in the representation of small-scale moist processes, like convection and clouds, and their interaction with the large scale circulation.

4 The fast response of the tropical circulation to CO₂ forcing

This Chapter includes the description of the newly defined metric for the tropical overturning circulation in Section 4.1, and the discussion of the detected circulation change, as well as the decomposition of this change into the contributions of radiative heating rate, stratification and subsidence area change, for the aqua-planet experiments (Section 4.2) and the amip experiments (Section 4.3). A brief investigation of the change in circulation variability is presented in Section 4.4. Section 4.5 compares these results with the circulation change detected in the coupled climate experiments.

4.1 The subsidence mass flow metric

I limit my analysis of the circulation change to the tropical subsidence regions. Following [Davis and Birner \[2013\]](#), the zero-crossings between 20 – 40° latitude (in both hemispheres) of the vertically-averaged zonal mean of mass stream function are considered as the tropics' limits for any given time step ([Fig. 4.1](#)). This allows the separation of the equatorward from the poleward air mass transport. An atmospheric column within the tropics is considered a subsidence column if the vertically-averaged vertical pressure velocity $\bar{\omega}$ is positive.

In the limits of the detected tropical subsidence regions, I define the subsidence mass flow SMF as follows:

$$SMF = \frac{1}{g} A_{\downarrow} \bar{\omega}, \quad (4.1)$$

where g is the gravitational acceleration, A_{\downarrow} is the subsidence area and $\bar{\omega}$ is the vertical velocity of each grid box. [Fig. 4.3](#), subplots (1a) and (1b), show the zonal mean of the subsidence mass flow averaged over the output of CNRM-CM5 for the aquaControl and aqua4xCO2 experiments, respectively. It is noticeable that the variation pattern of SMF is dominated by the variation of $\bar{\omega}$ ([Fig. 4.1a](#)), as the grid-box area in the limits of the subsidence regions does not vary strongly enough to have an impact on the pattern of the subsidence flux.

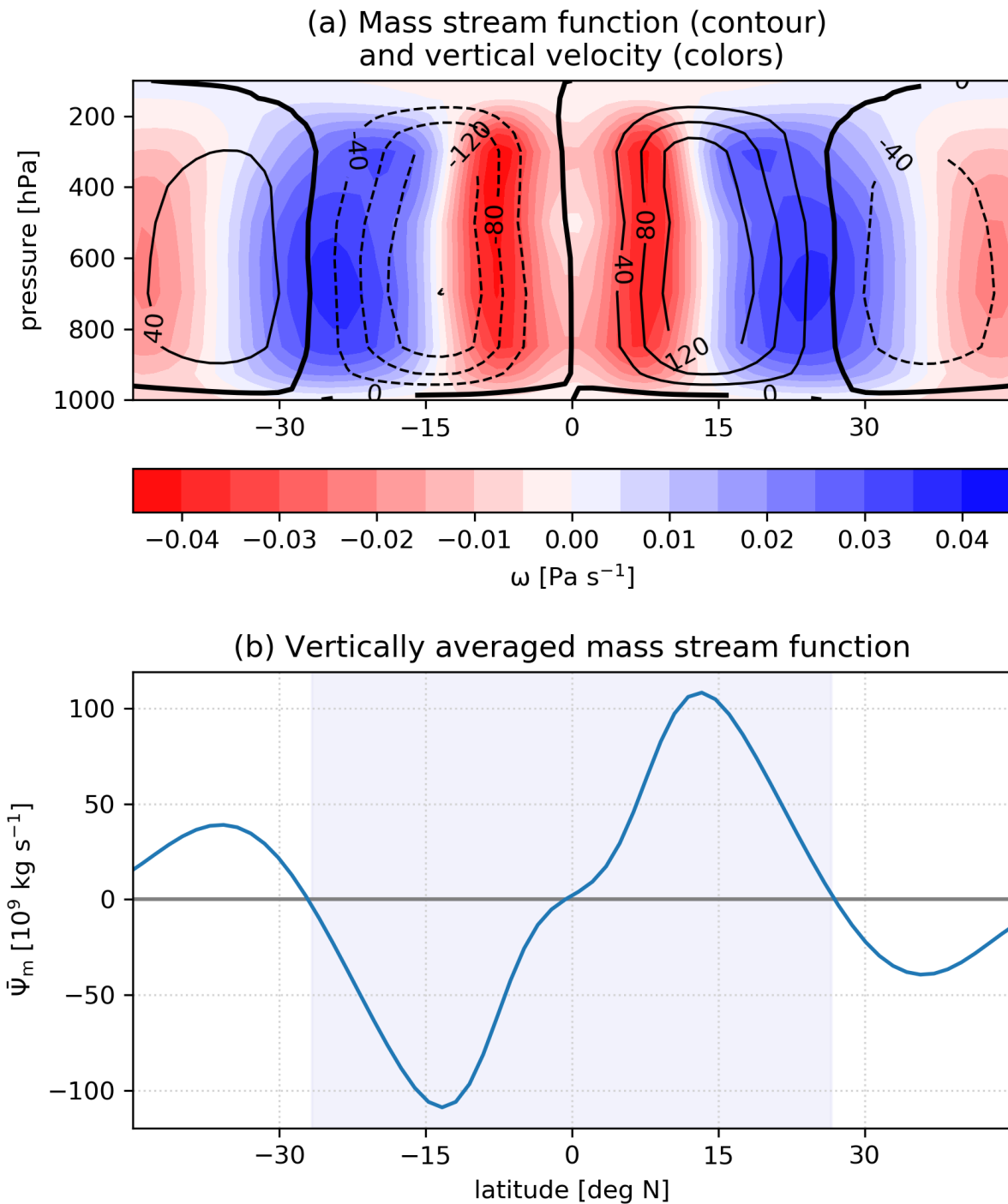


Figure 4.1: (a) Zonal mean of mass stream function in 10^9 kg s^{-1} (black contours) and of vertical velocity (color shading), averaged over the aquaControl output of CNRM-CM5. (b) Vertically-averaged zonal mean of mass stream function for the same output with the selected tropics expanse.

In the tropical subsidence regions the diabatic vertical motion ω balances diabatic heating Q_T , as horizontal temperature advection is almost insignificant [Zelinka and Hartmann, 2010;

Thompson et al., 2017]. As this work is limited strictly to these regions, I diagnose vertical velocity from the total diabatic heating rate Q_T and static stability σ :

$$\omega = -\frac{Q_T}{\sigma}, \quad (4.2)$$

therefore equation (4.1) becomes:

$$SMF = -\frac{1}{g} A \downarrow \frac{Q_T}{\sigma}. \quad (4.3)$$

I decompose the tropical total heating rate Q_T into the purely-radiative clear-sky heating rate Q_{rad} and a residual heating rate Q_{res} . The latter accounts for the cloud radiative effect, cloud microphysics and the heating resulting from lateral eddy mixing [Phillips, 1956]:

$$Q_T = Q_{rad} + Q_{res}. \quad (4.4)$$

The definition of subsidence mass flow in equation (4.1) and (4.3), and the consideration of equation (4.4) allow the decomposition of the change in subsidence mass flow as follows:

$$\frac{dSMF}{SMF} = \frac{dA \downarrow}{A \downarrow} - \frac{d\sigma}{\sigma} + \frac{dQ_T}{Q_T}, \quad (4.5)$$

and

$$\frac{dSMF}{SMF} = \frac{dA \downarrow}{A \downarrow} - \frac{d\sigma}{\sigma} + \frac{dQ_{rad}}{Q_T} + \frac{dQ_{res}}{Q_T}. \quad (4.6)$$

Therefore, I can investigate the relative change in subsidence flow SMF in comparison with the contribution of the relative change in the following parameters: subsidence area ($\frac{dA \downarrow}{A \downarrow}$), static stability ($-\frac{d\sigma}{\sigma}$), and heating rate ($\frac{dQ_T}{Q_T}$). The latter is also equivalent to the sum of changes in clear-sky heating rate Q_{rad} and residual heating rate Q_{res} relative to the total heating rate Q_T in the control setup ($\frac{dQ_T}{Q_T} = \frac{dQ_{rad}}{Q_T} + \frac{dQ_{res}}{Q_T}$).

PSRAD

For the decomposition of total heating rate into the clear-sky and residual components (equation (4.4)) I apply the radiative transfer model PSRAD [Pincus and Stevens, 2013] to calculate the clear-sky heating rate Q_{rad} . This model uses as input the vertical profiles for temperature, humidity, pressure, cloud properties, and absorption species' volume mixing ratios (CO₂, CH₄, N₂O, O₃). The absorption species volume mixing ratios were not available for all the investigated GCMs. I therefore used mean profiles for the 1979–2008 period (Fig. 4.2), averaged over MPI-ESM-LR, MRI-CGCM3, and four other GCMs that have available gas concentrations but are not investigated in this study (these GCMs were not run for the aqua-planet experiments):

CanESM2 [Arora et al., 2011], CESM1-BGC [Long et al., 2013], GFDL-ESM2G and GFDL-ESM2M [Dunne et al., 2012]. The GCM vertical profiles are limited in the stratosphere to 10 hPa. To account for this, I extend the remaining vertical range (10 – 0 hPa) with the tropical reference profiles FASCOD [Anderson et al., 1986]. These data provide stability to the PSRAD run and insure a realistic picture of heating rates above the tropopause without affecting the heating rate profile in the troposphere, which is my area of interest. Besides the vertical profiles, PSRAD uses surface temperature, surface pressure, surface albedo and solar zenith angle as input. For surface albedo I use the values of 0.07 and 0.2 for ocean and land surface, respectively. In the case of solar zenith angle I have to account for the fact that the GCM output is a monthly mean output. Therefore, I follow Cronin [2014] and Wing et al. [2018] and use a fixed zenith angle of 42.05° and an adjusted solar constant of 456.07 W m^{-2} to ensure a tropical mean annual insolation.

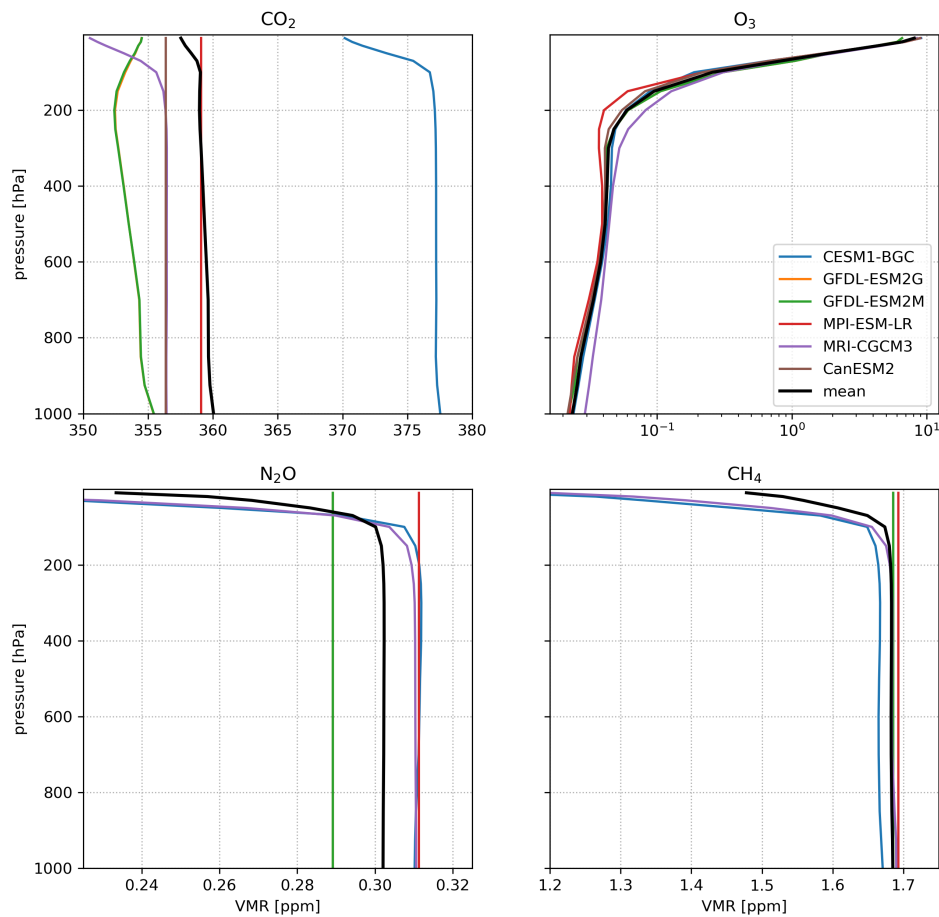


Figure 4.2: Mean profiles of CO₂, O₃, N₂O, and CH₄, averaged over the 1979–2008 period in the CMIP5 historical experiment output of CanESM2, CESM1-BGC, GFDL-ESM2G, GFDL-ESM2M and MPI-ESM-LR.

4.2 The circulation response in the aqua-planet experiments

I apply the methodology described above to the aquaControl output averaged over the entire experiment time range. In the case of aqua4xCO₂, I limit the averaging of the climate variable to years 2–5. This is to account for the abrupt CO₂ quadrupling which causes clear outlying values in the time series for the first year for most variables. Therefore, I will compare the mean control climate state (referred onward as aquaControl or control climate) with the quasi-equilibrium reached by the aqua-planet climate system after the sudden change in CO₂ forcing occurs (referred onward as aqua4xCO₂ or forced climate).

Because of the lack in land mass and seasons, the aqua-planet climate system is fairly symmetric meridionally and fairly uniform zonally. This enables the investigation of various variables just by looking at their zonal means. I use the CNRM-CM5 results to illustrate the zonal means for the subsidence mass flow SMF , static stability σ , heating rates (total Q_T , clear-sky Q_{rad} , and residual Q_{res}), and their difference between aquaControl and aqua4xCO₂ (Fig. 4.3). Note that the difference for the subsidence mass flow and static stability is shown in percentage, while for the heating rates it is in $K\ day^{-1}$: the latter have both negative and positive values, confusing the assessment of the change. The results indicate that in an aqua-planet setup the changes due to CO₂ quadrupling occur with respect to the magnitude, not the pattern of the various variables. The subsidence mass flow and therefore the circulation is in general weakening (Fig. 4.3, line 1), which is in agreement with previous studies [Held and Soden, 2006; Vecchi and Soden, 2007; Bony et al., 2013; He and Soden, 2015]. The only region where the values increase is in the vicinity of the ITCZ, suggesting that this convective region narrows. This is consistent with previous studies reporting this narrowing in Earth-like planet experiments [Lau and Kim, 2015; Byrne and Schneider, 2016]. Small change is seen in the static stability in the lower and mid troposphere (Fig. 4.3, line 2), but the upper troposphere shows a clear increase in stability. This may be related to the increase in high clouds and rise of the level of maximal meridional mass outflow in the upper troposphere, which enhance moisture divergence at these levels and promote stability increase [Zelinka and Hartmann, 2010; Lau and Kim, 2015]. The most evident change in the total heating rate is around 850 hPa (Fig. 4.3, line 3), where I find that in the forced climate the atmosphere cools less. This is dominated by clear-sky heating rate changes, as seen in its similar patterns of change (Fig. 4.3, line 4). The residual heating rate changes correspond to a narrowing of ITCZ and a drying of the atmosphere by entrainment in the regions close to the edges of ITCZ (Fig. 4.3, line 5). The parameters' values in the layer above the surface and in the stratosphere are either impossible to compute (these regions have little to no subsidence) or are too scattered to present a clear picture. Therefore for further analysis I consider only the results for the troposphere at pressures below 925 hPa.

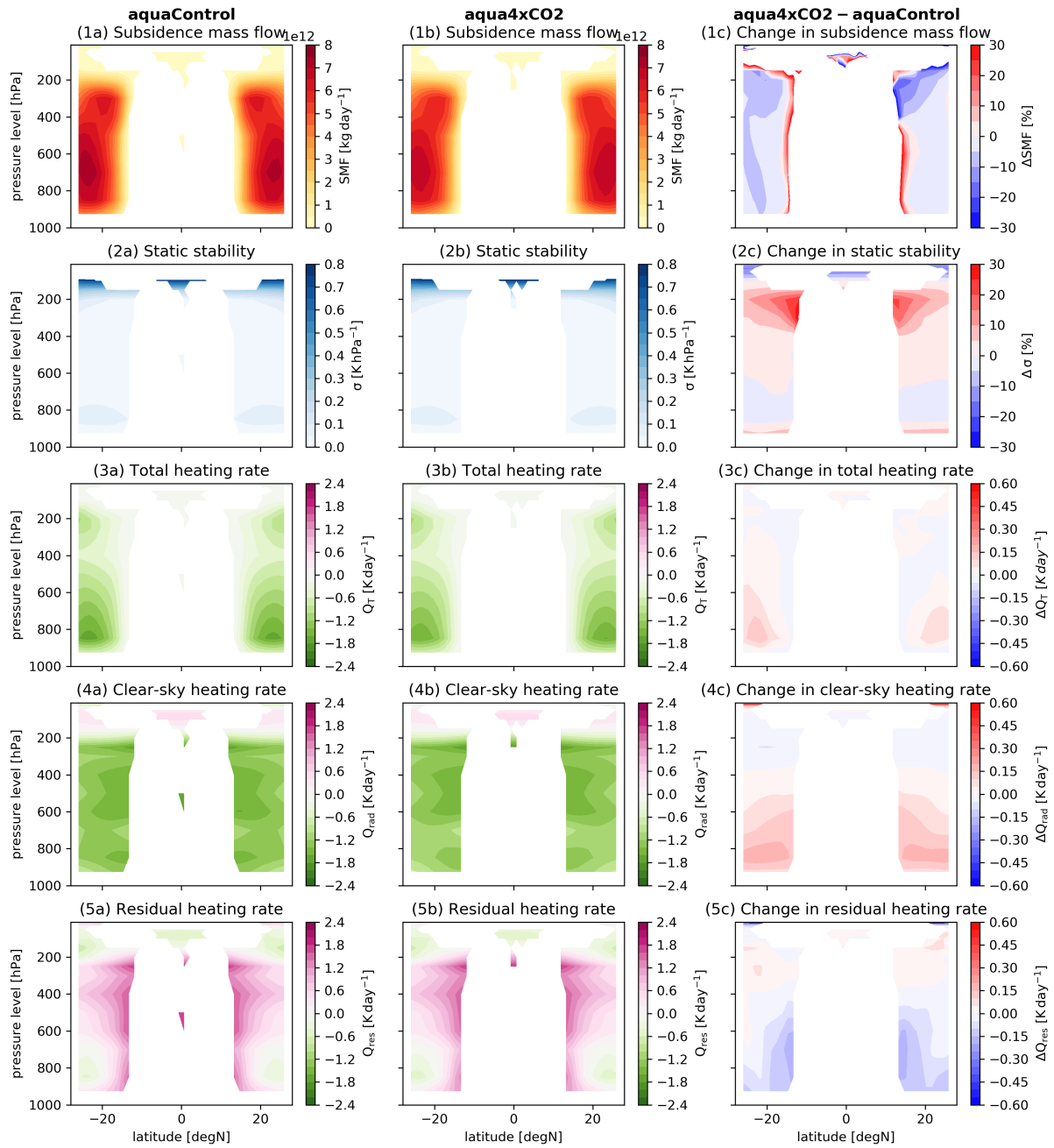


Figure 4.3: (first line) Zonal mean of subsidence mass flow, averaged for CNRM-CM5 over (a) the aquaControl and (b) the aqua4xCO2 experiment, as well as (c) the difference between the experiments. (lines 2–5) Same as in the first line, but for static stability, total diabatic heating rate, radiative heating rate and residual heating rate, respectively.

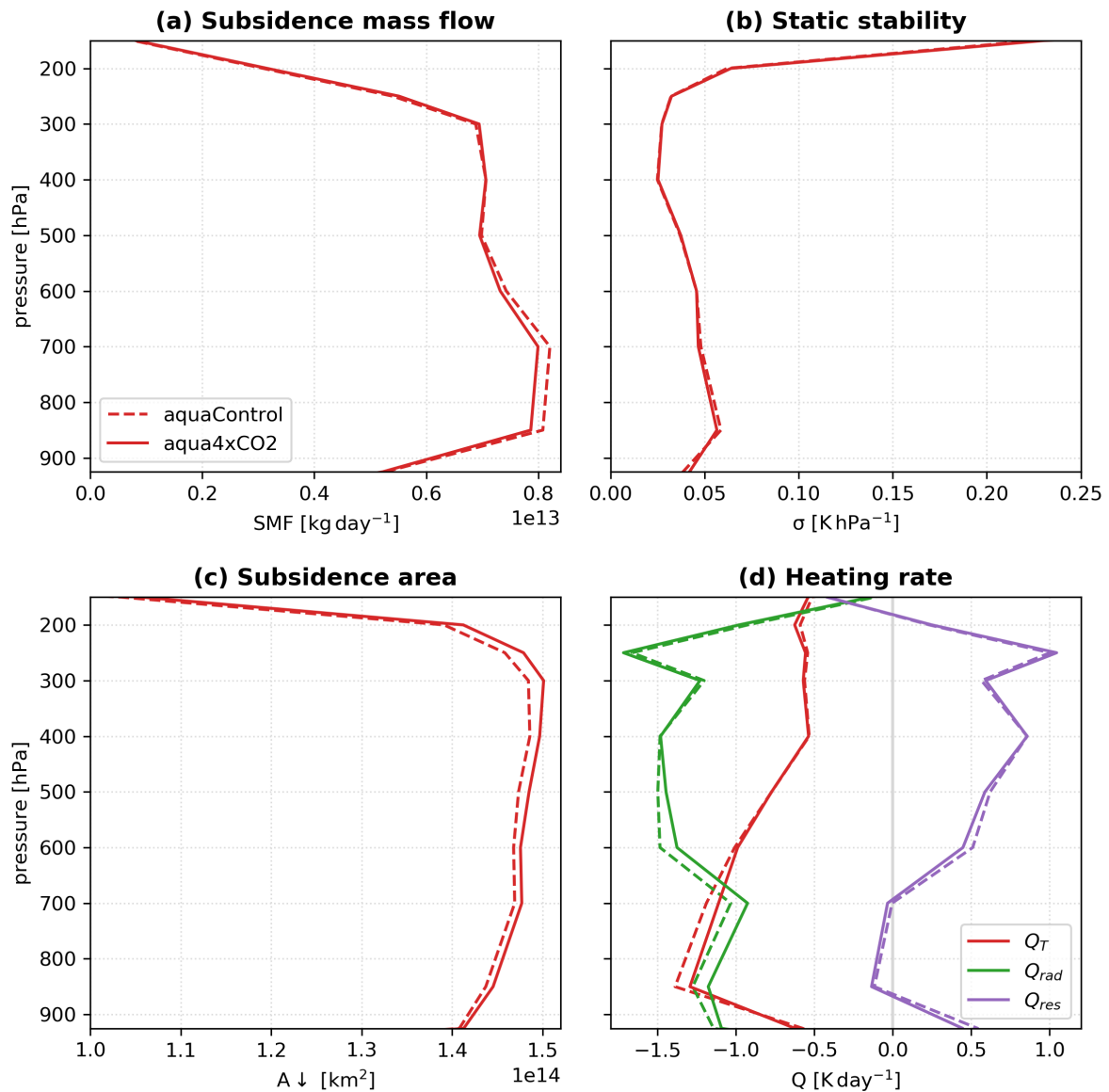


Figure 4.4: aquaControl (*dashed lines*) and aqua4xCO2 (*solid lines*) ensemble mean profiles of (a) subsidence mass flow, (b) static stability, (c) tropical subsidence area, and (d) total, clear-sky and residual heating rates (the profiles are averaged over the tropical subsidence areas).

Fig. 4.4 shows the ensemble mean tropical subsidence profiles for SMF , σ , $A \downarrow$, Q_T , Q_{rad} and Q_{res} for the control climate and the forced climate. The difference between the profiles confirms once more that the circulation weakens, most prominently in the lower part of the troposphere. As the surface is not allowed to heat, which would impact the lapse rate, the direct effect of CO_2 increase on the mean static stability is almost undetectable. This is not the case for the subsidence area and heating rates. The subsidence area increases throughout the height of the troposphere. In the case of Q_T the change is driven by the change in Q_{rad} , which means a weaker atmospheric cooling in the lower and mid troposphere.

After investigating the response of each variable to CO₂ forcing, I now look at the contribution of the respective change to the general change in tropical overturning circulation (Fig. 4.5). According to equations (4.5) and (4.6), a relative increase in subsidence area and in heating rate will force an increase in circulation intensity, while an increase in static stability will dampen the circulation. As mentioned above, the circulation weakens significantly in the lower and mid troposphere. I find that this weakening is of 3 – 5% in the ensemble mean (Fig. 4.5a, red line) and the ensemble spread of the maximum decrease in circulation strength is 1 – 8% (Fig. 4.5a, gray lines). Fig. 4.5b–f present the contributions of σ , $A \downarrow$, Q_T , Q_{rad} and Q_{res} changes, respectively. The static stability and subsidence area response to CO₂ forcing bring around 4% and 1% enhancement to the circulation, respectively. These are counteracted by the CO₂ effect on the total heating rate: Q_T decreases by 7 – 8% and causes a general weakening of the circulation. The change in total heating rate is dominated by the change in clear-sky heating rate, which is reduced by around 10%. However, above 400 hPa, the total and radiative heating rates become slightly more negative (the atmosphere cools more). At the same time $A \downarrow$ increases most prominently in this tropospheric region as well. These findings explain the slight increase in SMF in the upper troposphere, suggesting stronger subsidence. This result goes in line with the narrowing of the ITCZ, which intensifies the convection and the divergent mass flow at the tropopause height, with subsequent subsidence increase in the tropical upper troposphere.

I note that Fig. 4.5b–f show a clear outlier: HadGEM2-A. This may represent an effect of the model’s inability to accurately represent tropical precipitation processes [Haywood et al., 2016]. Also, in Fig. 4.4c I notice 3 distinct groups of GCMs. This grouping is caused not only by the model configuration, but also by the presence of a double ITCZ in the climate simulation of some models (CNRM-CM5, IPSL-CM5A-LR).

Considering the above, I find that the fast response of the tropical overturning circulation to CO₂ quadrupling in an aqua-planet setup exhibits a weakening of around 4%, similar to the one found by He and Soden [2015]. This weakening can be decomposed into a sum of contributions from static stability, subsidence area and heating rate. Fig. 4.5a shows that the calculated relative change in subsidence mass flow can be reasonably well approximated by the sums of contributions, as presented in equations (4.5) and (4.6). However, the sum from equation (4.6) is deviating stronger from the calculated change and this is most probably related to the calculation of Q_{rad} with PSRAD, as I use the same mean profiles of absorption species for all GCMs. Based on this decomposition, I find that the driver of the change in circulation is the radiative effect of CO₂ on the clear-sky heating rate, reconfirming previous studies [Bony et al., 2013; He and Soden, 2015]. The results from the ensemble GCMs still vary considerably due to the model configuration and initialization, visible even in the tropical mean surface temperature, which has a spread of 293.8 – 296.5 K in the control climate (not shown). But the resulting

ensemble variance in the change of the investigated variables supports the robustness of the circulation weakening.

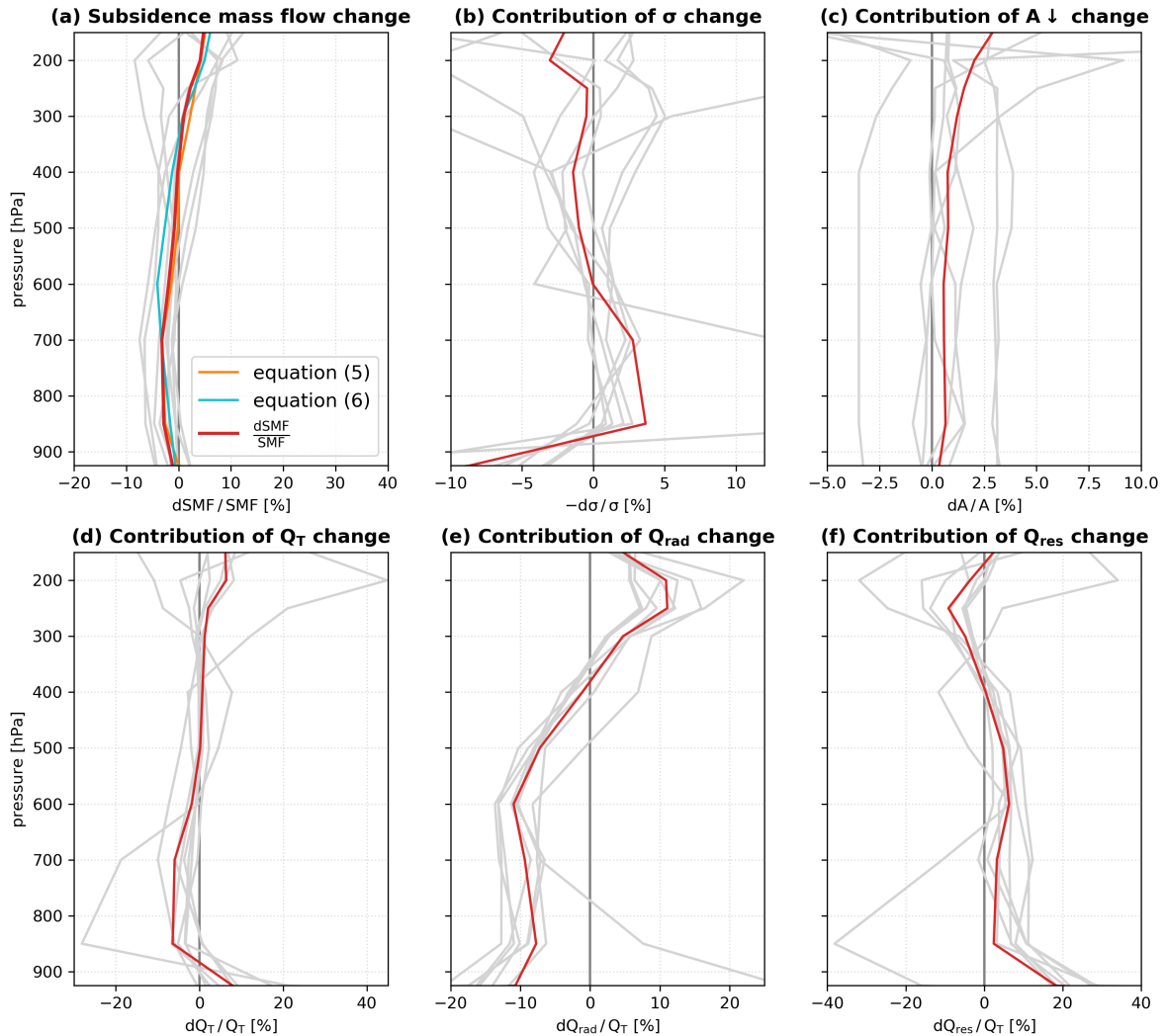


Figure 4.5: (a) Relative change of subsidence mass flow in the aqua-planet experiments. The solid line present a comparison of this change calculated following equations (4.1), (4.5) and (4.6). (b)–(f) The contribution to the change in SMF of static stability change, subsidence area change, total, clear-sky and residual heating rate change, respectively. The *grey lines* represent the corresponding results for every ensemble member (in (a) they show the change in SMF according to equation (4.1)).

4.3 The circulation response in the AMIP experiments

In comparison to the aqua-planet experiments, in the amip experiments I find that, on the mean, the circulation weakens (in response to CO_2 increase) throughout the troposphere (Fig. 4.6a), not only in its lower part. This more uniform tendency is driven by the different change pattern

between the subsidence areas over land and over ocean. The change over ocean is similar to the aqua-planet results: most of the change is projected for the lower troposphere. Over land, however, I detect a significant weakening in the upper troposphere as well. This is related to the increasing land surface temperatures and their effect on the air column above. Another difference between the aqua-planet and amip experiments is in the circulation intensity itself: the aqua-planet has a much more vigorous circulation in the tropics. This is easily explained by the setup of the experiments, as the aqua-planet has no axial tilting and therefore the tropics receive the same amount of solar energy year-round compared to the amip realistic planet system. This aspect can also explain the static stability profiles' difference between amip and aqua experiments. Judging by the height of the sudden increase in static stability, the tropopause is on the mean situated higher in the aqua-planet system than in the amip system (Fig. 4.6b). However, this does not change the response of σ to CO₂ quadrupling, as its profile barely changes. The differential heating of land and ocean in the amip experiments leads to opposing tendencies in subsidence area under increased CO₂ forcing: it shrinks over land and expands over ocean (Fig. 4.6c), as was shown previously by Bony et al. [2013]. Nonetheless, the total tropical subsidence area change is driven by the change over ocean, as here the area is around 3 times as big as the area over land. The heating rates have similar values in the aqua and amip experiments, as well as the same tendencies: I find again a less cooling atmosphere in the forced climate (Fig. 4.6d–f). There is, however, a clear difference between experiments in residual heating rates, which are larger in the amip experiment, especially in the lower troposphere. This difference between the aqua and amip experiments, as well as the larger difference within the amip experiments, may be related to a different cloud regime and a more irregular flow on a planet with land surfaces, and to the response of the extratropical systems to CO₂ forcing, such as the equatorward shift of the storm tracks and increased lateral eddy mixing [Butler et al., 2010].

As mentioned earlier, there is a much more vertically uniform change in circulation (subsidence mass flow) in the amip experiments in comparison to the aqua-planet experiments. As can be seen from Fig. 4.7, in the tropics this change amounts to 3 – 4% in the lower troposphere and is dominated by the change over ocean. Towards the tropopause the general change decreases to 0%; in comparison, in the aqua-planet experiments I find an increase of around 3% near the tropopause. Here the pattern is significantly impacted by the change over land, where the circulation decreases uniformly throughout the troposphere by around 4%. Such a difference between the lower and upper troposphere in comparison to the aqua-planet experiments is noticed in the other variables, too. However, this does not impact my findings related to the main contributor to the circulation weakening: in the amip experiments I find that it is again the decrease of radiative heating rate that dominates the circulation variation.

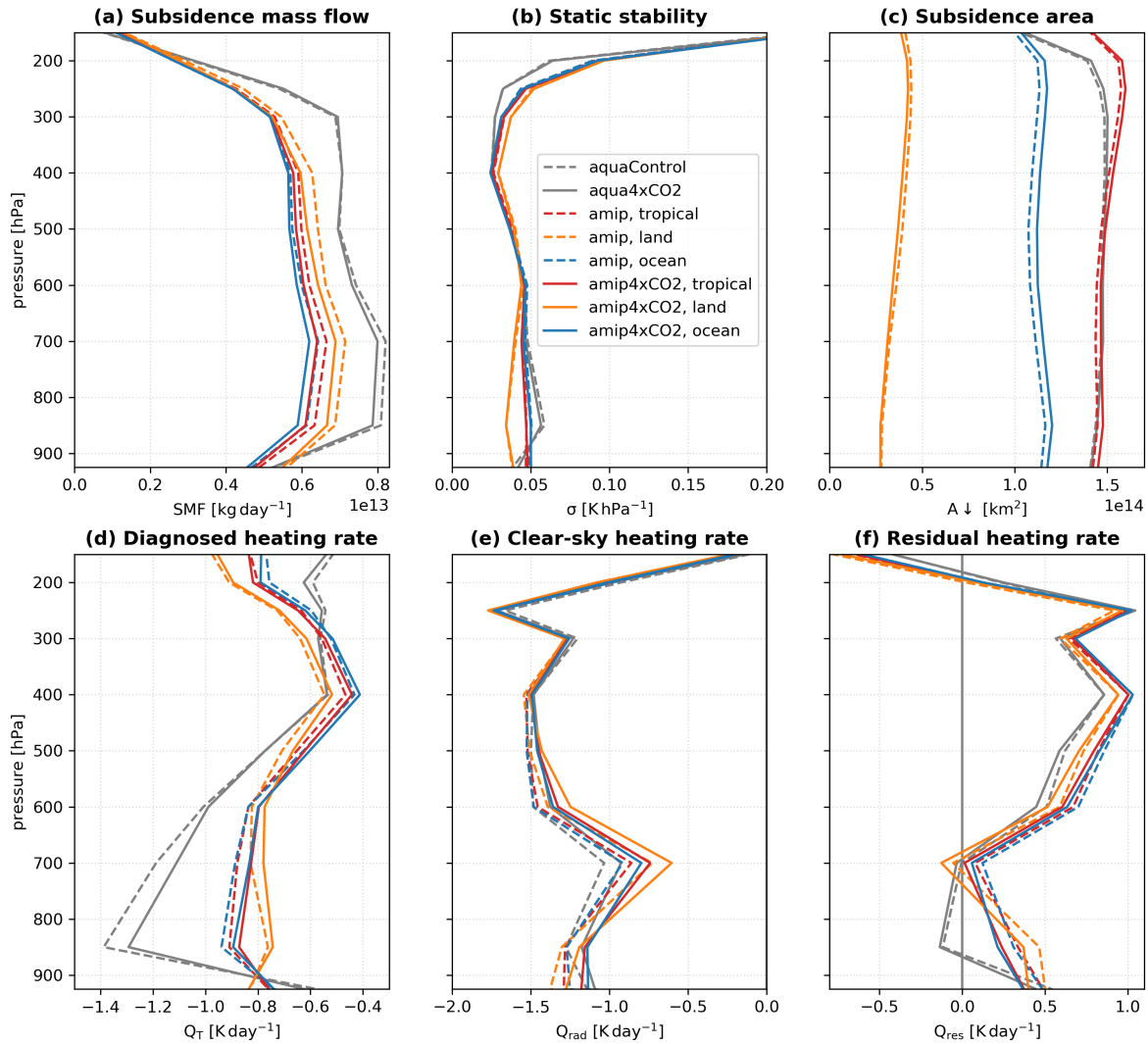


Figure 4.6: amip (*dashed lines*) and amip4xCO2 (*solid lines*) ensemble mean profiles of (a) subsidence mass flow, (b) static stability, (c) tropical subsidence area, (d) total, (e) clear-sky and (f) residual heating rates (the profiles are averaged over the tropical subsidence areas). The respective results are presented for the entire tropical subsidence area (*red lines*), as well as over land (*orange lines*) and over ocean (*blue lines*). The corresponding profiles from the aqua-planet experiments are presented in *grey lines* for comparison.

Although the amip experiments' setup introduces additional sources for the potential tropical circulation change, I find that regardless of the presence of land-sea contrast the circulation weakens. The main driver of this change in the amip case is also the direct effect of CO₂ increase on the radiative heating rate. However, the differential heating of land and ocean impacts the vertical distribution of this weakening by not limiting it to the lower troposphere.

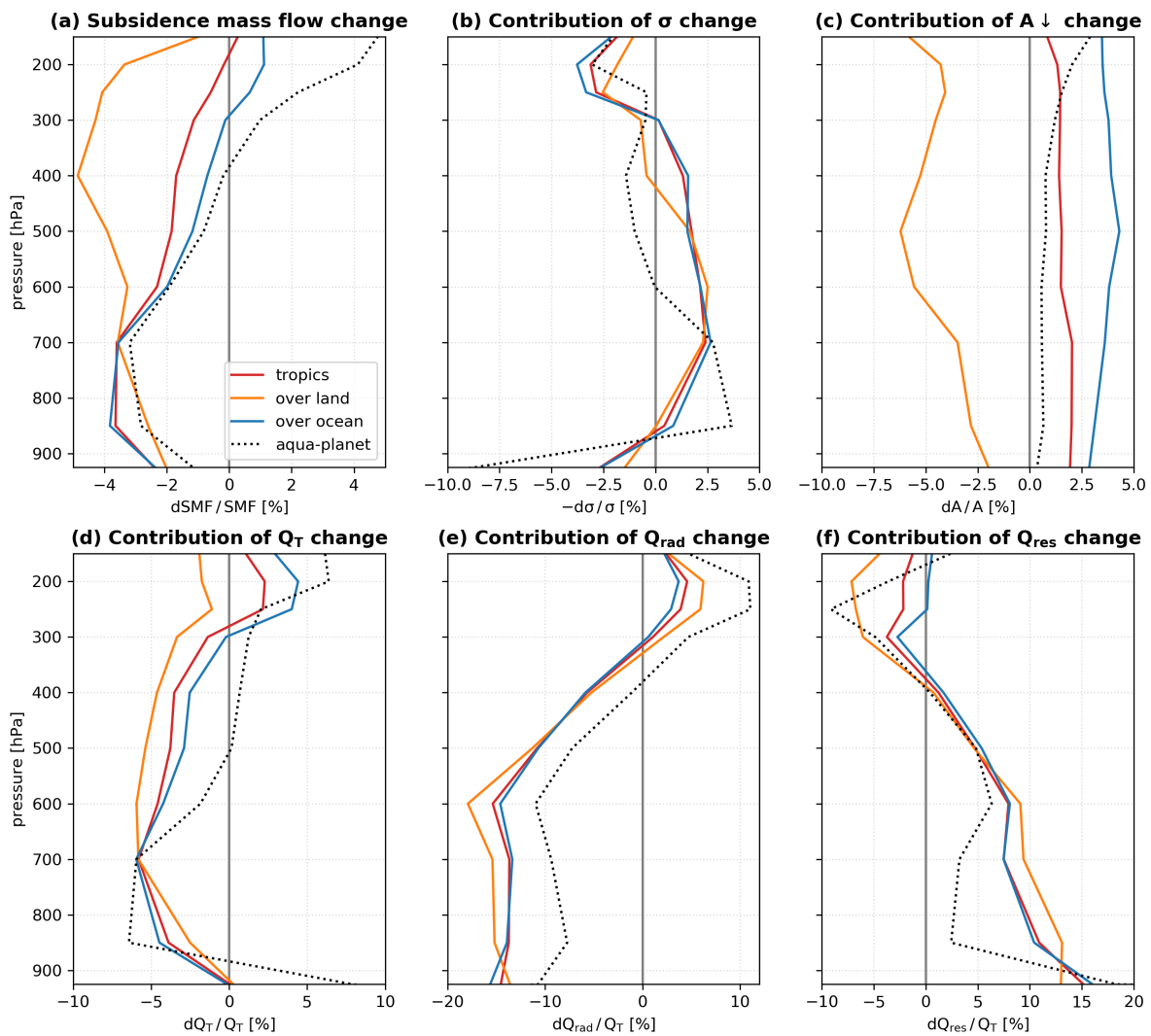


Figure 4.7: (a) Relative change of subsidence mass flow in the amip experiments. (b)–(f) The contribution to the change in *SMF* of static stability change, subsidence area change, total, clear-sky and residual heating rate change, respectively. The respective results are presented for the entire tropical subsidence area (red lines), as well as over land (orange lines) and over ocean (blue lines). The results from the aqua-planet experiments are presented in dotted lines for comparison.

4.4 Does CO₂ impact the variability of the circulation?

Fig. 4.3 shows a high zonal variance of patterns for the subsidence mass flow and the heating rates. Here I investigate in a simplistic approach whether the CO₂ forcing impacts the variability of these parameters: I use the ratio between the standard deviation and the mean of a time series, i.e. the coefficient of variance *CV*. This coefficient allows me to assess whether the forcing

impacts only the mean state (when CV does not change significantly, even though the mean and the standard deviation change) or the variability of the system (CV varies considerably).

Fig. 4.8 shows the corresponding standard deviation profiles for subsidence mass flow, static stability, subsidence area and heating rates, while Fig. 4.9 shows the corresponding coefficient of variance profiles. The standard deviation profiles for the two experiments are similar for each separate parameter, but there are apparent changes in the standard deviation of the heating rates, where the difference varies strongly on the vertical. The highest variance is present for SMF (Fig. 4.9a), where the standard deviation is around 50 – 60% of the mean. This is in accordance with the variance I already see in Fig. 4.3. The static stability varies quite narrowly in the lower troposphere in both aquaControl and aqua4xCO₂ (5 – 12% of the mean), but the value is slightly larger in the forced climate. The variance increases gradually towards the upper troposphere up to 15 – 20% in both experiments, the forced climate still surpassing the control climate. This links to the sudden increase of static stability close to the tropopause and the subsequent increase in its variance. The subsidence area also shows small variance throughout most of the troposphere (10 – 14%) and a sudden increase in the tropopause region. This picture is very similar for both experiments and the mentioned sudden increase may arise just from sampling, as close to the tropopause the area decreases significantly and the number of analysed profiles is small.

Though the heating rates' standard deviation differs evidently in the two aqua-planet experiments (Fig. 4.8d), the coefficient of variance suggests that the system is maintaining its variability throughout the atmosphere (Fig. 4.9d). The large negative values of the coefficient for Q_{res} in the layer 700 – 850 hPa are explained by the difference in magnitude between the experiments: e.g. at 700 hPa the mean is very close to zero (Fig. 4.4d), while the standard variation is 0.16 – 0.20 K day⁻¹ (Fig. 4.8d). Except for these outliers, Q_{res} also shows, as the other variables, that the climate system is adjusting to the forcing mostly by changing the mean values of the parameters, but not their variance. Additionally, I confirm that in the subsidence regions the atmosphere is quite uniform, except in the boundary layer and in the vicinity of the tropopause, where the local processes affect the variance.

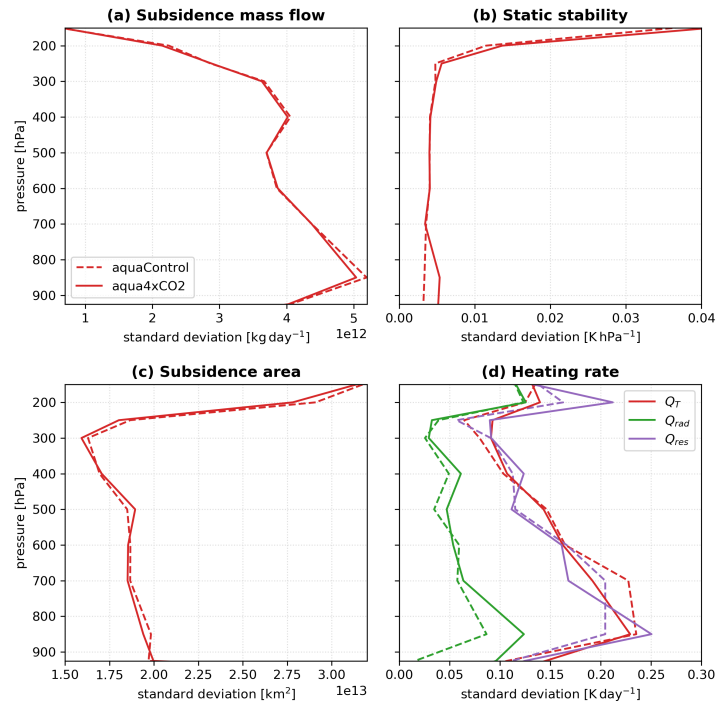


Figure 4.8: aquaControl (*dashed lines*) and aqua4xCO₂ (*solid lines*) ensemble standard deviation for the mean profiles of (a) subsidence mass flow, (b) static stability, (c) tropical subsidence area, and (d) total, clear-sky and residual heating rates (the profiles are averaged over the tropical subsidence areas).

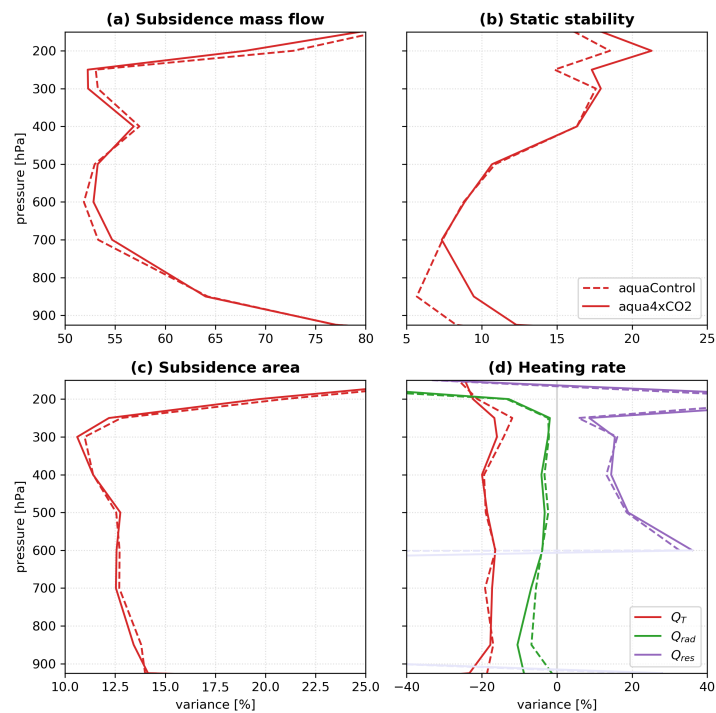


Figure 4.9: aquaControl (*dashed lines*) and aqua4xCO₂ (*solid lines*) ensemble coefficient of variance for the mean profiles of (a) subsidence mass flow, (b) static stability, (c) tropical subsidence area, and (d) total, clear-sky and residual heating rates (the profiles are averaged over the subsidence areas).

By applying the same simple analysis to the amip experiments (Fig. 4.10), I find that, except for the subsidence area and the residual heating rate, the variance of variables in the forced climate does not change or becomes smaller than in the control climate (note that the coefficient of variance for Q_T and Q_{rad} is negative and a positive change corresponds to a decrease in variance). This supports the findings from the aqua-planet experiments in that the forcing impacts the mean climate state more than its variability.

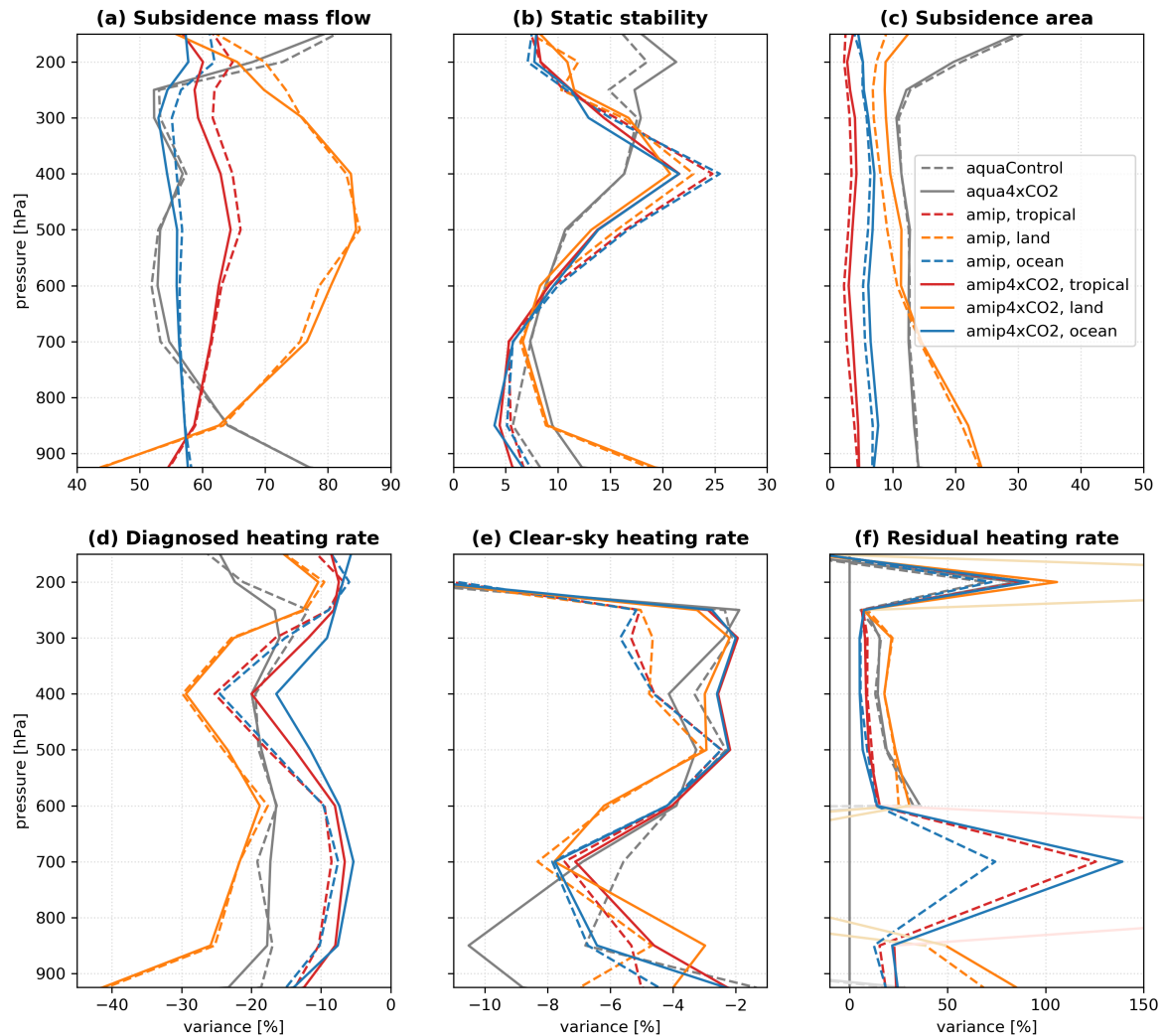


Figure 4.10: amip (*dashed lines*) and amip4xCO₂ (*solid lines*) ensemble coefficient of variance for the mean profiles of (a) subsidence mass flow, (b) static stability, (c) tropical subsidence area, (d) total, (e) clear-sky and (f) residual heating rates (the profiles are averaged over the tropical subsidence areas). *Note:* The respective results are presented for the entire tropical subsidence area (*red lines*), as well as over land (*orange lines*) and over ocean (*blue lines*). The corresponding profiles from the aqua-planet experiments are presented in *grey lines* for comparison.

4.5 The slow response of the tropical circulation to CO₂ forcing

A comparison of the fast response of the circulation with its slow response to CO₂ increase, in uncoupled and coupled experiments, can further the understanding of the time and space scales of the atmospheric dynamics response to anthropogenic forcing without limiting the contributions to the atmospheric processes only.

The slow response of the circulation to increased CO₂ refers here to the combined actions of the greenhouse effect amplification and the subsequent climate system feedbacks. The advantage of the CMIP5 tiered experiments is that I can separately investigate the effect of CO₂ and the subsequent (slower) increase in surface temperature by analysing the results from the aqua4xCO₂/amip4xCO₂ and aqua4K/amip4K. This comparative investigation will further our understanding of the changes detected in the coupled abrupt4xCO₂ experiment, in which the impact of the factors combine.

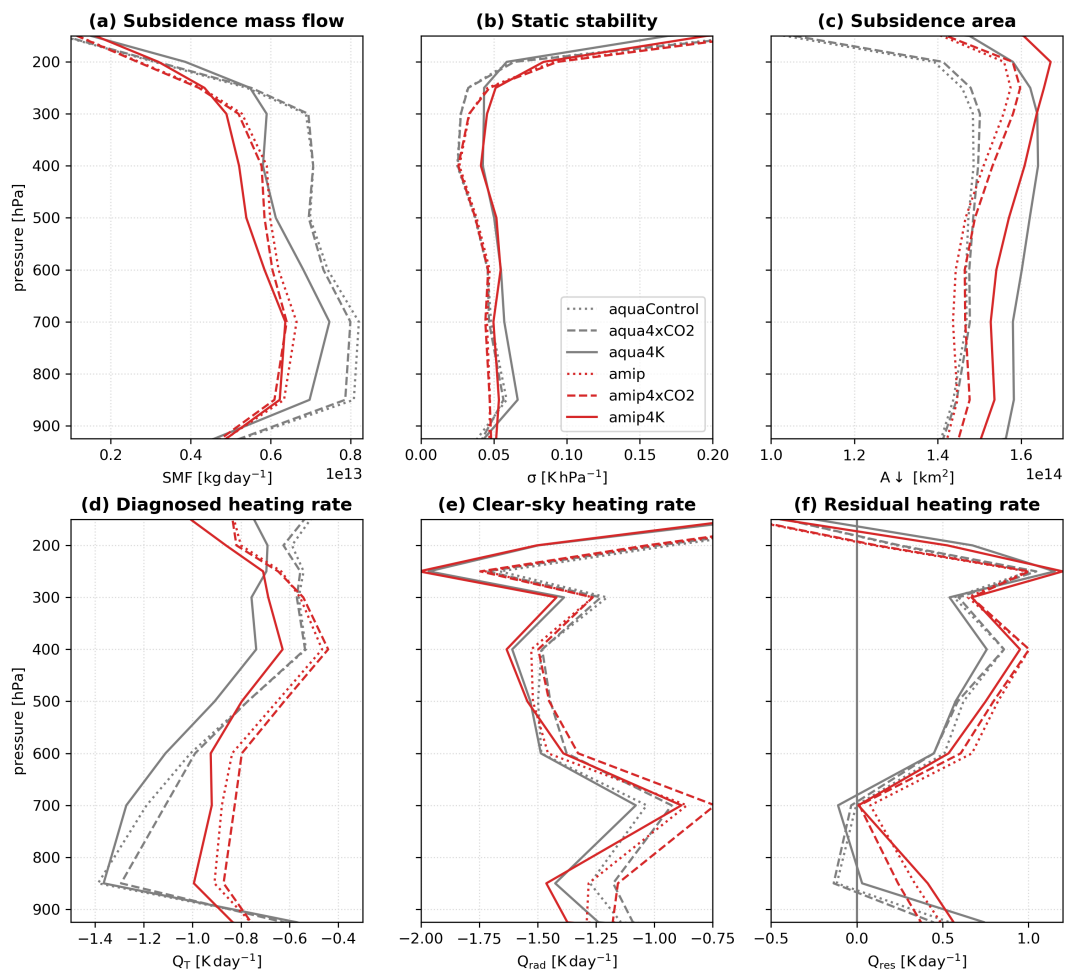


Figure 4.11: Ensemble mean tropical profiles of (a) subsidence mass flow, (b) static stability, (c) tropical subsidence area, (d) total, (e) clear-sky and (f) residual heating rates in the aqua-planet and amip experiments.

I continue the research approach from the previous sections by assessing the change in circulation induced by a sudden increase in surface temperature by 4 K. I find that the effect of this sudden increase is a stronger slowdown of the tropical circulation compared to the effect of CO₂ (Fig. 4.11a). The vertical pattern of change is again different between the aqua- and the Earth-like planets. Under the presence of land the circulation changes non-uniformly on the vertical: this time, the intensity decreases significantly in the upper-troposphere, while in the lower troposphere is close to the change induced by the quadrupling of CO₂.

The impact of the surface temperature rise on the static stability, subsidence area and diabatic heating rate is rather uniform vertically (Fig. 4.11b–d). The static stability increases significantly compared to its response to CO₂ increase. But the land-sea contrast appears to have an effect on the change in the lower troposphere, where the increase in static stability is around half as strong as in the upper troposphere (in the aqua-planet experiment there is also less increase in the lower troposphere, but the difference to the upper troposphere is smaller). Compared to aqua4xCO₂/amip4xCO₂, in the aqua4K/amip4K experiments the subsidence area increases considerably: the difference to the control is 10–12 times larger in the aqua-planet experiments and 3–4 times larger in the amip experiments. Whereas the total diabatic heating rate mostly increases as a response to CO₂ quadrupling, it becomes more negative when the surface heats: the atmosphere cools stronger, by up to 0.2 K day⁻¹ in the upper troposphere. This change is dominated largely by the response of the radiative heating rate to CO₂ forcing (Fig. 4.11e).

Fig. 4.12 shows the relative change in circulation and the contributions of each parameter's change. I find that the circulation weakens by 0–5% in the lower troposphere and that this response is dominated by the weakening over the ocean. In the upper troposphere the weakening is more intense: up to 12–18%. Here, the change in radiative heating rate leads mostly to a strengthening of the circulation (Fig. 4.12e), except in the middle troposphere. I can speculate that here the atmosphere cools less radiatively, but this effect is counteracted diabatically by advection of dry air (Fig. 4.12f), as suggested by Lu et al. [2008]. As a result, the total heating rate change as a result of surface warming has a positive effect on the circulation (Fig. 4.12d). The same goes for the subsidence area change that increases by around 6% and is dominated by the significant increase over land (Fig. 4.12c). However, these positive contributions to the circulation response are dominated by the negative contribution resulting from the increase in static stability. The latter increases by around 12% in the lower troposphere and by up to 60–70% in the upper troposphere (Fig. 4.12b), driving the overall vertical pattern of the circulation slowdown.

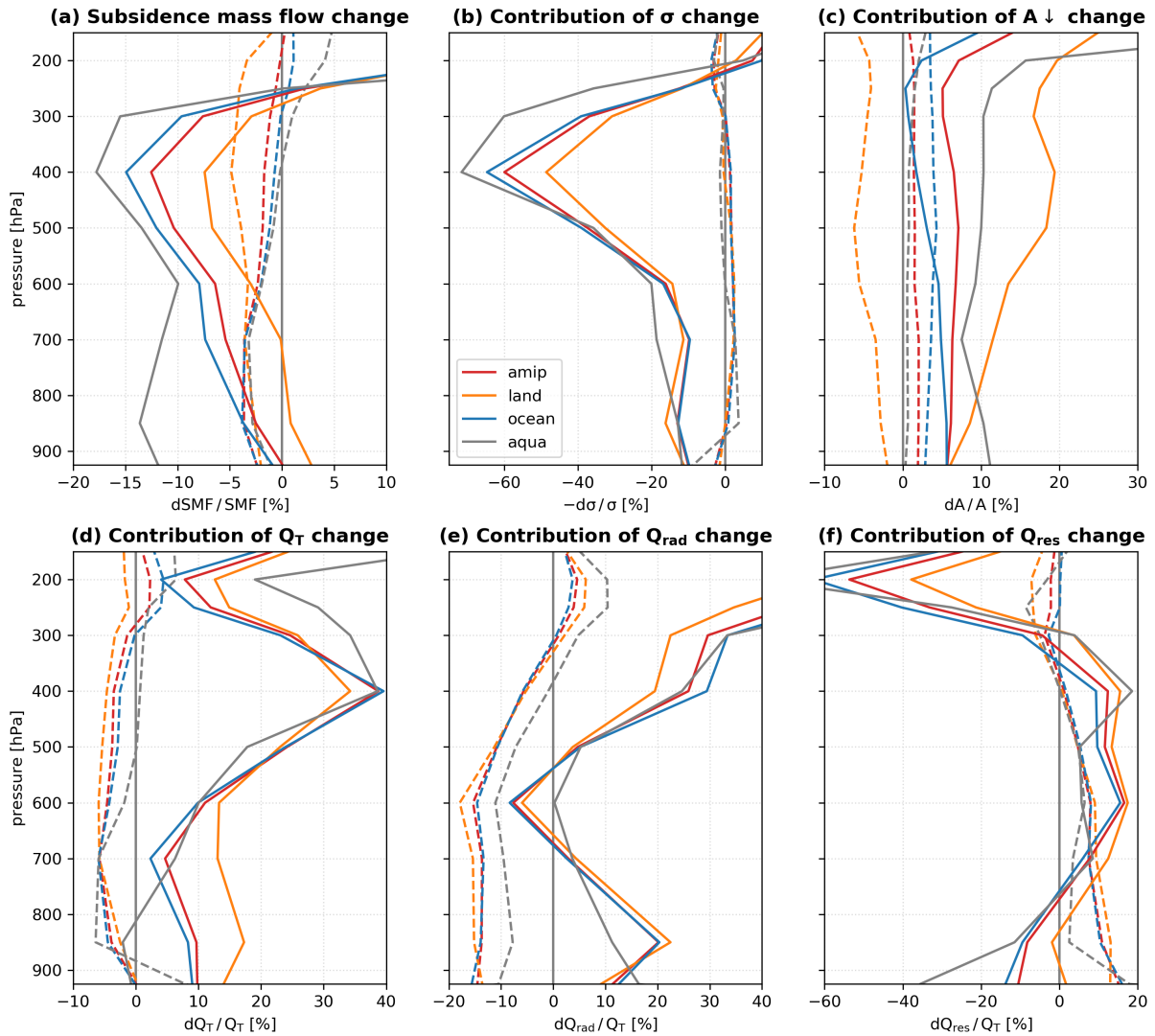


Figure 4.12: Ensemble mean tropical profiles of relative change in (a) subsidence mass flow, (b) static stability, (c) tropical subsidence area, (d) total, (e) clear-sky and (f) residual heating rates. The *grey lines* refer to the aqua-planet experiments, the *red lines* – to the mean tropical profile in the amip experiments, the *orange lines* – to the mean profile over land, the *blue lines* – to the mean profile over ocean; the *dashed lines* present the respective profile in the experiment with abrupt quadrupling of CO₂, the *solid lines* – in the experiment with abrupt 4 K increase in surface temperature.

As I see above, there are two main mechanisms driving the circulation weakening in a realistic climate system: the atmosphere cooling less as a result of CO₂ forcing increase and the enhanced static stability as a result of the rise of surface temperature. These effects are related, but occur in different time frames. Considering a coupled climate system in which the concentration of CO₂ is abruptly quadrupled and then kept at the same level (the abrupt4xCO₂ CMIP5 experiment), I find that the surface temperature starts increasing immediately, considering climate time-scales (by up to 1 K in the first year, Fig. 4.13). However, due to the slow rate of CO₂ exchange between

the surface waters and the deep ocean, it takes more than 50–200 years for the system to reach a quasi-equilibrium. Considering these distinct time frames, a brief investigation of the response of the circulation in a coupled climate system will be here attempted by comparing the means over the first year after CO₂ quadrupling, as an immediate response to the forcing, and over the last 110–140 years, as a quasi-equilibrium climate state.

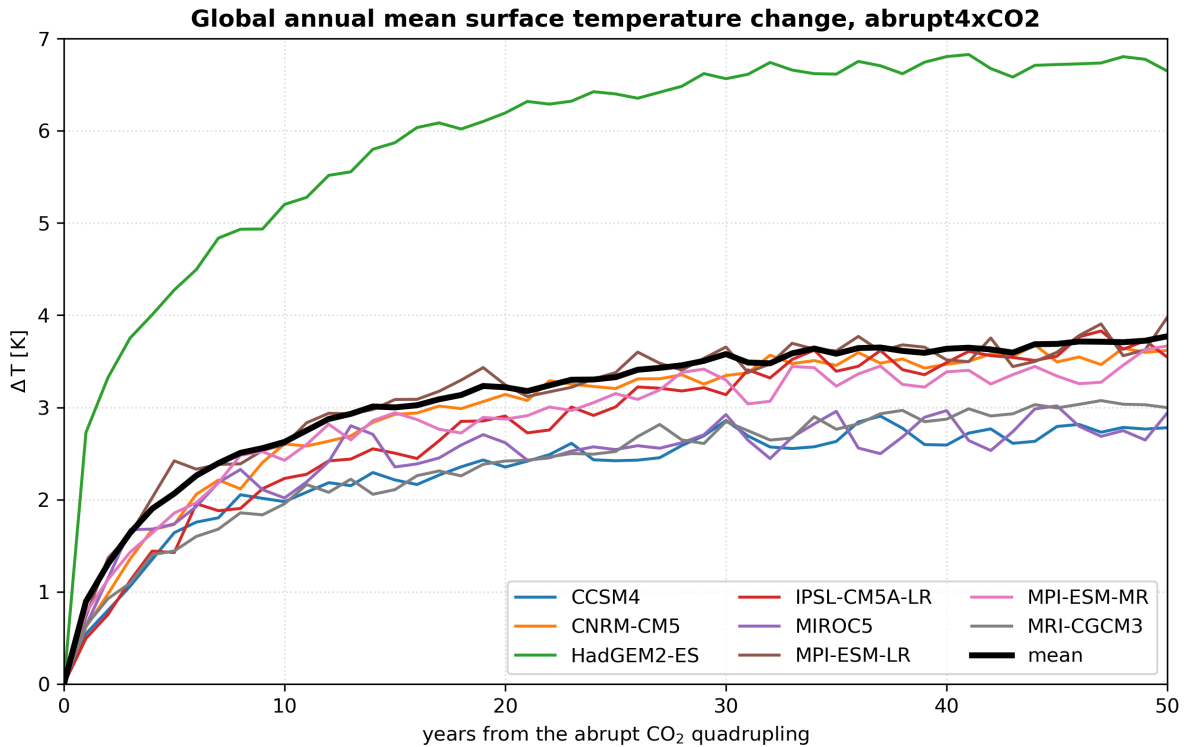


Figure 4.13: Global mean annual surface temperature variation after an abrupt CO₂ quadrupling, as found in 8 CMIP5 GCM runs for the abrupt4xCO₂ experiment.

The changes in the circulation intensity and the contributors to the change are shown in Fig. 4.14 for the first year and years 110–140 in abrupt4xCO₂ compared to the responses detected in the amip4xCO₂ and amip4K. Note that the impact of CO₂ increase is still present in the first year of the coupled experiment, as the radiative heating rate vertical profile of change is similar to the amip4xCO₂ profile. Evidently, the mean profile of change for the last 30 years of the experiment indicates to the effect of the increased surface temperature on the heating rate (Fig. 4.14e). In the case of the static stability change, the effect of the increase in temperature is observed already in the first year (Fig. 4.14b). Therefore, the fast response of the circulation to CO₂ can still be detected at time scales smaller than 1 year, consistent with the findings of Bony et al. [2013]. However, it is also noticeable that the circulation barely changes in the first year. The fact that in the first year the positive contribution of residual heating rate change is comparable to the sum of the negative contributions of the change in static stability and radiative heating rate (Fig. 4.14) suggests that the adjustment of the cloud systems and air masses

exchange to the increased forcing occurs at this time scale and has a considerable impact on the circulation.

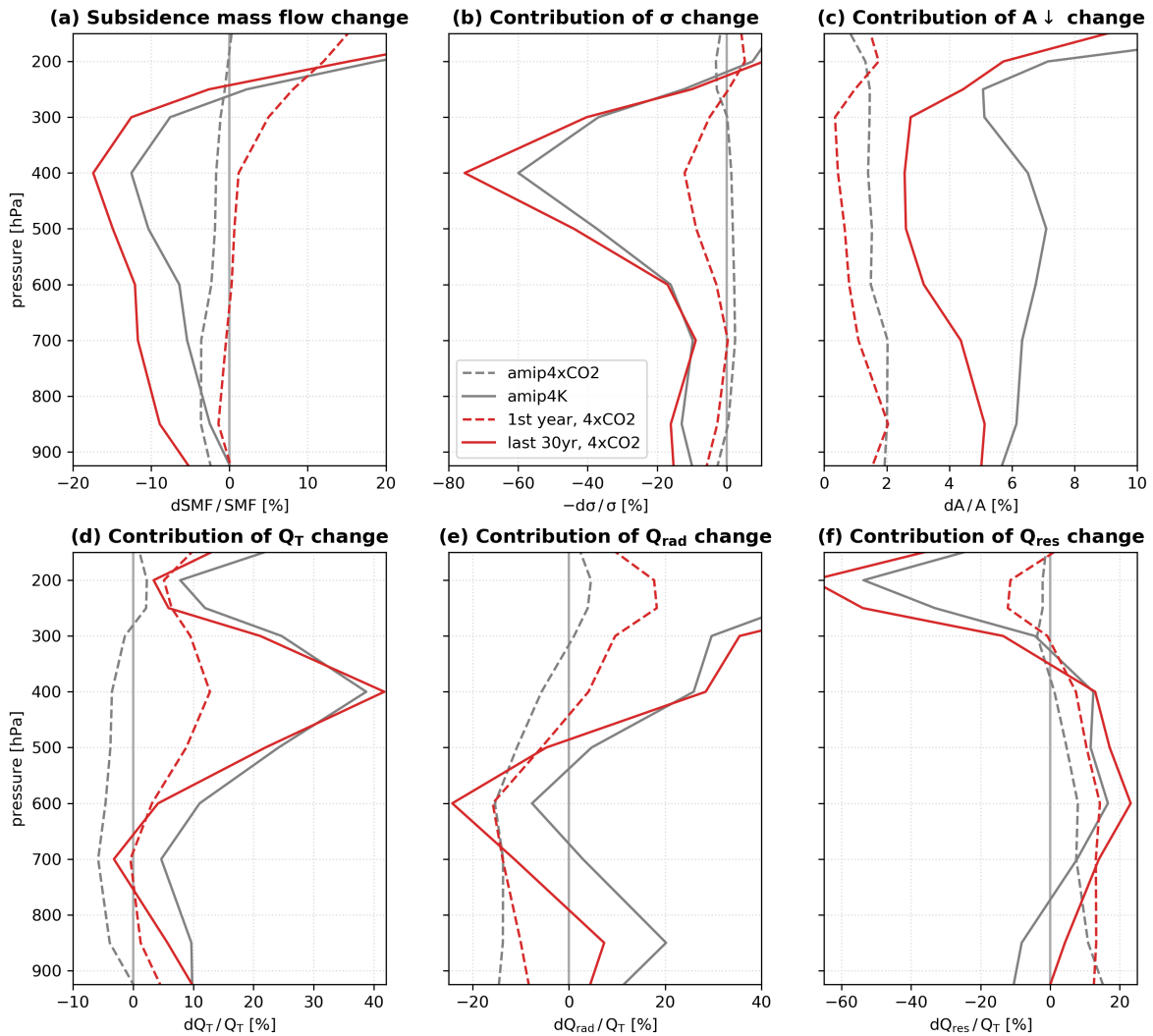


Figure 4.14: Ensemble mean tropical profiles of relative change in (a) subsidence mass flow, (b) static stability, (c) tropical subsidence area, (d) total, (e) clear-sky and (f) residual heating rates. The grey lines refer to the amip experiments, the red lines – to the coupled experiments (dashed lines for the 1st year mean in abrupt4xCO₂, solid lines for the last 30-year mean in abrupt4xCO₂).

Concluding, I found that the likely tropical circulation weakening as a result of increased CO₂ forcing is driven by different mechanisms depending on the investigated time frame. In the first months after a hypothetical sudden increase in CO₂ concentration, the circulation will respond mostly to the radiative effect of CO₂, i.e. the decreased atmospheric cooling rate. But the rapid increase in surface temperature would enhance the static stability quickly enough for this effect to be detectable (and to overtake the fast response) 1 year after the concentration increase.

5 Conclusions and outlook

5.1 Conclusions

In this work I investigated some aspects of the tropical circulation response to anthropogenic CO₂ forcing. This analysis consists of two parts, one investigating the robustness of the Walker circulation response to this forcing, and the other looking into the fast response of the tropical overturning circulation to the CO₂ radiative effect. In these two parts several sources of the current intermodel spread were considered, such as the current understanding of the circulation drivers, the mechanisms for the circulation change, the GCM configuration and parametrization schemes. Sources of uncertainty for the estimation of the circulation change were also discussed, such as the natural variability, the quantification of the circulation intensity, as well as the interaction between the large- and the small-scale processes.

The robustness of a weaker Pacific Walker circulation under constant increase in CO₂ forcing and its sensitivity to natural variability, GCM configuration and the chosen indexing method was investigated in the first part of the study (Chapter 3). The analysis was carried out on two ensembles of GCMs simulations of the CMIP5 1pctCO₂ experiment setting - the MPI ensemble (based on slightly perturbed initial climate states) and the CMIP5 ensemble, consisting of distinct GCMs. Three simple indices were used for the computation of the Walker circulation intensity time series.

I find that, regardless of the ensemble and chosen indexing method, a weakening Pacific Walker Cell is the most probable scenario for a transient CO₂ increase. The variance of this response is of comparable magnitude in the CMIP5 ensemble and the MPI ensemble, suggesting that the Walker circulation trend for the considered time period of 70-140 years is as dependent on the initial climate state as on the model physics. The comparison in the projection of mean surface temperature and circulation intensity change by the moment of CO₂ doubling shows much less variance in the surface temperature than in the circulation intensity, regardless of the ensemble. This difference seems to reflect the better understanding and simulation of the thermodynamical changes in GCMs than of the atmospheric circulation's response to increased forcing, a general point that has been argued by [Shepherd \[2014\]](#).

An index-only comparison between simulated Walker circulation changes must consider the variability and sensitivity of the index's base-parameter to increased CO₂ concentration. The MSLP-index (based on the MSLP anomaly difference between the East and West Pacific) is indicative of the intensity of the lower branch of the Pacific Walker Cell and is highly sensitive to the internal variability of MSLP and the parametrization of boundary layer processes within the GCM. The other two investigated indices are the ω_{500} -index, derived from the 500 hPa vertical velocity anomaly difference between East and West Pacific, and the χ_{200} -index, derived from the maximum 200 hPa velocity potential anomaly over the West Pacific. These two indices reveal a dependence on the cloud and convection parametrization of the climate model, as they represent the ascending branch and the upper tropospheric branch of the cell, respectively. Therefore, a future study of the Walker circulation change in a specific climate experiment should not take into account the model's physical basis and parametrizations exclusively. The quantification of the circulation's intensity variation should also consider the sensitivity of the index's base-parameter to various atmospheric processes and forcings.

This work was not aimed to identify the best index to represent the intensity of the Walker circulation. I considered widely accepted indices and showed that – though they relate to the same complex phenomenon, the Pacific Walker Cell – the correlation between their time series is not large enough to insure the same variance of the response. Also, because of these differences, in some GCMs the three indices suggest distinct changes of intensity. This analysis suggests that these indices are in fact each describing one distinct aspect of the complex Walker Cell phenomenon. The three indices regarded in this study all use quasi-surfaces, albeit at different altitudes and with focus on different parameters. The definitions of the MSLP- and ω_{500} - indices are based on fixed spatial boxes in the East and West Pacific. A spatial change in the structure of the cell (e.g. a decreased zonal extent) would likely require an update of this preset parameter. Also, as seen in the mean piControl cross-section of vertical velocity over the equatorial Pacific, there is significant variance in the representation of the Pacific Walker Cell in the GCMs, even in an unforced climate system. This result leads again to the possible need of adjusting the indices to each GCM and/or to the choice of indices that are not confined to a limited spatial box, as the MSLP- and ω_{500} - indices are. In perspective, another facet of the circulation change may be provided by an index describing the mass transport within the cell, which was beyond the scope of this study. Such an index, like the one based on zonal mass stream function, defined by [Yu and Zwiers \[2010\]](#), may indicate both intensity and structural changes of the cell.

I ranked the MPI and CMIP5 ensemble members according to their Walker circulation response and I investigated the differences between the runs/models that project the strongest weakening of the Pacific Walker Cell and those that project no change or a strengthening of the Cell. This revealed that the two groups are not obviously different in their representation

of the mean Walker circulation in the control climate; the difference only becomes apparent upon forcing. The forcing also amplifies the intermodel differences caused by the distinct representations of the interaction between small- and large-scale atmospheric processes. An analysis of the OLR changes over the tropical Pacific in the two identified groups also revealed that a strong weakening of the Walker circulation will be associated with a drier Maritime Continent, increased convection eastward from this region, and a warmer tropical Pacific in comparison to a strengthened circulation.

A secondary result of investigating the forced dynamical response of the Pacific Walker Cell is the apparent robustness of its structural response, that is the eastward shift of the ascending branch of the cell. This spatial response of the circulation may be detected in various indices, but also in basic climate elements, such as the pattern of OLR and surface temperature change across the tropical Pacific. This response to the warming climate may also partly explain the differences detected in the response of the Walker circulation: as two of the investigated indices are based on fixed boxes in the East and West Pacific, this shift of the ascending branch would impact the estimation of the MSLP and vertical velocity gradient across the Pacific.

Although the forced response, estimated from the CMIP5 ensemble mean, is a circulation slowdown, several individual ensemble members show a circulation strengthening even for quite long time periods. For CO₂ doubling during 70 years, 3–6 out of 28 CMIP5 ensemble members (depending on index) show a significant circulation speedup going against the ensemble mean trend, and for CO₂ quadrupling during 140 years, still 3–5 out of 28 models show this. This result is not limited to the CMIP5 ensemble: even in the MPI ensemble, where spread is driven exclusively by natural variability, up to 15 out of 68 members show a significant strengthening of the circulation going against the forced response, for the 70 year time period. And still 2 ensemble members show this for a 140 year time period, though the significance of the trend is slightly decreased. Thus, the uncertainty introduced in the simulation of the Walker circulation change by the GCM configuration and the choice of index, as well as the insufficient understanding of the circulation's internal variability, affect the confidence in and predictability of a weaker circulation under increased CO₂ forcing.

In summary, the answers to the research questions in the first part are:

- *What is the most probable response of the Walker circulation to a gradual increase in CO₂?* The Walker circulation is more likely to weaken in a warming climate system, with 54–75% of the CMIP5 GCMs supporting this statement.
- *How robust is this response?* The MPI ensemble members also support the weakening of the circulation as the most probable Walker circulation response (50–93% ensemble

members). However, this also shows that the natural variability plays an important role in the variation of the circulation, reducing the confidence in the robustness of the weakening.

- *Does the choice of metric for the Walker circulation intensity matter?* Yes. The choice of metric needs to correspond to the scope of any future studies, as each of the investigated indices for the intensity of the Walker circulation have been shown to describe a distinct feature in the atmospheric cell, to have distinct time variation and to have distinct sensitivity to boundary layer processes.
- *What are the reasons for the intermodel spread?* I found that the difference between the representation of the Walker circulation in the CMIP5 GCMs becomes apparent upon forcing. In general, the forcing amplifies the intermodel spread within the representation of the relation between the large scale climate features and the small scale processes. Also, I found that, as a result of the link between the Walker circulation and ENSO, the ensemble members projecting the most intense slowdown of the circulation, also project the highest warming of the equatorial surface Pacific.
- *How does the detected change compare to the natural variability of the circulation?* By comparing the results from the MPI and the CMIP5 ensembles, I find evidence that the natural variability signal affects the assessment of change considerably.

In the second part of this thesis (Chapter 4), I investigated the fast response of the tropical overturning circulation to CO₂ forcing. The analysis was performed on an ensemble of 8 GCMs for the CMIP5 aqua-planet and amip experiments with abrupt CO₂ quadrupling from control levels, but with fixed sea surface temperature. I define a new metric for the circulation, the subsidence mass flow, which characterizes the subsidence strength in the tropics. In addition to the assessment of the change, this metric allows the quantification of the contribution of various processes to the total circulation change. By limiting my analysis to the subsidence regions, I reduce the impact of uncertainties arising from the GCM precipitation and convection parametrizations on my results.

I have confirmed that the tropical circulation weakens with rising CO₂ concentration, even when surface temperature is held fixed, as has been argued by [Bony et al. \[2013\]](#). In my metric, the weakening is 3–4% for a quadrupling of the CO₂ concentration, similar to the results of [He and Soden \[2015\]](#). The driver of this change is the CO₂ radiative effect on the atmospheric heating rate: the atmosphere cools less (by up to 15%) with larger CO₂ content, reducing the radiatively driven subsidence. This change in radiative heating rate dominates the opposing positive contributions of static stability change (up to 2–4%), subsidence area expansion (up to 1–2%), and of residual heating rate (up to 5–9%). This result is similar in both the aqua-

planet and the amip experiments: the direct radiative effect of CO₂ dominates the circulation change also for the planets with land surface, and overshadows the land-sea contrast changes. Nonetheless, the differential land-ocean heating in the amip experiments impacts the vertical pattern of circulation change. Here I find that the weakening of the tropical circulation is not limited to the lower troposphere, but extends (gradually decreasing in magnitude) towards the tropopause. Such a pattern is driven by the surface heating over land and the subsequent change in radiative fluxes throughout the atmospheric column. I also notice that the results obtained in the amip experiments over ocean slightly differ from the aqua-planet results. This may relate to the regional land-sea boundary interactions [Kamae et al., 2014] and a stronger dynamical variability in the Earth-like climate system. The variation patterns found here are similar in most of the ensemble members, which indicates a likely robustness of my findings, even though the study was limited to the 8 CMIP5 models that performed the aqua-planet experiments.

To summarize the results of the second part, the answers to the research questions are:

- *How does the tropical circulation change as response to the CO₂ forcing, but with no surface temperature adjustment?* The overturning circulation weakens by 3–4%, most prominently in the lower troposphere.
- *What are the relative contributions of the change in radiative heating rate and in static stability to the total change in circulation intensity?* If surface temperature does not adjust to the CO₂ quadrupling, the change in static stability would lead to an enhancement of the circulation by 2–4%. However, this effect is cancelled by the significant change in radiative heating rate, which independently leads to a circulation weakening of up to 15%.
- *How does the effect of land-sea contrast on the circulation change compare to the CO₂ impact?* It was found that in the presence of land-sea contrast, the circulation change, as well as the contributions to the change, are similar to the aqua-planet case. However, the heating of land affects the vertical extent of the weakening, which is not limited to the lower troposphere anymore, reaching the tropopause in the amip experiments.
- *Is the fast response detectable in the coupled experiments?* At time scales smaller than 1 year the fast response of the circulation is still detectable, but is quickly overtaken by the slow response resulting from the surface temperature rise in response to the greenhouse effect.

5.2 Outlook

The current and future variation of the atmospheric circulation belongs now to the most investigated topics in climate science. The impact these variations have on the climate patterns at regional scale makes this line of research a priority, as climate change at this scale has the potential to undergo more dramatic change than on the global scale [IPCC, 2013]. An example for this is the risk for the Maritime Continent to get drier as the Walker circulation weakens. Further investigations at a higher resolution and/or with regional climate modelling may shed light on the space and time scale of the precipitation regime changes.

The atmospheric circulation, in general, and the Walker circulation, in particular, are tightly linked to the ocean circulation. The progressing ocean circulation representation in the next-generation GCMs will provide a more accurate simulation of the dynamics in the Earth system, but it will also raise the need for updating the current knowledge, as well as the metrics used to quantify the intensity of the circulation. Another aspect of this analysis may consider the link between the Walker circulation and ENSO. Collins et al. [2010] argue that El Niño events' magnitude and frequency is not related to the Walker circulation slowdown. However, the large spread of the response of the circulation still provides enough arguments for a comparative investigation of the atmospheric dynamics and various variability modes, such as ENSO.

In Chapter 4, I present a new metric for the intensity of the tropical circulation to investigate the fast response of the circulation to increased CO₂ forcing. Additional research on time scales smaller than 1 year in coupled experiments may give details on the time extent of this fast response. Idealized experiments with neglected cloud radiative effect, such as the COOKIE (Clouds On-Off Klimate Intercomparison Experiment) experiments [Stevens et al., 2012], can also improve our understanding of the adjustment of the cloud systems to the increased forcing and the subsequent effect on the circulation intensity.

The metric's application is easily extendable for other purposes, such as the assessment of the circulation in other climate setups and/or in reanalysis. As the metric is limited to the subsidence regions, it also is applicable for the investigation of the variability of the dry regions, which stand out evidently in the subsidence mass flow field. As these regions benefit from less contamination of the radiative signal because of the reduced amount of clouds and increased atmospheric stability, they are easily observable with space-borne instruments and offer a less uncertain view on the radiative fluxes than the cloudy regions [Pincus et al., 2015]. The subsidence mass flow metric may therefore prove efficient in tracking the circulation changes in present climate by analysing satellite data records.

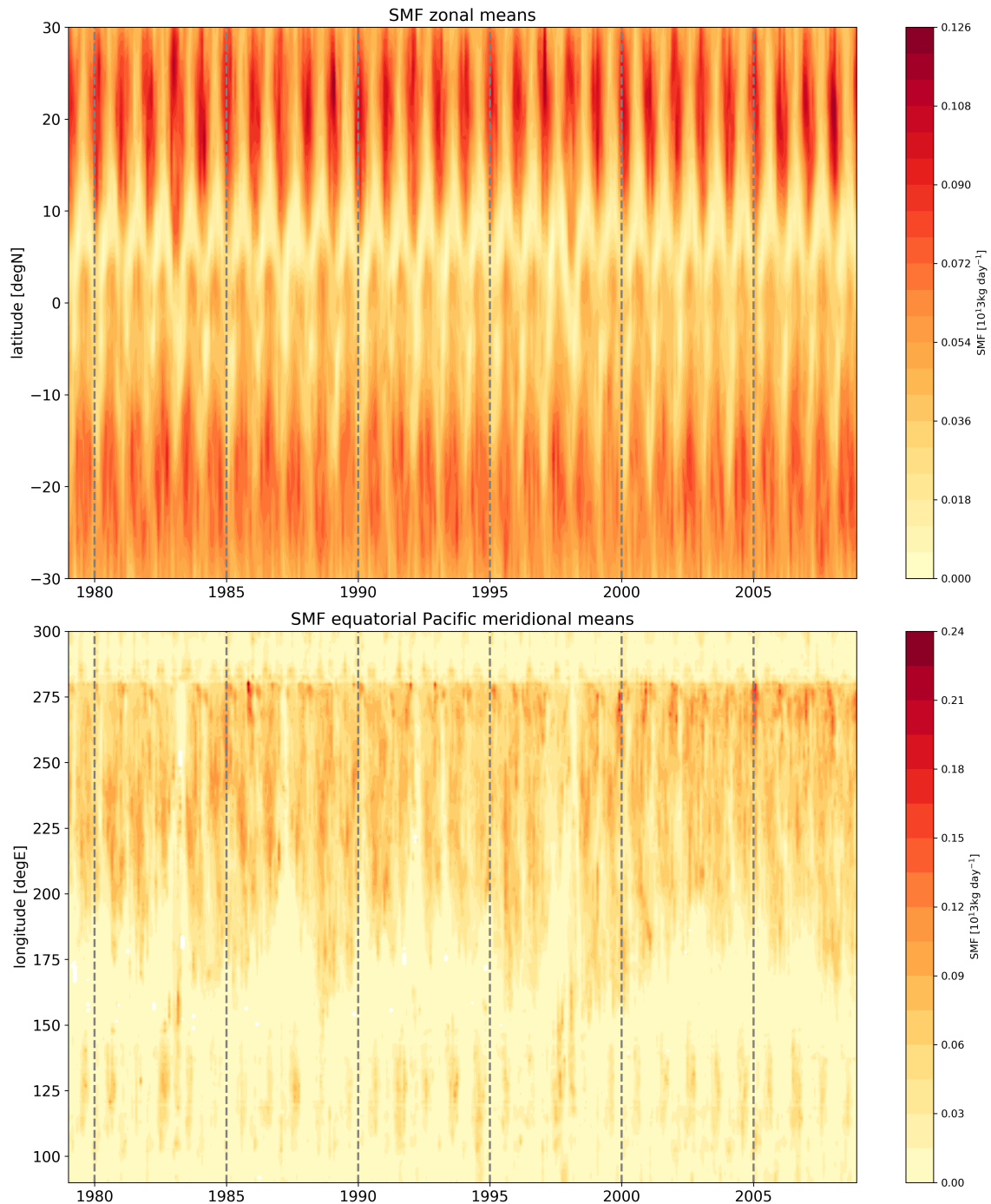


Figure 5.1: ERA-Interim monthly mean SMF, vertically averaged over the troposphere, presented in (*upper series*) zonal means and (*lower series*) meridional means over the equatorial Pacific (7.5°S-7.5°N, 90°E-60°W).

There is potential for the *SMF* metric to be applied for the investigation of the Hadley and Walker circulations' variation. Fig. 5.1 shows time series of zonal and meridional means of *SMF* in the ERA-Interim dataset. The seasonal cycle of the Hadley Cells is evident in the zonal means, as well as their intensity. The extent of the Pacific Walker Cell may be estimated

from the meridional means calculated over the tropical Pacific. Note here that the El Niño events of 1983–84 and 1997–98 stand out in both time series: in the zonal means (Hadley Cell) through extended strong subsidence area in the Northern Hemisphere and in the meridional means (Walker Cell) through very weak subsidence over the equatorial Pacific. The strong La Niña events of 1988–89, 1998–2000 and 2007–2008 also stand out over the equatorial Pacific through the eastward-extended subsidence areas. Supplementary, an orthogonal decomposition of the *SMF* field, similar to the decomposition proposed by [Tanaka et al. \[2004\]](#) for the velocity potential field, may be attempted in order to use this metric to quantify the Hadley and Walker circulations.

Publications

Peer-reviewed publications:

1. Plesca, E., Grützun, V., and Buehler, S. A. (2018). How robust is the weakening of the Pacific Walker circulation in CMIP5 idealized transient climate simulations? *Journal of Climate*, **31**(1): 81–97
2. Plesca, E., Buehler, S. A., Grützun, V. (2018, in review). The fast response of the tropical circulation to CO₂ forcing. *Journal of Climate*

Contribution to thesis supervision:

1. Lutzmann, J. (2017). Influence of ENSO on the astronomical observing conditions in the Atacama region. Master thesis, Universität Hamburg, Fachbereich Geowissenschaften, Meteorologisches Institut.

Bibliography

- Albern, N., Voigt, A., Buehler, S. A., and Grützun, V. (2018). Robust and non-robust impacts of atmospheric cloud-radiative interactions on the tropical circulation and its response to surface warming. *Geophysical Research Letters*.
- Alexander, M. A., Bladé, I., Newman, M., Lanzante, J. R., Lau, N.-C., and Scott, J. D. (2002). The atmospheric bridge: The influence of ENSO teleconnections on air–sea interaction over the global oceans. *Journal of Climate*, 15(16):2205–2231.
- Anderson, G. P., Clough, S. A., Kneizys, F., Chetwynd, J. H., and Shettle, E. P. (1986). AFGL atmospheric constituent profiles (0.120 km). Technical report, Air Force Geophysics Lab HANSCOM AFB MA.
- Arora, V., Scinocca, J., Boer, G., Christian, J., Denman, K., Flato, G., Kharin, V., Lee, W., and Merryfield, W. (2011). Carbon emission limits required to satisfy future representative concentration pathways of greenhouse gases. *Geophysical Research Letters*, 38(5).
- Bao, Q., Lin, P., Zhou, T., Liu, Y., Yu, Y., Wu, G., He, B., He, J., Li, L., Li, J., et al. (2013). The Flexible Global Ocean-Atmosphere-Land System model, spectral version 2: FGOALS-s2. *Advances in Atmospheric Sciences*, 30(3):561–576.
- Bayr, T., Dommenges, D., Martin, T., and Power, S. B. (2014). The eastward shift of the Walker circulation in response to global warming and its relationship to ENSO variability. *Climate Dynamics*, 43(9-10):2747–2763.
- Bentsen, M., Bethke, I., Debernard, J., Iversen, T., Kirkevåg, A., Seland, Ø., Drange, H., Roelandt, C., Seierstad, I., Hoose, C., et al. (2013). The Norwegian Earth system model, NorESM1-M. Part 1: Description and basic evaluation of the physical climate. *Geoscientific Model Development*, 6(3):687–720.
- Bi, D., Dix, M., Marsland, S. J., O’Farrell, S., Rashid, H., Uotila, P., Hirst, A., Kowalczyk, E., Golebiewski, M., Sullivan, A., et al. (2013). The ACCESS coupled model: description, control climate and evaluation. *Australian Meteorological and Oceanographic Journal*, 63(1):41–64.
- Bony, S., Bellon, G., Klocke, D., Sherwood, S., Fermepin, S., and Denvil, S. (2013). Robust direct effect of carbon dioxide on tropical circulation and regional precipitation. *Nature*

- Geoscience*, 6:447–451.
- Butler, A. H., Thompson, D. W., and Heikes, R. (2010). The steady-state atmospheric circulation response to climate change–like thermal forcings in a simple general circulation model. *Journal of Climate*, 23(13):3474–3496.
- Byrne, M. P. and Schneider, T. (2016). Narrowing of the ITCZ in a warming climate: Physical mechanisms. *Geophysical Research Letters*, 43(21): 11350–11357.
- Chadwick, R., Boutle, I., and Martin, G. (2013). Spatial patterns of precipitation change in CMIP5: Why the rich do not get richer in the tropics. *Journal of Climate*, 26(11):3803–3822.
- Chou, C. and Chen, C.-A. (2010). Depth of convection and the weakening of tropical circulation in global warming. *Journal of Climate*, 23(11):3019–3030.
- Chou, C., Neelin, J. D., Chen, C.-A., and Tu, J.-Y. (2009). Evaluating the "rich-get-richer" mechanism in tropical precipitation change under global warming. *Journal of Climate*, 22(8):1982–2005.
- Collins, M., An, S.-I., Cai, W., Ganachaud, A., Guilyardi, E., Jin, F.-F., Jochum, M., Lengaigne, M., Power, S., Timmermann, A., et al. (2010). The impact of global warming on the tropical Pacific Ocean and El-Niño. *Nature Geoscience*, 3(6):391–397.
- Collins, W., Bellouin, N., Doutriaux-Boucher, M., Gedney, N., Halloran, P., Hinton, T., Hughes, J., Jones, C., Joshi, M., Liddicoat, S., et al. (2011). Development and evaluation of an Earth-system model – HadGEM2. *Geoscientific Model Development*, 4(4):1051–1075.
- Cronin, T. W. (2014). On the choice of average solar zenith angle. *Journal of the Atmospheric Sciences*, 71(8):2994–3003.
- Cubasch, U., Meehl, G., Boer, G., Stouffer, R., Dix, M., Noda, A., Senior, C., Raper, S., and Yap, K. (2001). Projections of future climate change. , in: *JT Houghton, Y. Ding, DJ Griggs, M. Noguer, PJ Van der Linden, X. Dai, K. Maskell, and CA Johnson (eds.): Climate Change 2001: The Scientific Basis: Contribution of Working Group I to the Third Assessment Report of the Intergovernmental Panel*, pages 526–582.
- Davis, N. and Birner, T. (2016). Climate model biases in the width of the tropical belt. *Journal of Climate*, 29(5):1935–1954.
- Davis, N. A. and Birner, T. (2013). Seasonal to multidecadal variability of the width of the tropical belt. *Journal of Geophysical Research: Atmospheres*, 118(14):7773–7787.

- Dee, D. P., Uppala, S., Simmons, A., Berrisford, P., Poli, P., Kobayashi, S., Andrae, U., Balmaseda, M., Balsamo, G., Bauer, P., et al. (2011). The ERA-Interim reanalysis: Configuration and performance of the data assimilation system. *Quarterly Journal of the Royal Meteorological Society*, 137(656):553–597.
- Diaz, H. F., Hoerling, M. P., and Eischeid, J. K. (2001). ENSO variability, teleconnections and climate change. *International Journal of Climatology*, 21(15):1845–1862.
- Donner, L. J., Wyman, B. L., Hemler, R. S., Horowitz, L. W., Ming, Y., Zhao, M., Golaz, J.-C., Ginoux, P., Lin, S.-J., Schwarzkopf, M. D., et al. (2011). The dynamical core, physical parameterizations, and basic simulation characteristics of the atmospheric component AM3 of the GFDL global coupled model CM3. *Journal of Climate*, 24(13):3484–3519.
- Donohoe, A., Marshall, J., Ferreira, D., and Mcgee, D. (2013). The relationship between ITCZ location and cross-equatorial atmospheric heat transport: From the seasonal cycle to the last glacial maximum. *Journal of Climate*, 26(11):3597–3618.
- Dufresne, J.-L., Foujols, M.-A., Denvil, S., Caubel, A., Marti, O., Aumont, O., Balkanski, Y., Bekki, S., Bellenger, H., Benshila, R., et al. (2013). Climate change projections using the IPSL-CM5 Earth system model: from CMIP3 to CMIP5. *Climate Dynamics*, 40(9-10):2123–2165.
- Dunne, J. P., John, J. G., Adcroft, A. J., Griffies, S. M., Hallberg, R. W., Shevliakova, E., Stouffer, R. J., Cooke, W., Dunne, K. A., Harrison, M. J., et al. (2012). GFDL’s ESM2 global coupled climate–carbon Earth system models. Part I: Physical formulation and baseline simulation characteristics. *Journal of Climate*, 25(19):6646–6665.
- England, M. H., McGregor, S., Spence, P., Meehl, G. A., Timmermann, A., Cai, W., Gupta, A. S., McPhaden, M. J., Purich, A., and Santoso, A. (2014). Recent intensification of wind-driven circulation in the Pacific and the ongoing warming hiatus. *Nature Climate Change*, 4(3):222–227.
- Gaetani, M., Flamant, C., Bastin, S., Janicot, S., Lavaysse, C., Hourdin, F., Braconnot, P., and Bony, S. (2017). West African monsoon dynamics and precipitation: the competition between global SST warming and CO₂ increase in CMIP5 idealized simulations. *Climate Dynamics*, 48(3-4):1353–1373.
- Gastineau, G., Li, L., and Le Treut, H. (2009). The Hadley and Walker circulation changes in global warming conditions described by idealized atmospheric simulations. *Journal of Climate*, 22(14):3993–4013.

- Gershunov, A. and Barnett, T. P. (1998). Interdecadal modulation of ENSO teleconnections. *Bulletin of the American Meteorological Society*, 79(12):2715–2725.
- Giorgetta, M. A., Jungclaus, J., Reick, C. H., Legutke, S., Bader, J., Böttinger, M., Brovkin, V., Crueger, T., Esch, M., Fieg, K., et al. (2013). Climate and carbon cycle changes from 1850 to 2100 in MPI-ESM simulations for the Coupled Model Intercomparison Project Phase 5. *Journal of Advances in Modeling Earth Systems*, 5(3):572–597.
- Gregory, J. and Forster, P. (2008). Transient climate response estimated from radiative forcing and observed temperature change. *Journal of Geophysical Research: Atmospheres*, 113(D23).
- Haywood, J. M., Jones, A., Dunstone, N., Milton, S., Vellinga, M., Bodas-Salcedo, A., Hawcroft, M., Kravitz, B., Cole, J., Watanabe, S., et al. (2016). The impact of equilibrating hemispheric albedos on tropical performance in the HadGEM2-ES coupled climate model. *Geophysical Research Letters*, 43(1):395–403.
- He, J. and Soden, B. J. (2015). Anthropogenic weakening of the tropical circulation: The relative roles of direct CO₂ forcing and sea surface temperature change. *Journal of Climate*, 28(22):8728–8742.
- Held, I. M. and Soden, B. J. (2006). Robust responses of the hydrological cycle to global warming. *Journal of Climate*, 19(21):5686–5699.
- Hourdin, F., Grandpeix, J.-Y., Rio, C., Bony, S., Jam, A., Cheruy, F., Rochetin, N., Fairhead, L., Idelkadi, A., Musat, I., et al. (2013). LMDZ5B: the atmospheric component of the IPSL climate model with revisited parameterizations for clouds and convection. *Climate Dynamics*, 40(9-10):2193–2222.
- IPCC (2013). *Climate Change 2013: The Physical Science Basis. Contribution of Working Group I to the Fifth Assessment Report of the Intergovernmental Panel on Climate Change*. Cambridge University Press, Cambridge, United Kingdom and New York, NY, USA.
- Kamae, Y., Watanabe, M., Kimoto, M., and Shiogama, H. (2014). Summertime land–sea thermal contrast and atmospheric circulation over East Asia in a warming climate. Part II: Importance of CO₂-induced continental warming. *Climate dynamics*, 43(9-10):2569–2583.
- Kociuba, G. and Power, S. B. (2015). Inability of CMIP5 models to simulate recent strengthening of the Walker circulation: Implications for projections. *Journal of Climate*, 28(1):20–35.
- Lau, W. K. and Kim, K.-M. (2015). Robust Hadley circulation changes and increasing global dryness due to CO₂ warming from CMIP5 model projections. *Proceedings of the National Academy of Sciences*, 112(12):3630–3635.

- Li, L., Lin, P., Yu, Y., Wang, B., Zhou, T., Liu, L., Liu, J., Bao, Q., Xu, S., Huang, W., et al. (2013). The Flexible Global Ocean-Atmosphere-Land System model, grid-point version 2: FGOALS-g2. *Advances in Atmospheric Sciences*, 30(3):543–560.
- Li, X. and Ting, M. (2017). Understanding the Asian summer monsoon response to greenhouse warming: the relative roles of direct radiative forcing and sea surface temperature change. *Climate Dynamics*, 49(7-8):2863–2880.
- Long, M. C., Lindsay, K., Peacock, S., Moore, J. K., and Doney, S. C. (2013). Twentieth-century oceanic carbon uptake and storage in CESM1(BGC). *Journal of Climate*, 26(18):6775–6800.
- Lu, J., Chen, G., and Frierson, D. M. (2008). Response of the zonal mean atmospheric circulation to El-Niño versus global warming. *Journal of Climate*, 21(22):5835–5851.
- Ma, J. and Xie, S.-P. (2013). Regional patterns of sea surface temperature change: A source of uncertainty in future projections of precipitation and atmospheric circulation. *Journal of Climate*, 26(8):2482–2501.
- Ma, J., Xie, S.-P., and Kosaka, Y. (2012). Mechanisms for tropical tropospheric circulation change in response to global warming. *Journal of Climate*, 25(8):2979–2994.
- Ma, S. and Zhou, T. (2016). Robust strengthening and westward shift of the tropical Pacific Walker circulation during 1979–2012: A comparison of 7 sets of reanalysis data and 26 CMIP5 models. *Journal of Climate*, 29(9):3097–3118.
- McGregor, S., Timmermann, A., Stuecker, M. F., England, M. H., Merrifield, M., Jin, F.-F., and Chikamoto, Y. (2014). Recent Walker circulation strengthening and Pacific cooling amplified by Atlantic warming. *Nature Climate Change*, 4(10):888–892.
- McIlveen, R. (2010). *Fundamentals of Weather and Climate*. Oxford University Press.
- Medeiros, B., Stevens, B., and Bony, S. (2015). Using aquaplanets to understand the robust responses of comprehensive climate models to forcing. *Climate Dynamics*, 44(7-8):1957–1977.
- Meehl, G. A., Washington, W. M., Arblaster, J. M., Hu, A., Teng, H., Tebaldi, C., Sanderson, B. N., Lamarque, J.-F., Conley, A., Strand, W. G., et al. (2012). Climate system response to external forcings and climate change projections in CCSM4. *Journal of Climate*, 25(11):3661–3683.
- Merlis, T. M. (2015). Direct weakening of tropical circulations from masked CO₂ radiative forcing. *Proceedings of the National Academy of Sciences*, 112(43):13167–13171.

- NOAA Climate Prediction Center, National Weather Service. Description of changes to Ocean Niño Index (ONI), 1950–2018. URL: http://origin.cpc.ncep.noaa.gov/products/analysis_monitoring/ensostuff/ONI_change.shtml. [Online; accessed 19-January-2018].
- Phillips, N. A. (1956). The general circulation of the atmosphere: A numerical experiment. *Quarterly Journal of the Royal Meteorological Society*, 82(352):123–164.
- Pincus, R. and Stevens, B. (2013). Paths to accuracy for radiation parameterizations in atmospheric models. *Journal of Advances in Modeling Earth Systems*, 5(2):225–233.
- Pincus, R., Mlawer, E. J., Oreopoulos, L., Ackerman, A. S., Baek, S., Brath, M., Buehler, S. A., Cady-Pereira, K. E., Cole, J. N., Dufresne, J.-L., et al. (2015). Radiative flux and forcing parameterization error in aerosol-free clear skies. *Geophysical Research Letters*, 42(13):5485–5492.
- Power, S. B. and Kociuba, G. (2011a). The impact of global warming on the Southern Oscillation Index. *Climate dynamics*, 37(9-10):1745–1754.
- Power, S. B. and Kociuba, G. (2011b). What caused the observed twentieth-century weakening of the Walker circulation? *Journal of Climate*, 24(24):6501–6514.
- Rotstayn, L., Jeffrey, S., Collier, M., Dravitzki, S., Hirst, A., Syktus, J., and Wong, K. (2012). Aerosol-and greenhouse gas-induced changes in summer rainfall and circulation in the Australasian region: a study using single-forcing climate simulations. *Atmospheric Chemistry and Physics*, 12(14):6377–6404.
- Rybka, H. and Tost, H. (2014). Uncertainties in future climate predictions due to convection parameterisations. *Atmospheric Chemistry and Physics*, 14(11):5561–5576.
- Schmidt, G. A., Kelley, M., Nazarenko, L., Ruedy, R., Russell, G. L., Aleinov, I., Bauer, M., Bauer, S. E., Bhat, M. K., Bleck, R., et al. (2014). Configuration and assessment of the GISS ModelE2 contributions to the CMIP5 archive. *Journal of Advances in Modeling Earth Systems*, 6(1):141–184.
- Scoccimarro, E., Gualdi, S., Bellucci, A., Sanna, A., Giuseppe Fogli, P., Manzini, E., Vichi, M., Oddo, P., and Navarra, A. (2011). Effects of tropical cyclones on ocean heat transport in a high-resolution coupled general circulation model. *Journal of Climate*, 24(16):4368–4384.
- Shepherd, T. G. (2014). Atmospheric circulation as a source of uncertainty in climate change projections. *Nature Geoscience*, 7(10):703–708.
- Stevens, B., Bony, S., and Webb, M. (2012). Clouds On-Off Climate Intercomparison Experiment (COOKIE). Technical report. [Online; accessed 17-November-2017].

- Stevens, B., Giorgetta, M., Esch, M., Mauritsen, T., Crueger, T., Rast, S., Salzmann, M., Schmidt, H., Bader, J., Block, K., et al. (2013). Atmospheric component of the MPI-M Earth System Model: ECHAM6. *Journal of Advances in Modeling Earth Systems*, 5(2):146–172.
- Su, H., Jiang, J. H., Zhai, C., Shen, T. J., Neelin, J. D., Stephens, G. L., and Yung, Y. L. (2014). Weakening and strengthening structures in the Hadley circulation change under global warming and implications for cloud response and climate sensitivity. *Journal of Geophysical Research: Atmospheres*, 119(10):5787–5805.
- Tanaka, H., Ishizaki, N., and Kitoh, A. (2004). Trend and interannual variability of Walker, monsoon and Hadley circulations defined by velocity potential in the upper troposphere. *Tellus A*, 56(3):250–269.
- Taylor, K. E., Stouffer, R. J., and Meehl, G. A. (2012). An overview of CMIP5 and the experiment design. *Bulletin of the American Meteorological Society*, 93(4):485–498.
- Thompson, D. W., Bony, S., and Li, Y. (2017). Thermodynamic constraint on the depth of the global tropospheric circulation. *Proceedings of the National Academy of Sciences*, 114(31):8181–8186.
- Vecchi, G. A. and Soden, B. J. (2007). Global warming and the weakening of the tropical circulation. *Journal of Climate*, 20(17):4316–4340.
- Vecchi, G. A., Soden, B. J., Wittenberg, A. T., Held, I. M., Leetmaa, A., and Harrison, M. J. (2006). Weakening of tropical pacific atmospheric circulation due to anthropogenic forcing. *Nature*, 441(7089):73–76.
- Voltaire, A., Sanchez-Gomez, E., y Méliá, D. S., Decharme, B., Cassou, C., Sénési, S., Valcke, S., Beau, I., Alias, A., Chevallier, M., et al. (2013). The CNRM-CM5.1 Global Climate Model: description and basic evaluation. *Climate Dynamics*, 40(9-10):2091–2121.
- Volodin, E., Dianskii, N., and Gusev, A. (2010). Simulating present-day climate with the INMCM4.0 coupled model of the atmospheric and oceanic general circulations. *Izvestiya, Atmospheric and Oceanic Physics*, 46(4):414–431.
- Wang, C. (2002). Atmospheric circulation cells associated with the El-Niño-Southern Oscillation. *Journal of Climate*, 15(4):399–419.
- Watanabe, M., Suzuki, T., O’ishi, R., Komuro, Y., Watanabe, S., Emori, S., Takemura, T., Chikira, M., Ogura, T., Sekiguchi, M., et al. (2010). Improved climate simulation by MIROC5: mean states, variability, and climate sensitivity. *Journal of Climate*, 23(23):6312–6335.

- Watanabe, S., Hajima, T., Sudo, K., Nagashima, T., Takemura, T., Okajima, H., Nozawa, T., Kawase, H., Abe, M., Yokohata, T., et al. (2011). MIROC-ESM 2010: Model description and basic results of CMIP5-20C3M experiments. *Geoscientific Model Development*, 4(4):845.
- Wing, A. A., Reed, K. A., Satoh, M., Stevens, B., Bony, S., and Ohno, T. (2018). Radiative–Convective Equilibrium Model Intercomparison Project. *Geoscientific Model Development*, 11(2):793–826.
- Wu, T., Song, L., Li, W., Wang, Z., Zhang, H., Xin, X., Zhang, Y., Zhang, L., Li, J., Wu, F., et al. (2014). An overview of BCC climate system model development and application for climate change studies. *Journal of Meteorological Research*, 28(1):34–56.
- Yu, B. and Zwiers, F. W. (2010). Changes in equatorial atmospheric zonal circulations in recent decades. *Geophysical Research Letters*, 37(5).
- Yukimoto, S., Adachi, Y., Hosaka, M., Sakami, T., Yoshimura, H., Hirabara, M., Tanaka, T. Y., Shindo, E., Tsujino, H., Deushi, M., et al. (2012). A new global climate model of the Meteorological Research Institute: MRI-CGCM3 –model description and basic performance– *Journal of the Meteorological Society of Japan. Ser. II*, 90:23–64.
- Zelinka, M. D. and Hartmann, D. L. (2010). Why is longwave cloud feedback positive? *Journal of Geophysical Research: Atmospheres*, 115(D16).

List of Tables

2.1	Details of the CMIP5 General Circulation Models	14
3.1	Statistical results for the ERA-Interim reanalysis dataset	19
3.2	Statistical results for the MPI ensemble	21
3.3	MPI ensemble correlation between the change in Walker circulation on one side and TCR_{TP} and the OLR trend (until CO_2 doubling) on the other side (selected runs/GCMs refer to the runs/GCMs that show a significant trend in the Walker circulation intensity until CO_2 doubling)	24
3.4	Statistical results for the CMIP5 ensemble	25
3.5	CMIP5 ensemble correlation between the change in Walker circulation on one side and TCR_{TP} and the OLR trend (until CO_2 doubling) on the other side (selected runs/GCMs refer to the runs/GCMs that show a significant trend in the Walker circulation intensity until CO_2 doubling)	26

List of Figures

1.1	Schematic of the atmospheric circulation over the tropical Pacific Ocean and its relationship to the ocean circulation. The <i>color shading</i> describes the anomalous ocean circulation with the help of the equatorial and meridional mean trend in water temperature down to the 300 m depths as detected in the 1992–2011 period reanalysis (reprinted by permission from Springer Customer Service Centre GmbH: Nature Climate Change, England et al. [2014] , © 2014).	2
1.2	Sources of uncertainty and of intermodel spread in the assessment of the change in tropical circulation under anthropogenic CO ₂ forcing investigated in this work.	7
3.1	ERA-Interim reanalysis 1979–2008 mean fields for the parameters used to derive (a) the MSLP-index, (b) the ω_{500} -index, and (c) the χ_{200} -index. The Western and Eastern Pacific boxes used for the first two indices are marked in (a) and (b).	17
3.2	ERA-Interim reanalysis 1979–2008 time series for (a) the MSLP-index, (b) the ω_{500} -index, and (c) the χ_{200} -index. In every plot the ONI-index is presented in <i>dashed line</i> , with values on the second y-axis.	20
3.3	Pacific Walker Cell intensity trends detected for the CMIP5 ensemble 1pctCO ₂ experiment output. Trends detected until CO ₂ doubling are shaded <i>red</i> , until CO ₂ quadrupling - <i>blue</i> (hatched bars denote trends with confidence level below 80%). The <i>red solid line</i> represents the MPI ensemble mean trend, the <i>dashed lines</i> - the range of 1σ variance, the <i>dotted lines</i> - the total spread of the MPI ensemble.	27
3.4	Pacific Walker Cell intensity trend until CO ₂ doubling compared to the TCR _{TP} in the CMIP5 and MPI ensembles' output of the 1pctCO ₂ experiment (the values corresponding to the MPI ensemble are denoted by circles with smaller diameter). The correlation coefficient between the two sets is given for each ensemble separately.	28

- 3.5 MPI and CMIP5 ensemble members' index-based ranking (in ascending order) according to the projected trend in the intensity of the Pacific Walker Cell until CO₂ doubling within the 1pctCO₂ experiment (MPI-ESM-LR runs and GCMs are ordered according to their mean rank). The *blue shading* denotes the low-ranking ensemble members (LRM, projecting on average the strongest weakening of the Walker circulation), the *red shading* - high-ranking members (HRM, projecting on average the smallest weakening of the Walker circulation or its strengthening). 30
- 3.6 (a) Meridional cross-section of vertical velocity ω_X between 10°N and 10°S, calculated for the mean piControl output of MPI-ESM-LR. (b) CMIP5 ensemble vertically-weighted mean $\bar{\omega}_X$ of the meridional cross-section presented above. (c) Changes in $\bar{\omega}_X$ at the moment of CO₂ doubling with respect to the control run for the CMIP5 ensemble LRMs (GISS-E2-H, MIROC-ESM, HadGEM2-ES) and HRMs (INMCM4, NorESM1-M).
Notes: The thick black lines at the bottom of plot (a), as well as the grey stripes in (b) and (c), represent land surface on the equator, corresponding to Sumatra, Borneo and South America. The beige stripes in (b) and (c) refer to the zonal extent of the boxes used to compute the MSLP-index; the hatched stripes refer to the zonal extent of the boxes used to compute the ω_{500} -index. 32
- 3.7 (a), (b) - Ensemble mean OLR in the pre-industrial control experiment (pi-Control) for the MPI and CMIP5 ensembles, respectively. (c), (d) - Ensemble mean trend in OLR variation until CO₂ doubling in the 1pctCO₂ output. (e), (f) - Mean trend in OLR variation until CO₂ doubling in the 1pctCO₂ output, averaged for the low-ranking ensemble members (LRM). (g), (h) - Mean OLR trend until CO₂ doubling, averaged for the high-ranking ensemble members (HRM). *Note: Regions with trends having $\geq 80\%$ confidence level are hatched.* 33
- 3.8 Mean OLR trend difference between HRMs and LRMs for the MPI ensemble (a) and the CMIP5 ensemble (b). The *crossed hatching* shows the regions where the sign of the trend differs between LRMs and HRMs. *Blue areas without hatching* are where the models with less circulation slowdown (HRM) have a stronger increase in cloudiness (lower OLR) than the areas with a stronger circulation slowdown (LRM). 34
- 3.9 Surface temperature change at the moment of CO₂ doubling in the 1pctCO₂ experiment output, averaged for the LRM (a) and HRM (b) CMIP5 models. . . 35

- 4.1 (a) Zonal mean of mass stream function in 10^9 kg s^{-1} (*black contours*) and of vertical velocity (*color shading*), averaged over the aquaControl output of CNRM-CM5. (b) Vertically-averaged zonal mean of mass stream function for the same output with the selected tropics expanse. 38
- 4.2 Mean profiles of CO_2 , O_3 , N_2O , and CH_4 , averaged over the 1979–2008 period in the CMIP5 historical experiment output of CanESM2, CESM1-BGC, GFDL-ESM2G, GFDL-ESM2M and MPI-ESM-LR. 40
- 4.3 (*first line*) Zonal mean of subsidence mass flow, averaged for CNRM-CM5 over (a) the aquaControl and (b) the aqua4xCO2 experiment, as well as (c) the difference between the experiments. (*lines 2–5*) Same as in the first line, but for static stability, total diabatic heating rate, radiative heating rate and residual heating rate, respectively. 42
- 4.4 aquaControl (*dashed lines*) and aqua4xCO2 (*solid lines*) ensemble mean profiles of (a) subsidence mass flow, (b) static stability, (c) tropical subsidence area, and (d) total, clear-sky and residual heating rates (the profiles are averaged over the tropical subsidence areas). 43
- 4.5 (a) Relative change of subsidence mass flow in the aqua-planet experiments. The solid line present a comparison of this change calculated following equations (4.1), (4.5) and (4.6). (b)–(f) The contribution to the change in *SMF* of static stability change, subsidence area change, total, clear-sky and residual heating rate change, respectively. The *grey lines* represent the corresponding results for every ensemble member (in (a) they show the change in *SMF* according to equation (4.1)). 45
- 4.6 amip (*dashed lines*) and amip4xCO2 (*solid lines*) ensemble mean profiles of (a) subsidence mass flow, (b) static stability, (c) tropical subsidence area, (d) total, (e) clear-sky and (f) residual heating rates (the profiles are averaged over the tropical subsidence areas). The respective results are presented for the entire tropical subsidence area (*red lines*), as well as over land (*orange lines*) and over ocean (*blue lines*). The corresponding profiles from the aqua-planet experiments are presented in *grey lines* for comparison. 47
- 4.7 (a) Relative change of subsidence mass flow in the amip experiments. (b)–(f) The contribution to the change in *SMF* of static stability change, subsidence area change, total, clear-sky and residual heating rate change, respectively. The respective results are presented for the entire tropical subsidence area (*red lines*), as well as over land (*orange lines*) and over ocean (*blue lines*). The results from the aqua-planet experiments are presented in *dotted lines* for comparison. 48

- 4.8 aquaControl (*dashed lines*) and aqua4xCO2 (*solid lines*) ensemble standard deviation for the mean profiles of (a) subsidence mass flow, (b) static stability, (c) tropical subsidence area, and (d) total, clear-sky and residual heating rates (the profiles are averaged over the tropical subsidence areas). 50
- 4.9 aquaControl (*dashed lines*) and aqua4xCO2 (*solid lines*) ensemble coefficient of variance for the mean profiles of (a) subsidence mass flow, (b) static stability, (c) tropical subsidence area, and (d) total, clear-sky and residual heating rates (the profiles are averaged over the subsidence areas). 50
- 4.10 amip (*dashed lines*) and amip4xCO2 (*solid lines*) ensemble coefficient of variance for the mean profiles of (a) subsidence mass flow, (b) static stability, (c) tropical subsidence area, (d) total, (e) clear-sky and (f) residual heating rates (the profiles are averaged over the tropical subsidence areas). *Note:* The respective results are presented for the entire tropical subsidence area (*red lines*), as well as over land (*orange lines*) and over ocean (*blue lines*). The corresponding profiles from the aqua-planet experiments are presented in *grey lines* for comparison. 51
- 4.11 Ensemble mean tropical profiles of (a) subsidence mass flow, (b) static stability, (c) tropical subsidence area, (d) total, (e) clear-sky and (f) residual heating rates in the aqua-planet and amip experiments. 52
- 4.12 Ensemble mean tropical profiles of relative change in (a) subsidence mass flow, (b) static stability, (c) tropical subsidence area, (d) total, (e) clear-sky and (f) residual heating rates. The *grey lines* refer to the aqua-planet experiments, the *red lines* – to the mean tropical profile in the amip experiments, the *orange lines* – to the mean profile over land, the *blue lines* – to the mean profile over ocean; the *dashed lines* present the respective profile in the experiment with abrupt quadrupling of CO₂, the *solid lines* – in the experiment with abrupt 4 K increase in surface temperature. 54
- 4.13 Global mean annual surface temperature variation after an abrupt CO₂ quadrupling, as found in 8 CMIP5 GCM runs for the abrupt4xCO2 experiment. 55
- 4.14 Ensemble mean tropical profiles of relative change in (a) subsidence mass flow, (b) static stability, (c) tropical subsidence area, (d) total, (e) clear-sky and (f) residual heating rates. The *grey lines* refer to the amip experiments, the *red lines* – to the coupled experiments (*dashed lines* for the 1st year mean in abrupt4xCO2, *solid lines* for the last 30-year mean in abrupt4xCO2). 56

-
- 5.1 ERA-Interim monthly mean SMF, vertically averaged over the troposphere, presented in (*upper series*) zonal means and (*lower series*) meridional means over the equatorial Pacific (7.5°S-7.5°N, 90°E-60°W). 63

Acknowledgments

I acknowledge the Cluster of Excellence CliSAP (EXC177), Universität Hamburg, funded through the German Science Foundation (DFG), that provided not only the financial support for this work, but also the scientific environment I have truly enjoyed in the last 4 years here in Hamburg. My analysis is based on datasets kindly made publicly available by the World Climate Research Programme's Working Group on Coupled Modelling, which is responsible for CMIP5, the institutions responsible for the models listed in Tab. 2.1, as well as ECMWF, which maintains the ERA-Interim reanalysis. Special thanks go to the Max-Planck Institute for Meteorology for providing the MPI-ESM-LR ensemble.

I am immensely grateful to Prof. Dr. Stefan Buehler and Dr. Verena Grützun for being the awesome supervisors they are, for their guidance, engagement, support, advice, trust and motivating remarks, as well as for the time invested in listening and encouraging me. I have enjoyed this work essentially thanks to your kind attitude.

Prof. Dr. Bjorn Stevens I thank for the time taken to be my Advisory Panel Chair, for the constructive comments and the supportive demeanor. I am also thankful to Thorsten Mauritsen, Brian Soden, Thomas Birner, Chris Bretherton for the interesting discussions and comments on my findings.

Special thanks go to the School of Integrated Climate System Sciences and especially to Berit Hachfeld and Ingo Harms, who are always helpful and approachable. I have greatly enjoyed being part of this Graduate School, as well as meeting and befriending the other PhD students. I want to also mention my gratitude to SICSS for organizing the many soft-skill courses, especially the Writing Course. On this note I thank Dallas Murphy for probably the most effective change of perspective on writing.

I can't begin to express how lucky I consider myself for working with everyone in the Radiation and Remote Sensing group – you are truly RaRe! I thank Oliver Lemke for 'magically' making everything work and I am very grateful to Jörg and Leo for providing the final proof-read of this dissertation.

To my dear Theresa Mieslinger and Mareike Burba I want to thank for being the best office mates one could ask for and for having the patience with my German. I am grateful to Oleksandr

'Alex' Bobryshev for being my friend from day 1 and for indulging my 'sunny' moments. I thank Imke Hans for being a great and funny listener, as well as a fellow Tolkienite. To Manfred 'Freddy' Brath I am thankful for the much-needed healthy dose of sarcasm.

I am lucky to have made amazing friends in the last 4 years! Jairo Segura, Tim Dudeck and Jessi Toboldt, big hugs go to you (and Suma) for just being my people. Larissa Schultze and Leo Borchert, you are truly inspiring and great partners in putting together events, great brunches, lunches, dinners, and coffee and ice-cream breaks (with this I solemnly swear to also contribute to the supply of ice-cream). Vera Köpsel, you are a true inspiration for me, on so many levels. Nana Molina Gamez, thanks for always having the best comments and advice, and also for the pure trekkiness. Marjan Ghobadian, I am very grateful to you for being the genuine and joyful person you are. Maciej Miernecki, thanks for bringing the craziness around. Yulia Polkova, I am especially grateful to you for organizing the Scientific Writing Group, and to Normann Rüggen, Dorothea Mayer, Mihael Machado de Souza, Aурpita Saha, Anju Sathyanarayanan and the other members of this group for the friendly but critically constructive atmosphere.

Last but certainly not least, I want to thank my big family and friends back home. To my parents and grandparents I want to thank for their love and for supporting and encouraging me to do what I like, no matter how far from home it is. And my most exclusive gratitude goes to the Berlin part of the family: Ina, Iwan, Tami and Garyk, thank you for being the wonderful, talented and loving family you are!

Eidesstattliche Versicherung

Hiermit versichere ich an Eides statt, dass ich die vorliegende Dissertation mit dem Titel "The Tropical Circulation in a Changing Climate" selbstständig verfasst und keine anderen als die angegebenen Hilfsmittel – insbesondere keine im Quellenverzeichnis nicht benannten Internet-Quellen – benutzt habe. Alle Stellen, die wörtlich oder sinngemäß aus Veröffentlichungen entnommen wurden, sind als solche kenntlich gemacht. Ich versichere weiterhin, dass ich die Dissertation oder Teile davon vorher weder im In- noch im Ausland in einem anderen Prüfungsverfahren eingereicht habe und die eingereichte schriftliche Fassung der auf dem elektronischen Speichermedium entspricht.

Hamburg, den 18. April 2018

Elina Plesca